THE RHEOLOGY AND FLOW BEHAVIOUR OF HIGH CONCENTRATION MINERAL SLURRIES

by

R.I.G. NEILL

BSc (Civil Engineering)
University of Cape Town

A thesis submitted in partial fulfilment of the requirement for the degree of Master of Science in the Department of Civil Engineering, University of Cape Town.

September 1988

Civil Engineering Department
University of Cape Town
South Africa

DEDICATION

To my parents.

ACKNOWLEDGEMENTS

The author would like to thank the following people -

Associate Professor J.H. Lazarus for his encouragement and creative input into this thesis and for sharing his expertise in the field of hydrotransport.

Miss P. Mc Cabe for her unfailing support.

Mr P.T. Slatter for his introduction to and expertise on rheology.

Mrs P. Jordaan for typing this thesis.

Associate Professor F.A. Kilner, the staff of the Department of Civil Engineering and the members of Hydrotransport Research for the seminars, stimulating discussions and advice.

The technical and laborotory staff for their assistance.

Dr. L. Bayvel and Mr. J. Knight for the particle size analyses.

Mr D. Gerneke of the Electron Microscope Unit for the micrographs.

For financial support:

The Council for Scientific and Industrial Research.
The University of Cape Town.
The Chamber of Mines of South Africa.
Dr. J. von Theurheim of Bornemann Pumps.

SYNOPSIS

The rheology and flow behaviour of high concentration backfill tailings are investigated using a modified Balanced Beam Tube Viscometer. The viscometer is capable of producing reliable data using a computer based data acquisition system and three different tube diameters.

The aim of this research is to determine the rheology of backfill tailings in order to predict friction head losses.

The backfill tailings were prepared into four different particle size distributions each with a different maximum particle size. Each particle size distribution was tested over a range of high concentrations in the viscometer.

The rheology of the lower concentration backfill tailings was successfully characterized using the yield-pseudoplastic model.

It has been found that at high concentrations rheological characterization is impossible because the laminar flow region of the pseudo-shear diagram varies with tube diameter. This anomalous behaviour in the form of diameter dependence has been recorded in the literature.

The results of high concentration tests on backfill tailings are investigated using the following theories to establish and account for the cause of the anomalous behaviour:

Effective slip analysis	- corrects the measured data for effective slip.
Dense-Phase Model	- based on the sliding friction between solid particles and the tube wall.
Wall Effect	- based on a reduction of *in situ* concentration due to a wall effect.
Boundary-Layer Effect	- corrects for the effect of a boundary-layer of liquid at the wall.
Modified Friction Factors	- takes into account the hydrodynamic lubrication between the solid particles and the tube wall.

The existence of a thin layer of liquid at the wall is credible but not yet proven. The anomalous behaviour is linked to this layer. However a suitable method for correcting the measured data has not yet been established.

TABLE OF CONTENTS

LIST OF FIGURES

LIST OF TABLES

NOMENCLATURE

Symbol	Description	Units
A	cross sectional area	m^2
C_m	maximum packing concentration	
C_{vd}	delivered volumetric concentration	
C_{vt}	*in situ* volumetric concentration	
C_{wd}	*in situ* mass concentration	
D	internal tube diameter	m
d	particle diameter	μm
F	force	N
f	Fanning friction factor = $\tau_o/\frac{1}{2}\rho V^2$	
f_ℓ	friction factor for the liquid phase	
f_n	function of	
g	gravitational constant = 9.81	m/s^2
i_m	hydraulic gradient of mixture in units of water per length of pipe	m/m
i_w	hydraulic gradient of water flowing at velocity V_m in pipe diameter D	m/m
K	fluid consistency index	
K	constant defined by the equation in which it is used	
L	tube length	m
Log	decimal logarithm	
ln	natural logarithm	
M	mass flow rate	kg/s
m	mass	kg
m	constant defined by the equation in which it is used	
n	flow behaviour index	
n	number of	
n'	apparent flow behaviour index	
p	pressure	Pa
Δp	pressure drop	Pa
Q	volumetric flow rate	m^3/s
Q_m	volumetric flow rate of mixture	m^3/s

R	radius of tube	m
r	radial distance	m
r_{plug}	radius containing plug flow	m
Re	Newtonian Reynolds number = $\rho VD/\mu$	
S_m	relative density of mixture	
S_s	relative density of solids	
S_w	relative density of water = 1	
t	time	s
u	local velocity	m/s
u_{core}	velocity of core	m/s
u_{plug}	velocity of plug	m/s
u_s	effective slip velocity	m/s
v	volume	m^3
v	voltage	V
v	velocity	m/s
V	mean velocity	m/s
V_m	mean mixture velocity = Q_m/A	m/s
x	direction of uniform flow	
y	direction perpendicular to x	
α	shear stress ratio (τ_y/τ_o)	
β	effective slip coefficient	
δ	boundary layer thickness	m
Δ	increment	
ϵ	initial pseudo-shear diagram slope	Pa s
η_p	plastic viscosity	Pa s
λ	a function of concentration defined by equation 2.37	
μ	dynamic viscosity	Pa s
μ_w	dynamic viscosity of water = $1{,}005 \times 10^{-3}$	Pa s
μ_s	coefficient of sliding friction	
π	3.146	
ρ	density	kg/m^3
ρ_m	density of mixture	kg/m^3
ρ_s	density of solids	kg/m^3
ρ_w	density of water = 998,2	kg/m^3
τ	shear stress	Pa
τ_o	shear stress at wall	Pa
τ_y	yield stress	Pa

Subscripts

d	delivered
i	i-th component
l	liquid phase
m	mixture
o	at the tube wall
s	solid phase
t	*in situ*
v	volumetric basis
w	weight basis
w	water
calc	calculated
obs	observed

CHAPTER 1

INTRODUCTION

This dissertation documents an investigation into the flow behaviour and the rheology of high concentration mineral slurries using a novel Balanced Beam Tube Viscometer (BBTV). The intention of this research is to theoretically model the effect of particle size distribution and concentration on rheology.

It has been shown extensively in the literature that high concentration slurries may exhibit anomalous behaviour. This behaviour is associated with a rheology that is pipe diameter dependent. Several theories have been proposed to explain this behaviour. Extensive tests on backfill tailings using the Balanced Beam Tube Viscometer are used to evaluate these theories.

The objectives of this research are as follows:

- Investigate the anomalous behaviour that occurrs at high concentrations in slurries.
- Evaluate theories in the literature that attempt to explain this anomalous behaviour.
- Develop a method for predicting the friction headlosses of these slurries.

This thesis is a continuation and development of the work presented by Slatter (1986).

1.1 THE HYDRAULIC TRANSPORT OF SOLIDS IN PIPES

The hydraulic transport of solids in pipes is an established and reliable method of transporting solids. The theory governing the design and optimization of hydraulic transport systems is still in its infancy. This is evident in the fact that friction headloss of a single phase Newtonian fluid is a function of five variables whereas the friction headloss of a two phase slurry is a function of fourteen variables (Lazarus (1985)).

1.2 RHEOLOGY

Rheology (rheos - flow; logos - knowledge) describes the deformation of a body of fluid under the influence of stress. More specifically rheology means the characterization of the relationship between shear stress and shear rate in a fluid. The process of rheological characterization involves the measurement of shear stress at various shear rates. This data is plotted on a graph called a rheogram and characterized using a rheological model.

In the context of this thesis a fluid is defined a material capable of continuous flow when stressed beyond its yield stress. A slurry is defined as a mixture of solids and liquids.

1.3 VISCOMETERS

The most common viscometers used in hydrotransport are rotational and tube viscometers (Barr (1931)), Green (1949), (Scott Blair (1969)).

The rotational viscometer consists of two coaxial cylinders. The gap between the cylinders is filled with a sample. One cylinder is rotated at various speeds and the applied torque measured. From this the shear rate and the shear stress can be calculated and the rheology can be determined.

The tube viscometer consists of a tube of known length and diameter through which a sample flows. The friction head loss across the tube at various velocities is measured. From this the shear stress and shear rate at the tube wall can be calculated and the rheology can be determined. The viscometer used in this thesis is of a tube variety and is capable of producing reliable rheological and pipeline data.

Lazarus and Slatter (1986) showed that rotary viscometers are less suitable than tube viscometers for the rheological characterization of slurries.

CHAPTER 2

LITERATURE AND THEORY

2.1 INTRODUCTION

This review is based on the literature obtained from journals and books dating from 1687 to 1987. The main references for this chapter are Govier and Aziz (1972) and Skelland (1967).

2.2 SHEAR STRESS AND SHEAR RATE

Consider two parallel plates a distance y apart containing a fluid. One plate is fixed and a force F moves the other at a velocity v creating a velocity distribution shown in Fig. 2.1. The shear stress τ is given by

$$\tau = \frac{F}{A} \quad (Pa) \qquad (2.1)$$

The shear rate is given by

$$\frac{dv}{dy} = \frac{v}{y} \left(\frac{1}{s}\right) \qquad (2.2)$$

A rheogram is defined as a graph of shear stress on the vertical axis versus shear rate on the horizontal axis shown in Fig. 2.2.

2.3 NEWTONIAN RHEOLOGY

In its simplest form hypothesized by Newton in his Principia of 1687, the "resistance arising from the lack of slipperiness in a fluid" is defined by one independent variable. Maxwell later named this variable the coefficient of dynamic viscosity (μ) (Barr (1931)). Schramm (1981) defined the viscosity as "the resistance of a fluid against any irreversible positional change of its volume elements". The mathematical formulation of this concept is given by

$$\tau = \mu \left(\frac{dv}{dy}\right) \qquad (2.3)$$

The viscosity (μ) has the units (Pa s) and is equal to the slope of the Newtonion rheological curve shown in Fig. 2.2.

The incremental viscosity (μ_i) is defined as the tangent to the rheological curve at a fixed shear rate as shown in Fig. 2.3. It can be likened to the thickness of a fluid at a fixed shear rate. The incremental viscosity of a Newtonian fluid remains constant with shear rate as shown in Figs. 2.2 and 2.3. Many common fluids such as water and oil are Newtonian.

2.4 NON-NEWTONIAN RHEOLOGY

The more complex case of non-Newtonian fluids exhibit a variation in incremental viscosity with shear rate shown in Fig. 2.3. This is associated with a non-linear rheogram shown in Fig. 2.2. These fluids may also exhibit a dependence of incremental viscosity on shear history called time dependence

Shear thinning (pseudoplasticity) occurs when incremental viscosity decreases with increasing shear rate shown as a flattening rheological curve in Fig. 2.2. Shear thickening (dilatency) occurs when incremental viscosity increases with increasing shear rate shown as a steepening rheological curve (Fig. 2.2).

Non-Newtonian fluids may also exhibit a yield stress (τ_y) shown in Fig. 2.2. This occurs in fluids such as toothpaste that only flow when they are stressed above their yield stress.

In order to account for rheogram curvature and yield stress Herchell-Bulkley proposed the yield-pseudoplastic model. The mathematical formulation of this model is given by

$$\tau = \tau_y + K \left(\frac{dv}{dy}\right)^n \qquad (2.4)$$

This model and its variations are shown on a rheogram in Fig. 2.2. The corresponding variations in the incremental viscosity with shear rate are shown in Fig. 2.3.

The fluid consistency index (K) corresponds to the steepness of the rheogram and to the thickness of the fluid. The deviation of the flow behaviour index (n) from unity corresponds to the amount of curvature of the rheogram and to the degree of non-Newtonian behaviour.

Many industrial fluids such as paints,creams and polymer melts and most slurries are non-Newtonian.

2.5 SLURRY RHEOLOGY

A slurry is defined as a mixture of solid particles and liquid. For analytical purposes researchers such as Lazarus (1988), Sive (1988) and Wasp et al (1979) considered a fictitious fine portion of the solids to combine with the free water to form the vehicle. The vehicle is the conveying fluid for the larger particles. The vehicle is analysed as non-settling and shows virtually no vertical concentration gradient. If all the solid particles form part of the vehicle then the slurry is analysed as a single phase homogeneous fluid although in a strict sense it is a two phase mixture.

Experience has shown that the vehicle is usually non-Newtonian and shows minimal time dependence.

The rheology of fine solid-liquid mixtures is dependent on several variables listed below.

Slatter (1986) showed that concentration and particle size distribution have a significant effect on the rheology shown in Fig. 2.4 and Fig. 2.5.

Horsley and Reizes (1980) showed that a change in the surface chemical characteristics such as zeta potential has an effect on the rheology as shown in Fig. 2.6.

Davis and Shrivastava (1982) showed that an increase in the temperature has the effect of reducing the consistency.

The slurry rheology is also dependent on other variables such as particle shape and particle roughness (Lazarus (1985)).

Hanks and Hanks (1982) describe a method of determining the critical particle size below which all the particles are rheologically active (vehicle). By adding successive fractions of coarser particles to the finest material the critical particle size is defined as the size above which any addition of coarser particles causes no further change in rheology.

2.6 TUBE FLOW THEORY

The fundamental problem in tube flow is the evaluation of the friction head loss. Research into this field showed that tube flow can occur in two states namely: laminar and turbulent. In laminar flow the friction head loss is mainly proportional to viscous forces. In turbulent flow the friction head loss is mainly proportional to the inertial forces. In laminar flow adjacent annuli shear telescopically past each other with axial symmetry as shown in Fig. 2.7. This shearing action is governed by the rheology of the fluid. For this reason data collected from laminar flow is used for rheology.

The following assumptions are made for the development of tube flow theory:

- steady state flow exists
- the fluid is homogeneous
- no slip occurs at the tube wall

The shear stress at the wall of a tube can be evaluated from a force balance on a section of fluid shown in Fig. 2.8 and is given by

$$\tau_o = \frac{D\Delta p}{4L} \qquad (2.5)$$

The continuity equation for tube flow is given by

$$Q = \pi R^2 V \qquad (2.6)$$

The shear rate at the wall $\left(-\frac{du}{dr}\right)_o$ cannot be evaluated directly so a pseudo-shear rate (bulk shear rate) 8V/D derived from Poiseuille's equation (eqn. 2.16) is used.

A typical tube flow pseudo-shear diagram obtained from the Balanced Beam Tube Viscometer is shown in Fig. 2.9.

Rabinowitch and Mooney derived a relation from first principals that converts the pseudo-shear rate into true shear rate which is given by

$$\left(-\frac{du}{dr}\right)_o = \left(\frac{3n'+1}{4n'}\right)\frac{8V}{D} \qquad (2.7)$$

where $n' = \dfrac{d(\ln(\tau_o))}{d(\ln\left(\frac{8V}{D}\right))}$

This relation effectively converts a pseudo-shear diagram into a rheogram and a full derivation is given in Appendix A. An analysis of this relation is shown in Appendix A revealed that the pseudo-shear diagram resembles a rheogram with a logarithmically compressed X axis. Slatter (1986) showed that the relation cannot be used because n' is not constant and its value at a particular shear rate cannot be accurately determined.

A new technique for data reduction has been developed and is described in Section 2.10.

A typical yield-pseudoplastic fluid shown in Fig. 2.2, has a velocity profile, shear rate distribution and shear stress distribution shown in Fig. 2.10.

By rearranging equation 2.4 the velocity gradient is given by

$$-\left(\frac{du}{dr}\right) = \left(\frac{1}{K}\right)^{1/n} (\tau - \tau_y)^{1/n} \tag{2.8}$$

The plug is defined as an unsheared zone in the center of the tube in which $\tau \leq \tau_y$.

The plug is bound by

$$r_{plug} = \frac{2\,\tau_y}{\left(-\frac{dp}{dL}\right)} \tag{2.9}$$

and moves at a velocity given by

$$u_{plug} = \frac{\left(\frac{1}{K}\right)^{1/n}}{\left(-\frac{dp}{2dL}\right)} \frac{n}{n+1} \left(\tau_o - \tau_y\right)^{\frac{n+1}{n}} \tag{2.10}$$

Integrating equation 2.8 with respect to r and substituting the boundary condition u = 0 at r = R yields the velocity profile given by

$$u = \frac{\left(\frac{1}{K}\right)^{1/n}}{\left(-\frac{dp}{2dL}\right)} \frac{n}{n+1} \left[\left(\tau_o - \tau_y\right)^{\frac{n+1}{n}} - \left(\tau - \tau_y\right)^{\frac{n+1}{n}}\right] \tag{2.11}$$

The discharge is the sum of the flow through the sheared region ($R > r > r_{plug}$) and the plug region ($r < r_{plug}$) given by

$$Q = \int_{r_{plug}}^{R} 2\,\pi\, r\, u\, dr + \pi\, r_{plug}^{\,2}\, u_{plug} \tag{2.12}$$

Setting $\tau_o = \frac{D\Delta p}{4L}$ and integrating gives

$$\frac{8V}{D} = \frac{4n}{K^{1/n}\,\tau_o^3}(\tau_o - \tau_y)^{\frac{n+1}{n}}\left[\frac{(\tau_o - \tau_y)^2}{1+3n} + \frac{2\,\tau_y(\tau_o - \tau_y)}{1+2n} + \frac{\tau_y^2}{1+n}\right] \quad 2.13$$

A full derivation of equation 2.13 is given in Appendix B.

By applying various conditions the flow equations for other models can be derived (detailed derivations are shown in Appendix B).

If $n > 1$ then the fluid is yield-dilatant and if $n < 1$ then the fluid is yield-pseudoplastic. In both cases equation 2.13 is used.

In the case of a Bingham plastic fluid (n=1) equation 2.13 reduces to the Buckingham equation given by

$$\frac{8V}{D} = \frac{4}{\eta_p}\left[1 - \frac{4}{3}\left(\frac{\tau_y}{\tau_o}\right) + \frac{1}{3}\left(\frac{\tau_y}{\tau_o}\right)^4\right] \quad (2.14)$$

In the case of a power law fluid ($\tau_y = 0$) equation 2.13 reduces to

$$\frac{8V}{D} = \frac{4n\,\tau_o^{1/n}}{K^{1/n}(1+3n)} \quad (2.15)$$

In the case of a Newtonian fluid ($n = 1$ and $\tau_y = 0$) equation 2.13 reduces to the Poiseuille equation given by

$$Q = \frac{\pi R^4 \Delta p}{8 \mu L} \quad (2.16)$$

2.7 FRICTION FACTORS AND REYNOLDS NUMBERS

Tube viscometer data can also be presented on a friction factor Reynolds number diagram provided that the rheology is known. A general form of the diagram is shown in Fig. 2.11.

Reynolds found that the transition between laminar and turbulent flow occurred at a lower bound value of 2320 of a dimensionless group called the Reynolds number. This is defined as

$$Re = \frac{\text{inertial forces}}{\text{viscous forces}} = \frac{\rho L^2 V^2}{\mu V L} = \frac{\rho V D}{\mu} \qquad (2.17)$$

for Newtonian fluids. For non-Newtonian fluids the Reynolds number contains a more complex version of the viscous term.

The Fanning friction factor is defined as

$$f = \frac{\tau_o}{\frac{1}{2} \rho V^2} \qquad (2.18)$$

where $1/2\ \rho\ V^2$ is the maximum dynamic pressure that may be obtained from a stream velocity V (Lazarus (1983)).

In the case of laminar flow of Newtonian fluids the shear stress is a function of the following variables

$$\tau_o = \text{fn}\ (\rho;\ V;\ D;\ \mu)$$

Dimensional analysis gives

$$\tau_o = \text{fn}\ \left(\frac{\rho V D}{\mu}\right) = \text{fn}\ (Re) \qquad (2.19)$$

Substituting the equations 2.5, 2.6 and 2.16 into equation 2.18 gives

$$f = \frac{16}{\frac{\rho V D}{\mu}} = \frac{16}{Re} \qquad (2.20)$$

In the flow of a solid-liquid mixture the shear stress is a function of the following variables

$$\tau_o = fn\ (V_m;\ D;\ C_{vt};\ \rho_m;\ \mu_w;\ d)$$

The rheology which is a function of C_{vt}, d and μ is contained intrinsically in this statement.

Dimensional analysis gives

$$f = \frac{\tau_o}{\frac{1}{2} \rho V^2} = fn\left(\left(\frac{\rho_m V_m D}{\mu_w}\right)\left(\frac{d}{D}\right)(C_{vt})\right) \qquad (2.21)$$

2.8 NEW METHOD OF DATA REDUCTION

A method of data reduction for tube viscometer data yielding the slurry's rheological parameters is needed.

2.8.1 Existing Rheological Characterization Procedure

The procedure was developed by Slatter (1986) to take the place of the Rabinowitch-Mooney derivation which was found to be unsuitable. The method is as follows

1. The raw data is plotted on a pseudo-shear diagram.
2. The yield-pseudoplastic equation 2.13 is the used to fit a curve to the yield stress and the coordinates of two judiciously selected points.

3. This is done three times with two different points each time.
4. The three curves are then plotted back onto the pseudo-shear diagram with the original data.
5. The best curve is then selected by eye and its rheological parameters are used to plot the rheogram.

2.8.2 New Rheological Characterization Procedure

A study revealed that the rheological parameters are highly sensitive to the selection of points. A program that fitted the curve with the minimum least-squares error described in Appendix C was then written and used. The new procedure is as follows

1. The raw data is plotted on a pseudo-shear diagram.
2. The yield-pseudoplastic equation 2.13 is the used to fit the best curve to the data.
3. The rheological parameters calculated in step 2 are then used to plot a rheogram.

2.9 ANOMALOUS BEHAVIOUR AT HIGH CONCENTRATIONS

At low concentrations it has been shown that the laminar section of the pseudo-shear diagram coincides for different tube diameters as shown in Fig. 2.9. Anomalous behaviour at high concentrations refers to the mechanism that causes the rheology to be dependent on tube diameter shown in Fig. 2.12. The behaviour is anomalous because rheology is a property of the fluid and should not be dependent on diameter.

This behaviour was first recorded by Green and Bingham in 1919 when they discovered that the "mobility" of certain paints is higher in smaller tubes.

Schofield and Scott Blair (1930) documented the anomalous behaviour at high concentrations naming it the sigma phenomenon. It was thought that a thin layer of liquid at the tube wall may cause a reduction in *in situ* concentration. Tests showed no such reduction occurred. Mechanical interaction between the solid particles and the wall does not allow their centers to move closer than one particle radius to the wall as shown in Fig. 2.13. Solid particles may be moved towards the pipe axis by Magnus forces which are the lift force caused by a velocity gradient across a sphere. It was noted that at high concentrations mechanical interaction was more likely than Magnus forces to create a thin liquid layer at the wall.

The presence of a thin layer of liquid at the wall will reduce the concentration and therefore the "viscosity" in close proximity to the wall. The geometry indicates that the increase in the concentration in the center of the tube is minimal provided the tube is large in comparison with the solid particles.

Bain and Bonnington (1970) document that the flow of fibrous paper pulp consists of a central plug with a flat velocity distribution and an annulus of clear water lubricating the plug. This is caused by the alignment of the fibres at the wall.

The most common method of analysing this anomalous behaviour is effective slip described in Section 2.10.

It is expected that the effect of mechanical interactions between the solid particles and the wall for polydisperse systems would be to change the particle size distribution in close proximity to the wall.

Several other researchers namely Barr (1931), Green (1949), Van Waser (1963), Thomas (1963), Cheng (1975) and Baker et al (1979) have also documented this phenomenon.

2.10 EFFECTIVE SLIP

2.10.1 Introduction

A prominent rheologist Mooney (1931) introduced the concept of effective slip with the following description:

> In addition to an unknown rheology effective slip may also be encountered. This effective slip may in reality be an abnormally large velocity gradient in a thin layer next to the wall. This is treated mathematically as a discontinuity (slip velocity) at the wall if the thickness of the layer is small in comparison with the viscometer dimensions.

Mooney (1931) developed the analysis technique described in Section 2.10.2.

Effective slip should not be confused with a slip velocity defined by Schramm (1981) as a lack of sufficient adherence between the wall and the fluid to transmit the applied shear stress.

Oldroyd (1948) documented that effective slip manifested itself as a tube diameter dependence on a pseudo-shear diagram. It was advised that at least two tube diameters be used for tube rheology. He maintained that a thin layer with anisotropic rheological properties caused the anomalous behaviour. The analysis technique described in Section 2.10.2 was presented.

Windhab and Gleissle (1984) used cone and plate, rotary and tube viscometers to determine the rheology of high concentration kaolin slurry. The analysis technique described in Section 2.10.2 was presented and used to correct the tube viscometer data for effective slip. It was shown that the modified tube viscometer rheogram corresponded well with the other two rheograms. A slip limit was defined as the shear stress above which slip starts to occur.

Wasp et al (1979) and Skelland (1967) both document that at high concentrations solid particles move away from the wall leaving a layer of liquid. This leads to a reduction in the "viscosity" of the mixture at the wall, the consequences of which are analogous to those if slip occurred. Skelland (1967) presented the analysis technique described in Section 2.10.2.

Several other researchers namely Thomas (1962), Stepanoff (1964), Kentchington (1974), Harris and Quader (1971) and Hanks and Hanks (1982) have also documented effective slip and the associated diameter dependence

2.10.2 Effective Slip Analysis Technique

This technique has been described in detail by Mooney (1931), Oldroyd (1948), Skelland (1967) and Windhab and Gleissle (1984).

The general equation for tube flow derived in appendix A is given by:

$$Q = \frac{\pi R^3}{\tau_o^3} \int_0^{\tau_o} \tau^2 \; f(\tau) \; d\tau \qquad (2.22)$$

Note that this equation is valid for any type of rheological model.

Mooney (1931) postulates an effective slip velocity at the wall given by

$$u_s = \beta \tau_o \qquad (2.23)$$

where β is the effective slip coefficient.

To account for the thin abnormal layer near the wall a modified boundary condition is used giving

$$Q = \pi u_s R^2 + \frac{\pi R^3}{\tau_o^3} \int_o^{\tau_o} \tau^2 \; f(\tau) \; d\tau \qquad (2.24)$$

this can be rewritten as

$$\frac{Q}{\pi R^3 \tau_o} = \frac{u_s}{R \tau_o} + \frac{1}{\tau_o^4} \int_o^{\tau_o} \tau^2 \; f(\tau) \; d\tau$$

$$= \frac{\beta}{R} + \frac{1}{\tau_o^4} \int_o^{\tau_o} \tau^2 \; f(\tau) \; d\tau \qquad (2.25)$$

Equation 2.25 has the form of a straight line where beta is equivalent to the slope of the graph of $Q/\pi R^3 \tau_o$ versus $1/R$ at a fixed τ_o. By calculating values of β over a range of τ_o values a graph of slip velocity $u_s = \tau_o \beta$ versus τ_o may be plotted.

The equation to correct the collected data is given by

$$Q \text{ corrected for slip} = Q \text{ measured} - \beta \tau_o \pi R^2 \qquad (2.26)$$

$$= \frac{1}{\tau_o^4} \int_o^{\tau_o} \tau^2 \; f(\tau) \; d\tau$$

Using this technique the slip function for a fluid tested in different diameters can be calculated. This is used to reduce the pseudo-shear diagram for each diameter onto one curve representing the fluid rheology.

2.11 DENSE-PHASE MODELS

Dense-phase flow occurs when the submerged weight of the solid particles is transferred to the pipe invert by particle-particle interactions. Typically this type of slurry has a small proportion of fine particles and a large proportion of coarse particles.

In dense-phase flow the wall friction of the sliding bed is the largest factor contributing to the overall head loss. A smaller component of the overall head loss is due to the flow of the vehicle through the interstitial spaces of the coarse solids.

Streat (1986) developed a equation to predict the hydraulic gradient of dense-phase flow given by

$$i_m = 2 \mu_s (S_s - S_w) C_{vt} + S_m i_w \qquad (2.27)$$

Streat (1986) showed that if the dense-phase flow condition existed equation 2.27 was applicable.

2.12 WALL EFFECT (Maude and Whitmore (1955))

Maude and Whitmore (1955) hypothesized that the a wall effect occurs due to the a redistribution of the solid particles at the wall. This is caused by the mechanical interaction between the solid particles and the wall as they enter the tube. This causes a reduction in the in situ concentration (C_{vt}). Tests were performed using polystyrene spheres (d_{so} = 965 μm) in a glass tube with a diameter D = 1.876 mm ($d_{so}/D = \pm 0.5$). The tests showed that the *in situ* volumetric concentration (C_{vt}) maybe as much as 75% lower than the delivered volumetric concentration (C_{vd}). It was proposed that the redistribution of particles away from the wall would have no effect on the rheological measurements.

It was hypothesized that the reduction in the *in situ* concentration and not effective slip was the cause of anomalous behaviour at high concentrations. This reduction will be more significant in a small tube therefore the rheology measured in a small tube will appear less viscous.

2.13 BOUNDARY-LAYER EFFECT

Reiner (1934) and Smoldyrev and Safonov (1979) both document that an inward radial migration of solid particles near the tube wall occurred increasing the concentration of the slurry in the core and leaving a thin boundary layer of lubricating fluid at the wall.

Assume that a layer of thickness δ and viscosity μ exists at the wall as shown in Fig. 2.14.

Assume that the velocity distribution in the boundary layer is linear. Using equation 2.3 the rate of shear at the wall for $\tau_o < \tau_y$ is given by

$$\left(-\frac{du}{dr}\right)_o = \frac{\tau_o}{\mu} + \frac{u_{core}}{\delta} \qquad (2.28)$$

and the flow is given by

$$Q = \pi (R - \delta)^2 u_{core} + \pi \frac{u_{core}}{2} (2 R \delta - \delta^2) \qquad (2.29)$$

assuming that δ is infinitesimally small in relation to R

$$Q = \pi R^2 u_{core} \qquad (2.30)$$

and substituting equations 2.6 and 2.28 into equation 2.30 gives

$$\frac{8V}{D} = \frac{8 \delta \tau_o}{\mu R} \qquad (2.31)$$

For values of $\tau_o < \tau_y$ the less viscous boundary layer will allow the core to move at a velocity u_{core}. This is shown on a pseudo-shear diagram in Fig. 2.15. The initial slope of the rheogram is given by

$$\epsilon = \frac{\tau_o}{\left(\frac{8V}{D}\right)} \qquad (2.32)$$

The thickness of the boundary layer can be solved for by combining eqn. 2.31 and eqn 2.32 giving

$$\delta = \frac{\mu R}{8 \epsilon} \tag{2.33}$$

The measured data is then corrected as follows

$$V_{actual} = V_{measured} - u_{core} \tag{2.34}$$

where

$$u_{core} = \frac{\tau_o \delta}{\mu} \tag{2.35}$$

Using this technique the thickness of the boundary layer can be determined from a pseudo-shear diagram. This is then used to correct the pseudo-shear diagram shown in Fig. 2.15 which can then be rheologically characterized.

2.14 MODIFIED FRICTION FACTORS

Shook (1985) hypothesized that the friction factor for a solid-liquid mixture was due partly to the liquid friction and partly to the hydrodynamic lubrication between solid particles and the tube wall. The final form of this equation derived from hydrodynamic lubrication theory is given as

$$f = (1 - C_v)\, f_\ell + K \lambda C_v \left(\frac{d}{D}\right)^{m-0.5} R_e^{-0.5} \tag{2.36}$$

$$\text{where } \lambda = \frac{1}{\left(\left(\frac{C_m}{C_v}\right)^{1/3} - 1\right)} \tag{2.37}$$

and K and m are dimensionless coefficients, and C_m is the maximum packing concentration.

On a log f versus log Re diagram the variation of K and m shift the curve parallel to its original position. The slope of this curve is fixed because the power of the Reynolds number is fixed at -0.5.

2.15 CONCLUSIONS

The theory of rheology has been presented. Several varying theories exist for the analysis of anomalous behaviour.

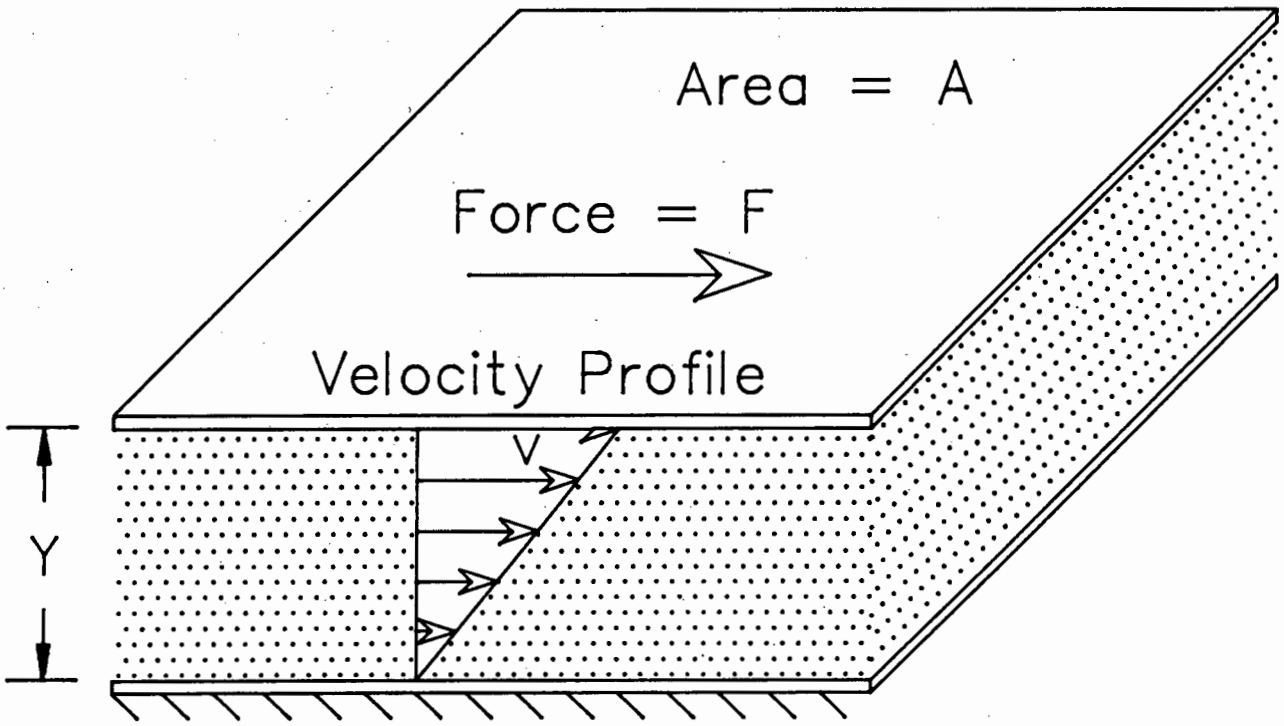

$$\text{Shear Stress } \tau = F / A$$

$$\text{Shear Rate } \frac{dv}{dy} = V / Y$$

Fig. 2.1 Shear stress and shear rate in a fluid sheared between parallel plates.

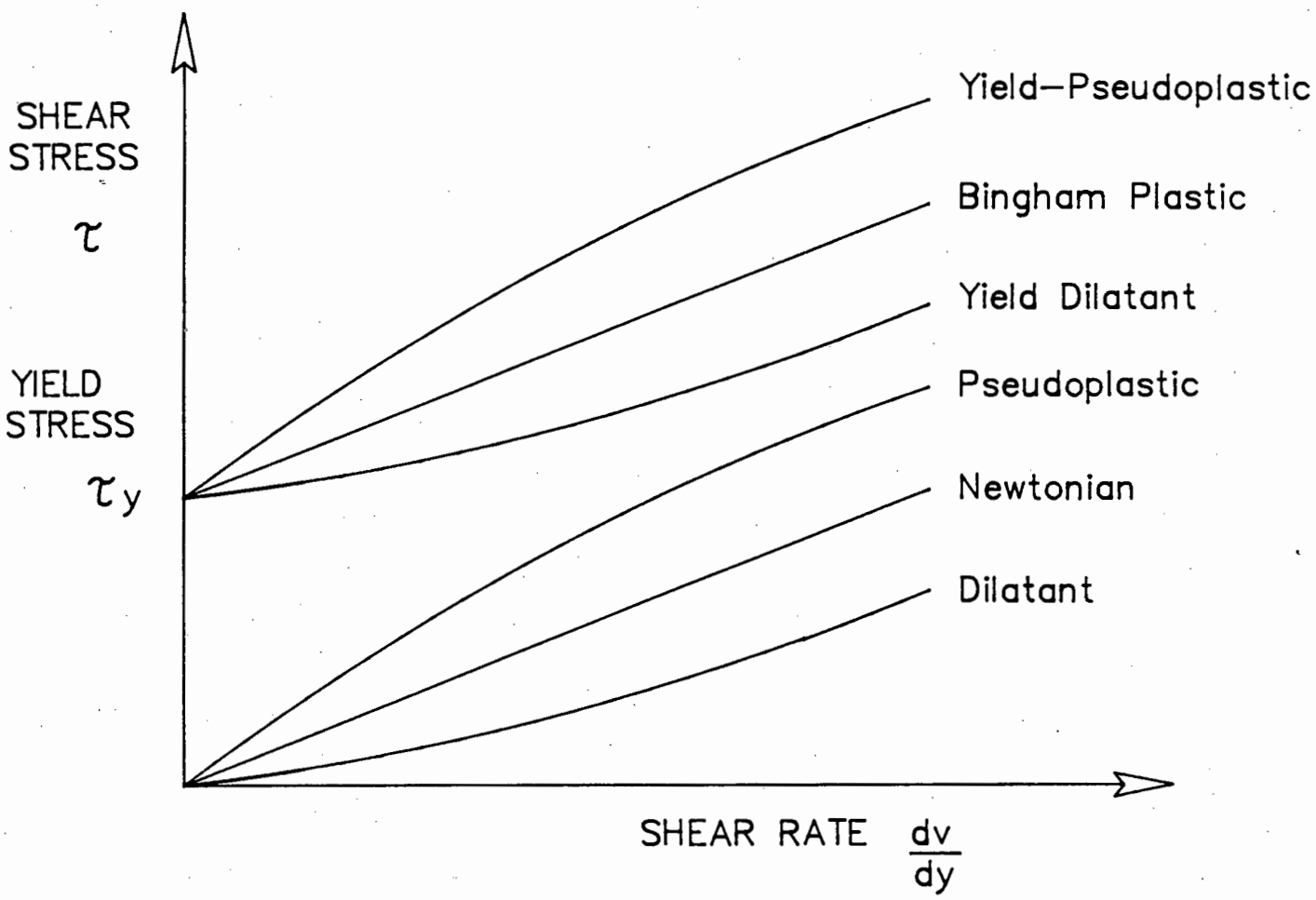

Fig. 2.2 Rheograms of various rheological models.

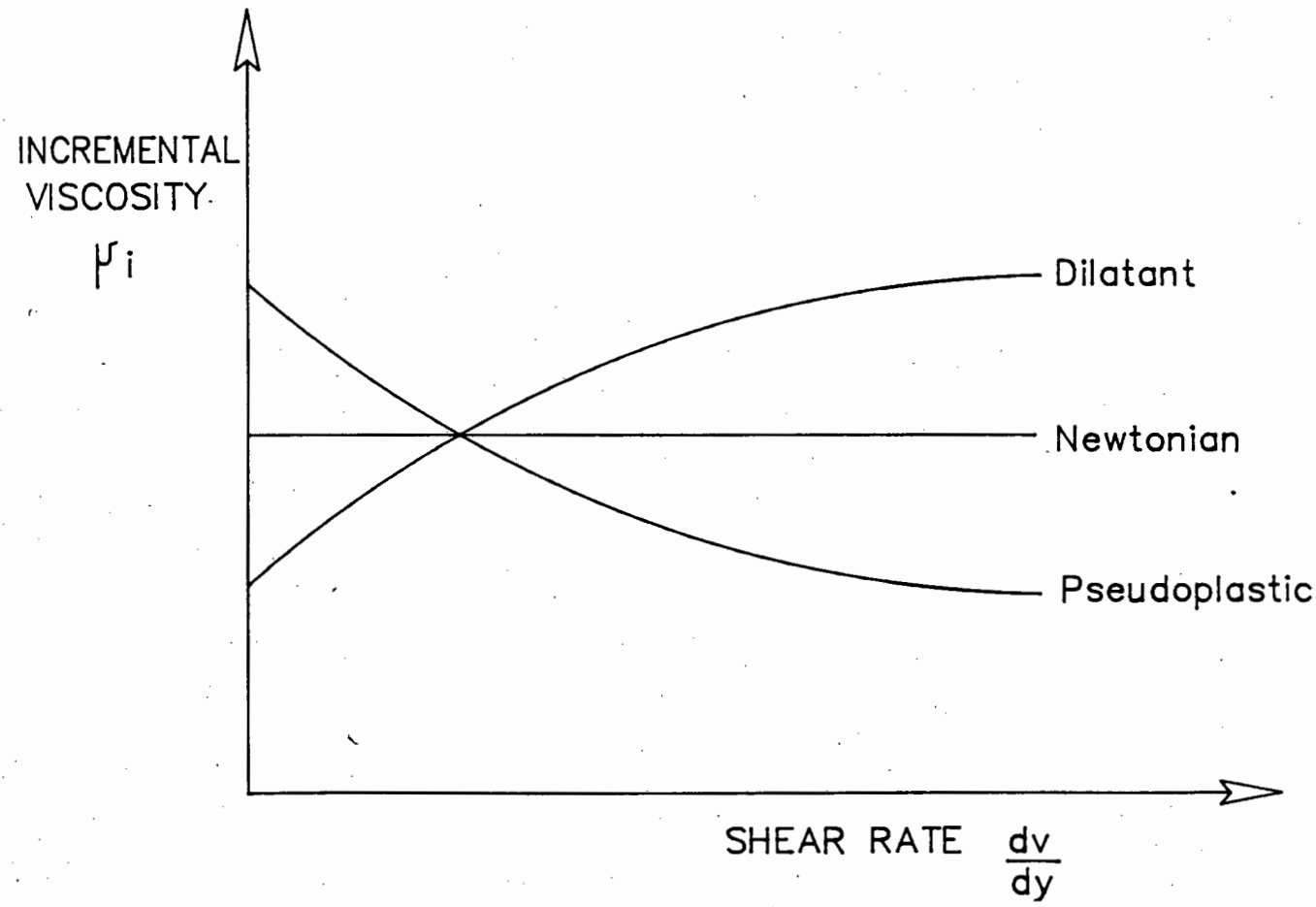

Fig. 2.3 A graph of incremental viscosity versus shear rate for various rheological models.

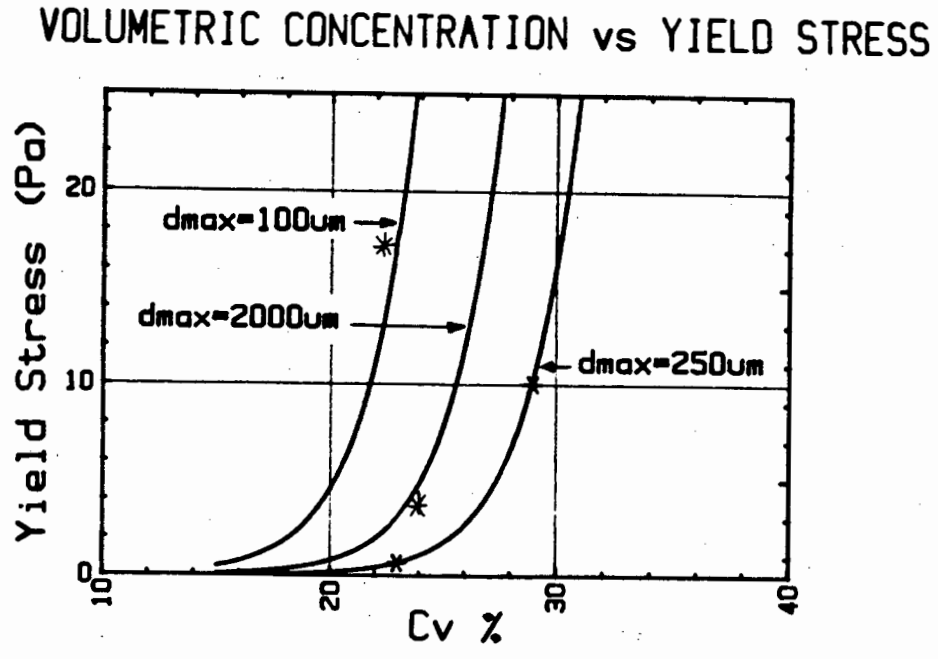

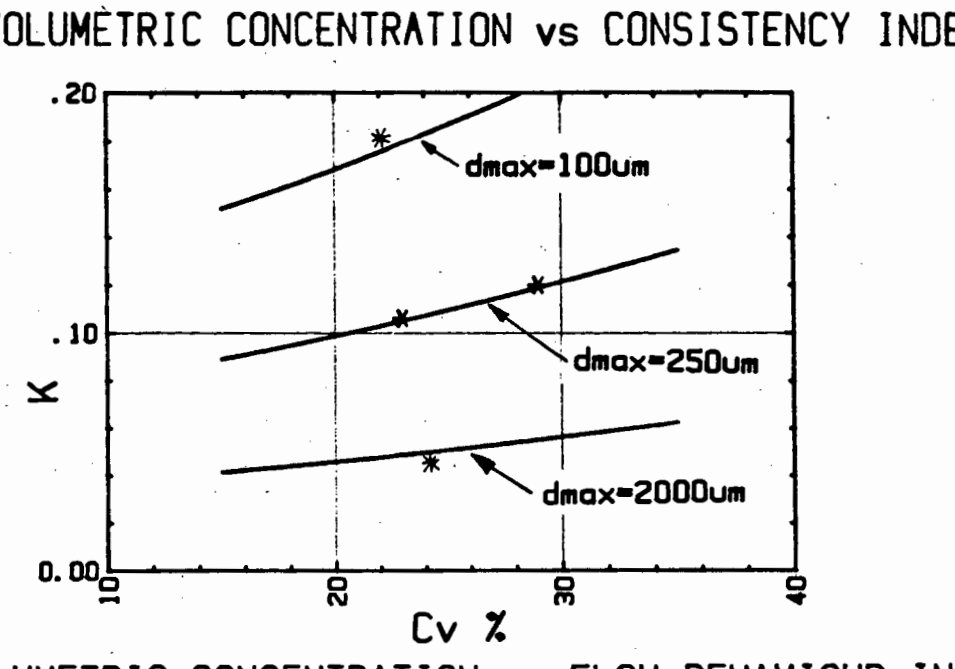

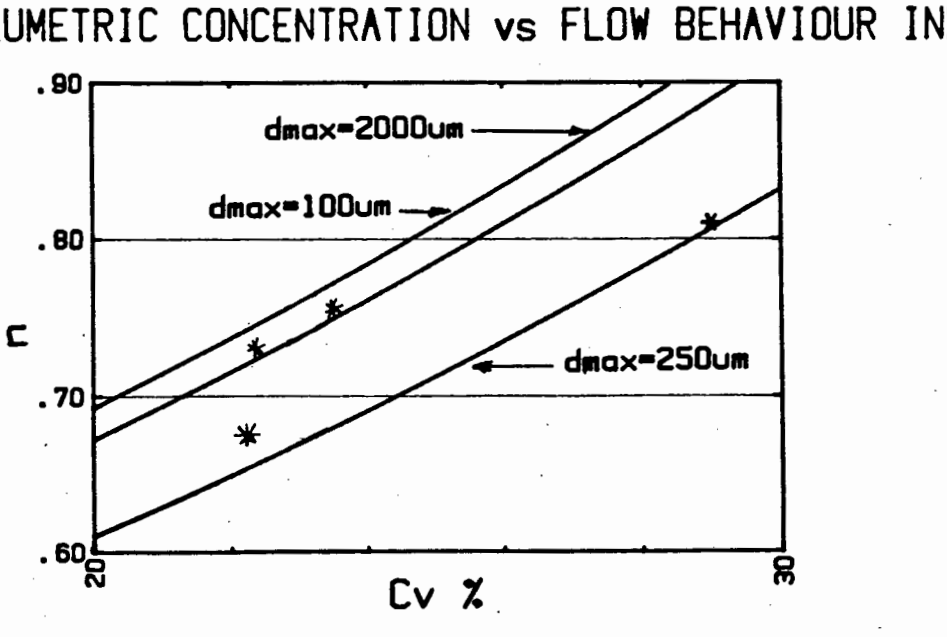

Fig. 2.4 A typical effect of concentration on rheology (Slatter (1986).

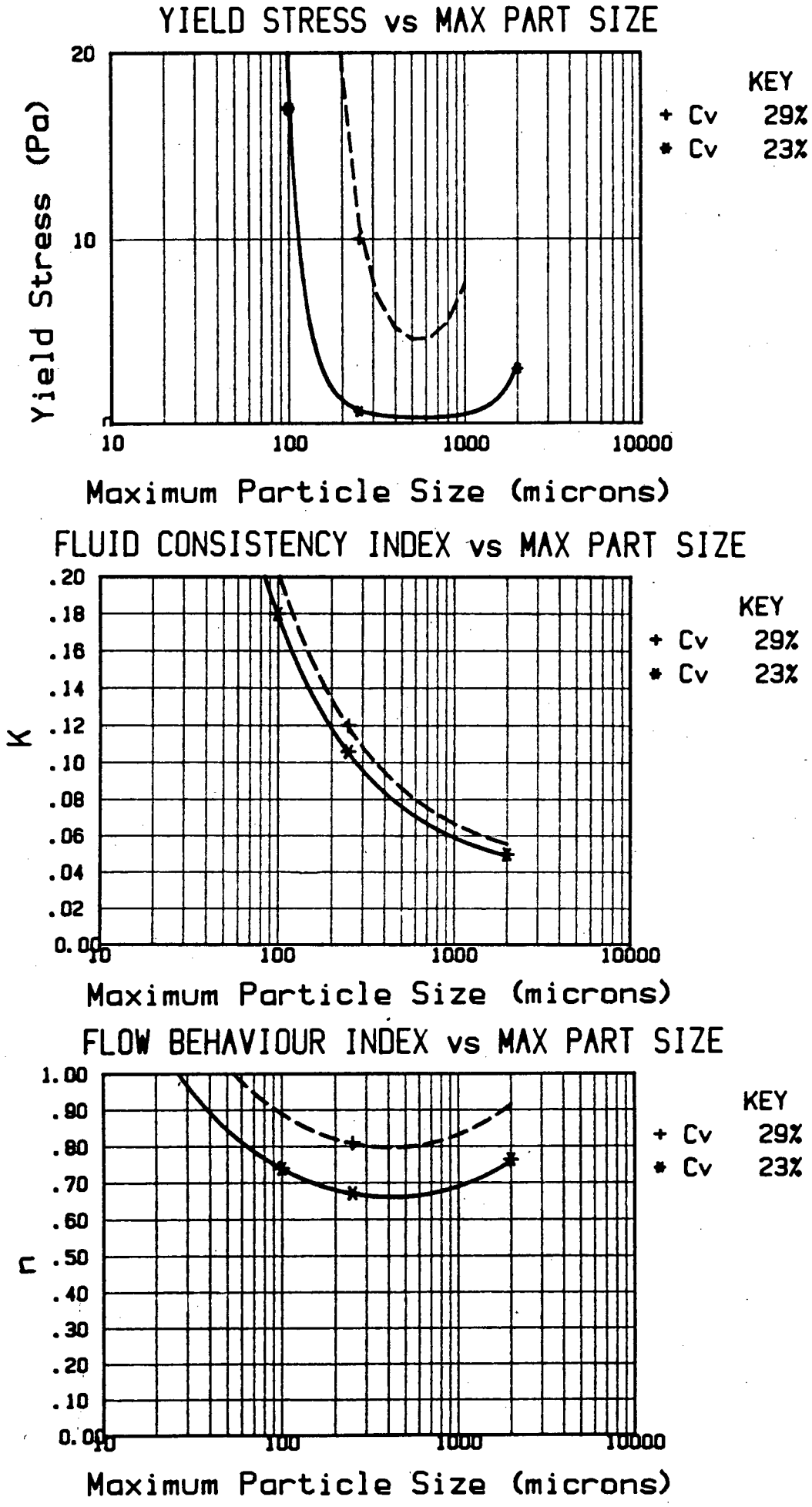

Fig. 2.5 A typical effect of maximum particle size on rheology (Slatter (1986).

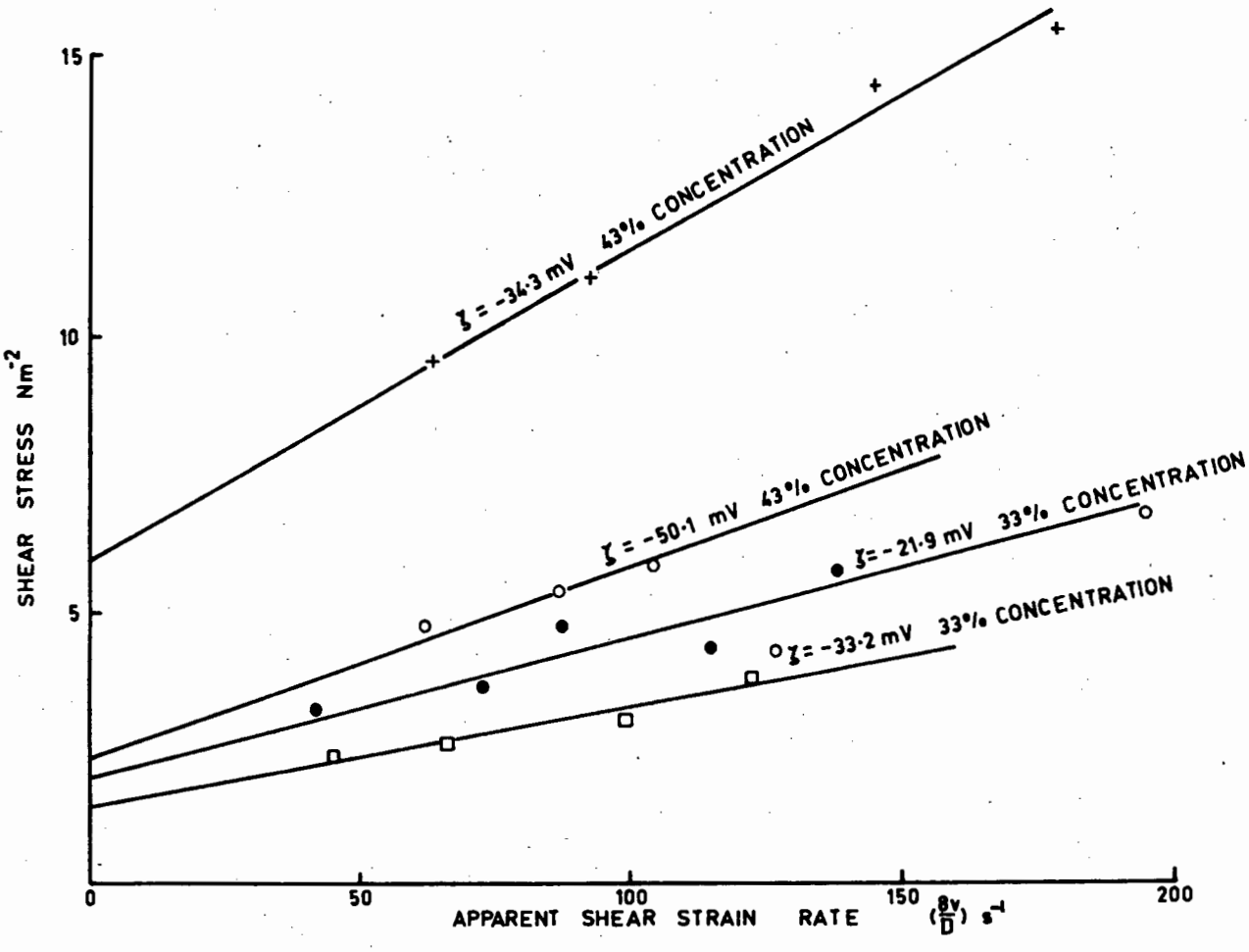

Fig. 2.6 The effect of zeta potential on rheology (Horsley and Reizes (1980)).

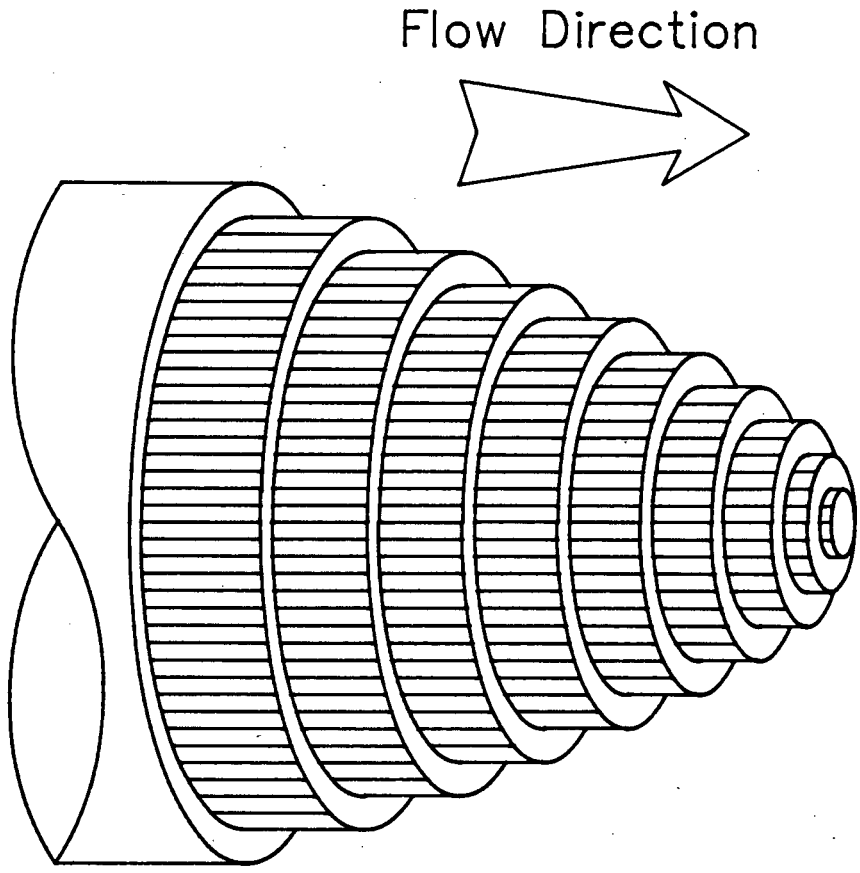

Fig. 2.7 Tube flow analogy.

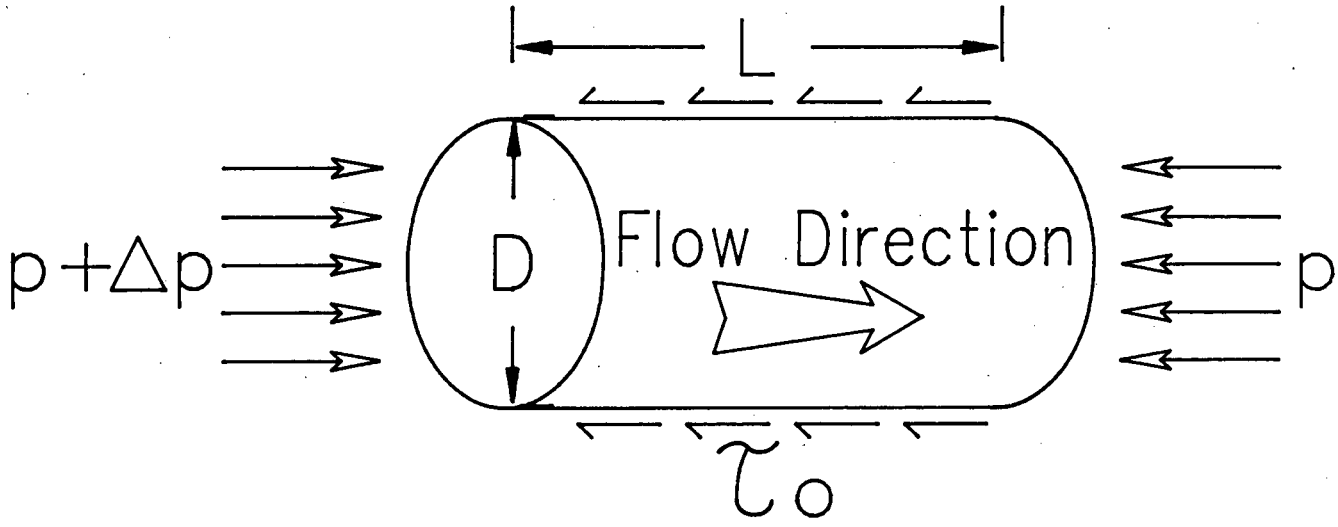

Force Balance:

$$\tau_o = \frac{D\Delta p}{4L}$$

Fig. 2.8 Derivation of the shear stress at the wall.

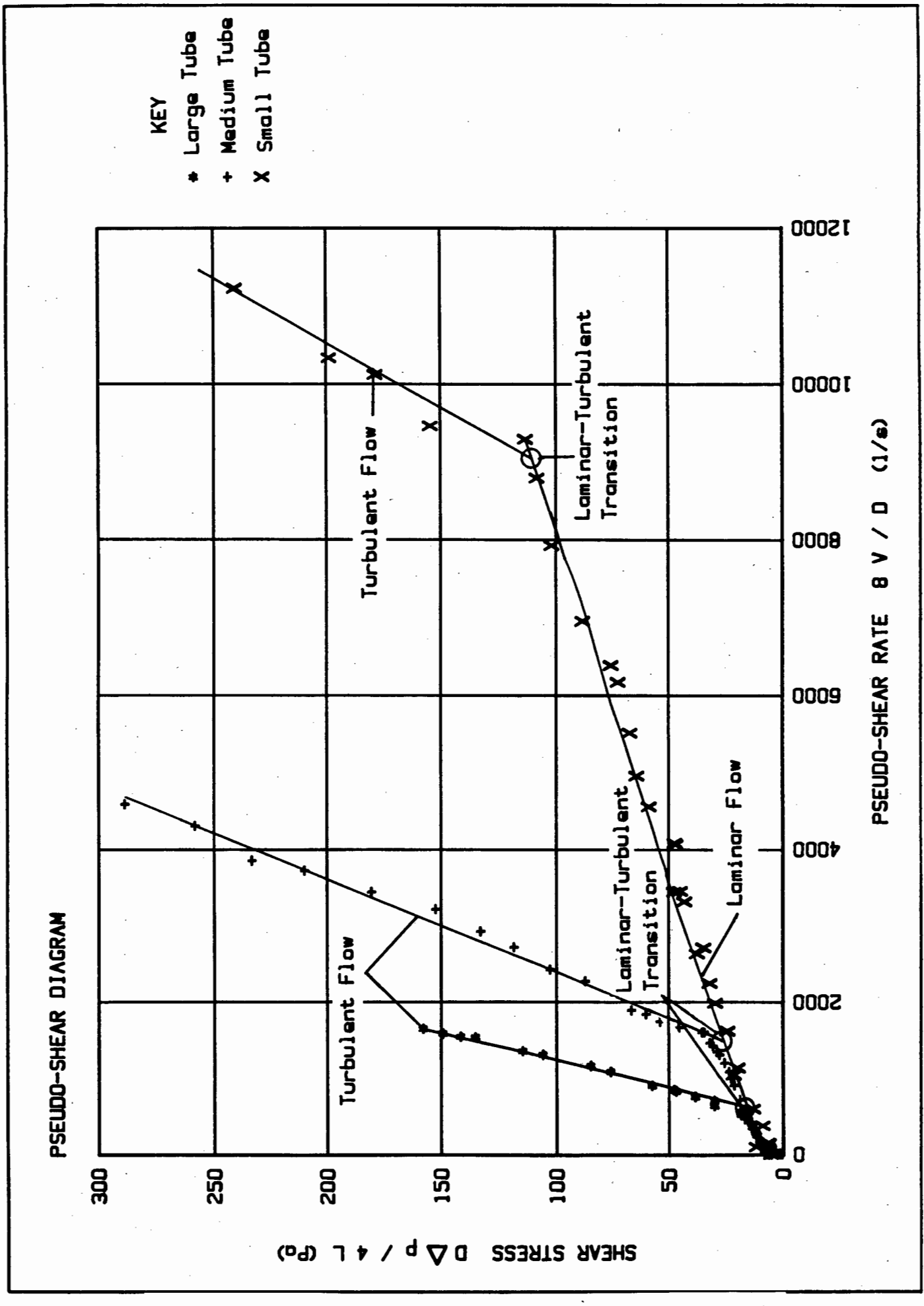

Fig. 2.9 A typical pseudo-shear diagram using three tube diameters.

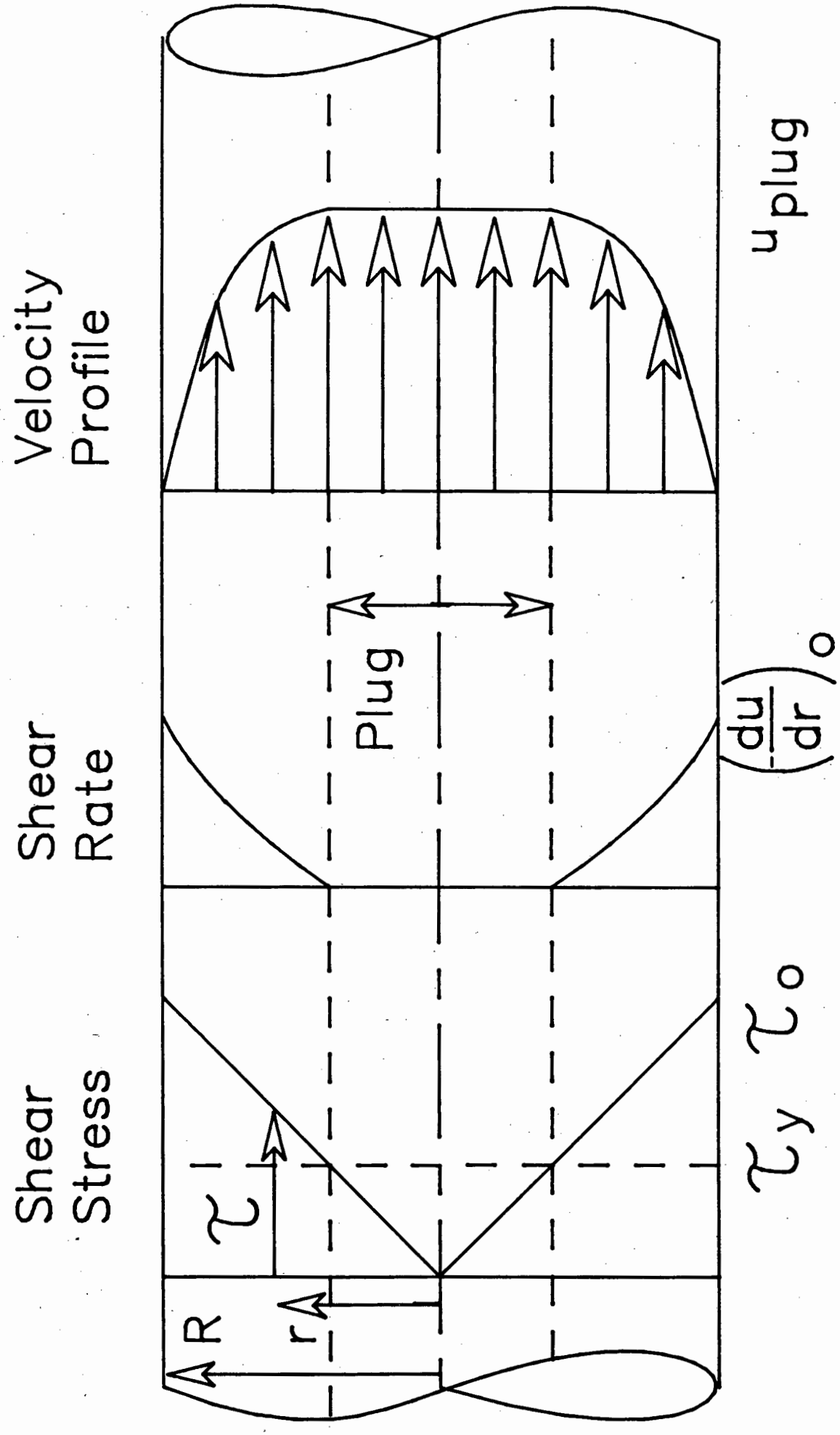

Fig. 2.10 Shear stress and shear rate distributions and the velocity profile for the flow of a yield-pseudoplastic fluid through a tube.

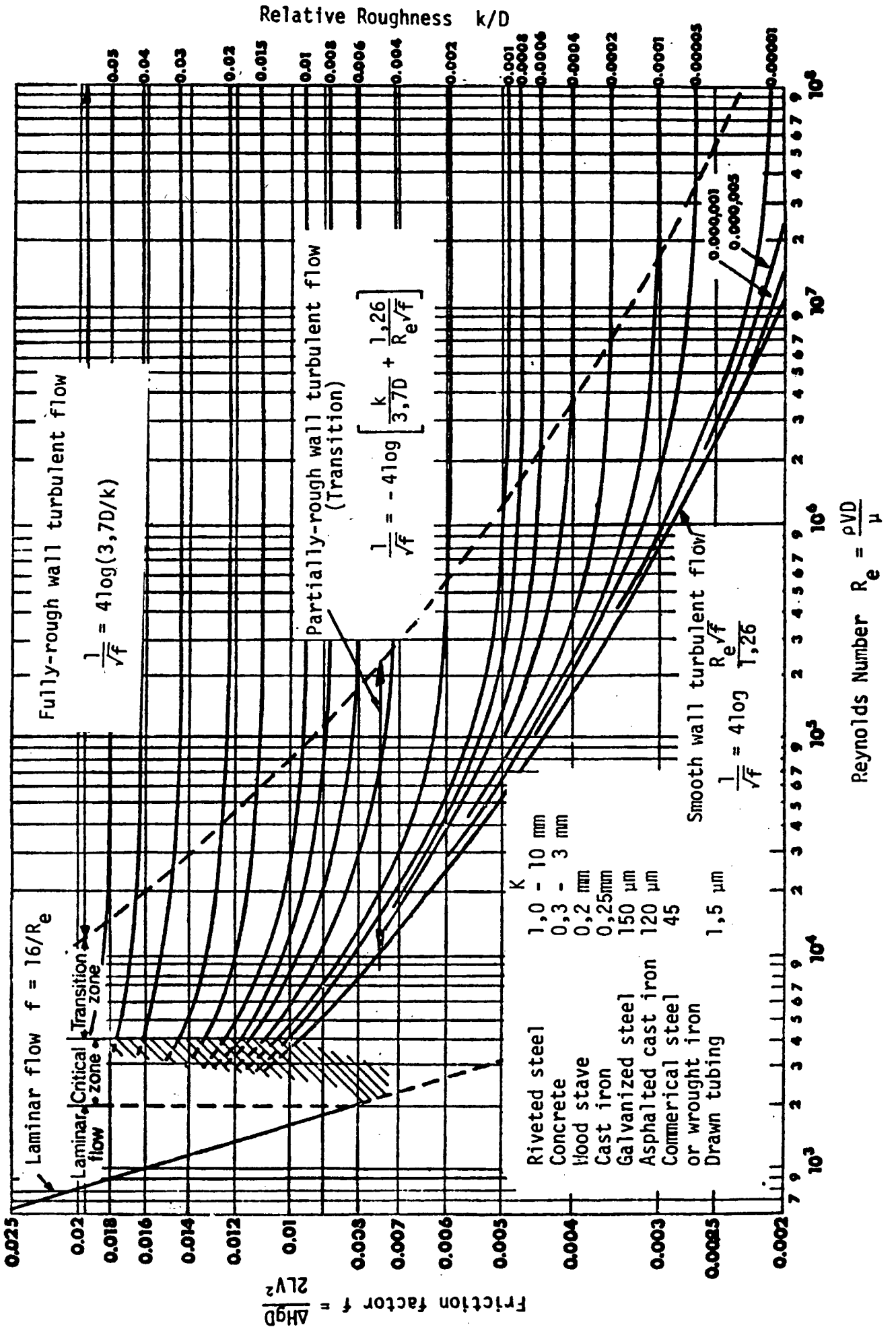

Fig. 2.11 Friction factor Reynolds number diagram.

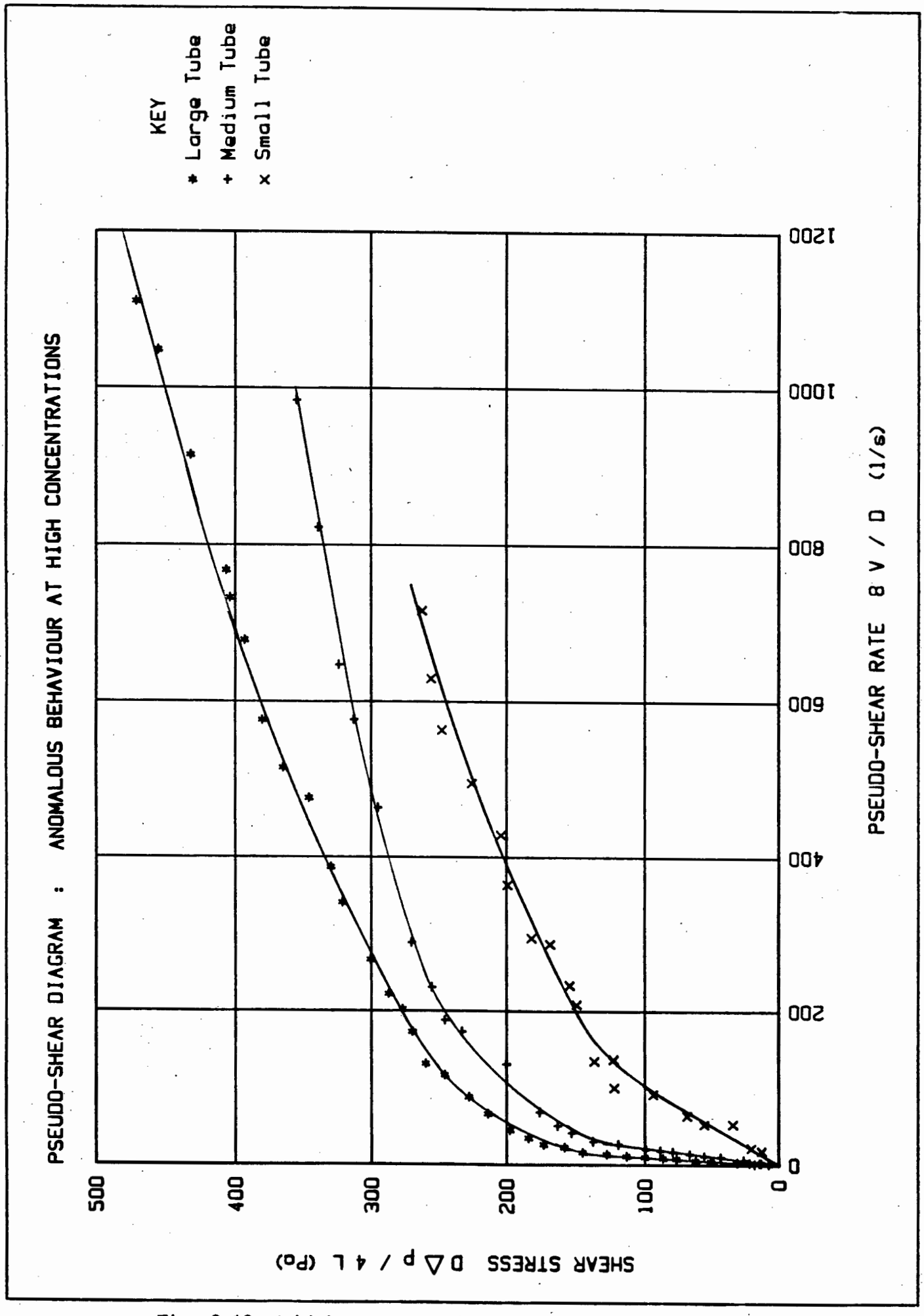

Fig. 2.12 A high concentration pseudo-shear diagram showing anomalous behaviour.

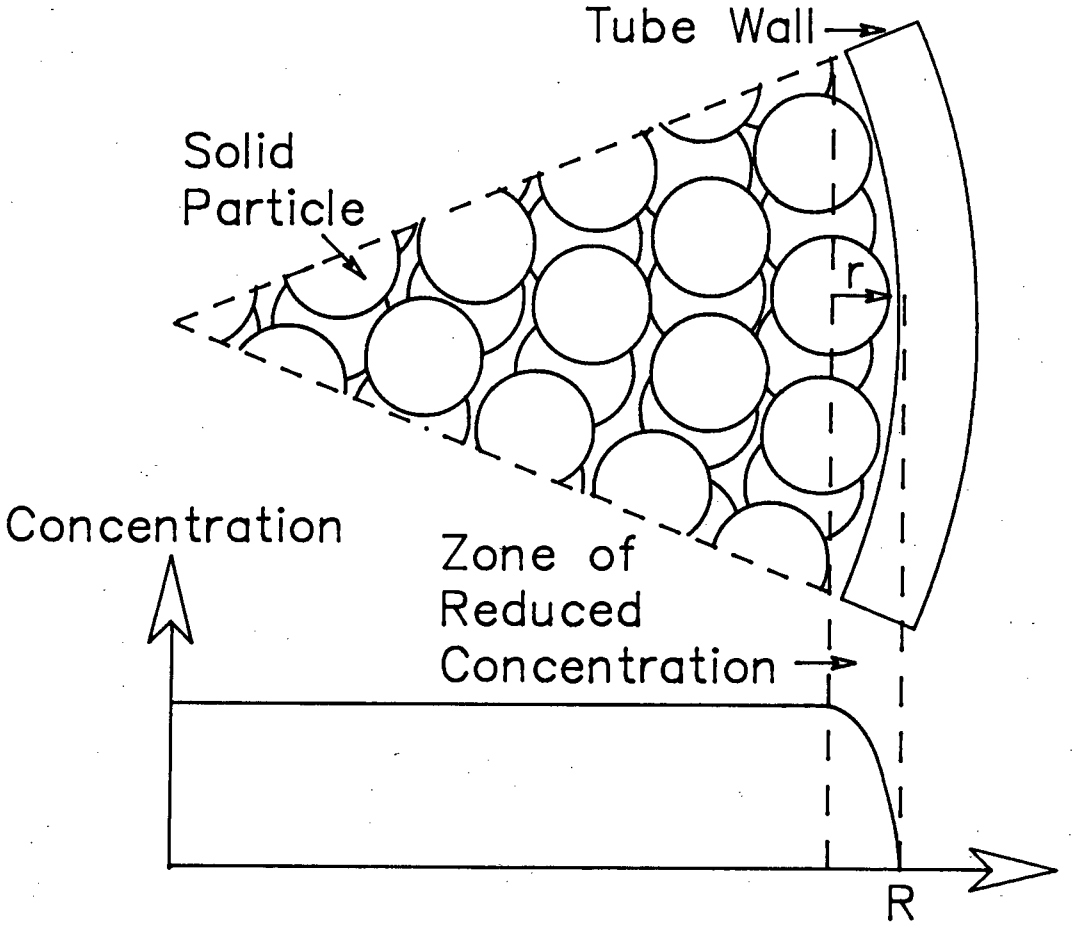

Fig. 2.13 Inward radial migration of solid particles and the associated reduction in concentration in the proximity of the tube wall.

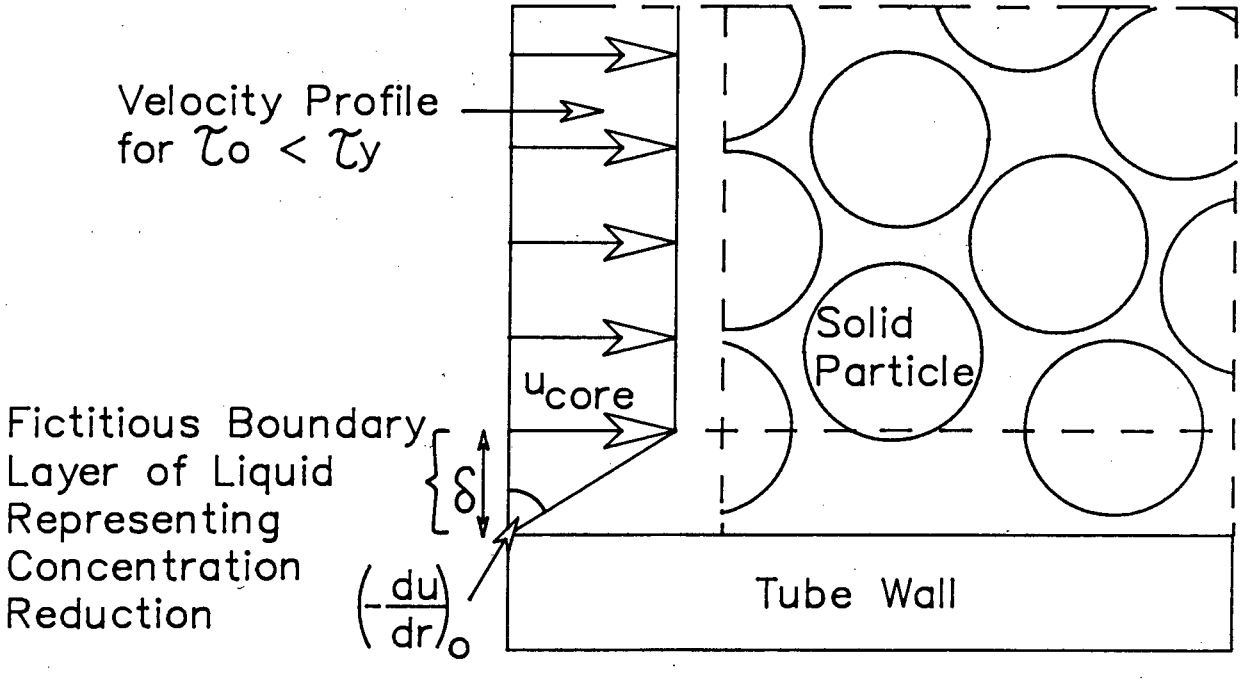

Fig. 2.14 Boundary-layer of liquid at the tube wall.

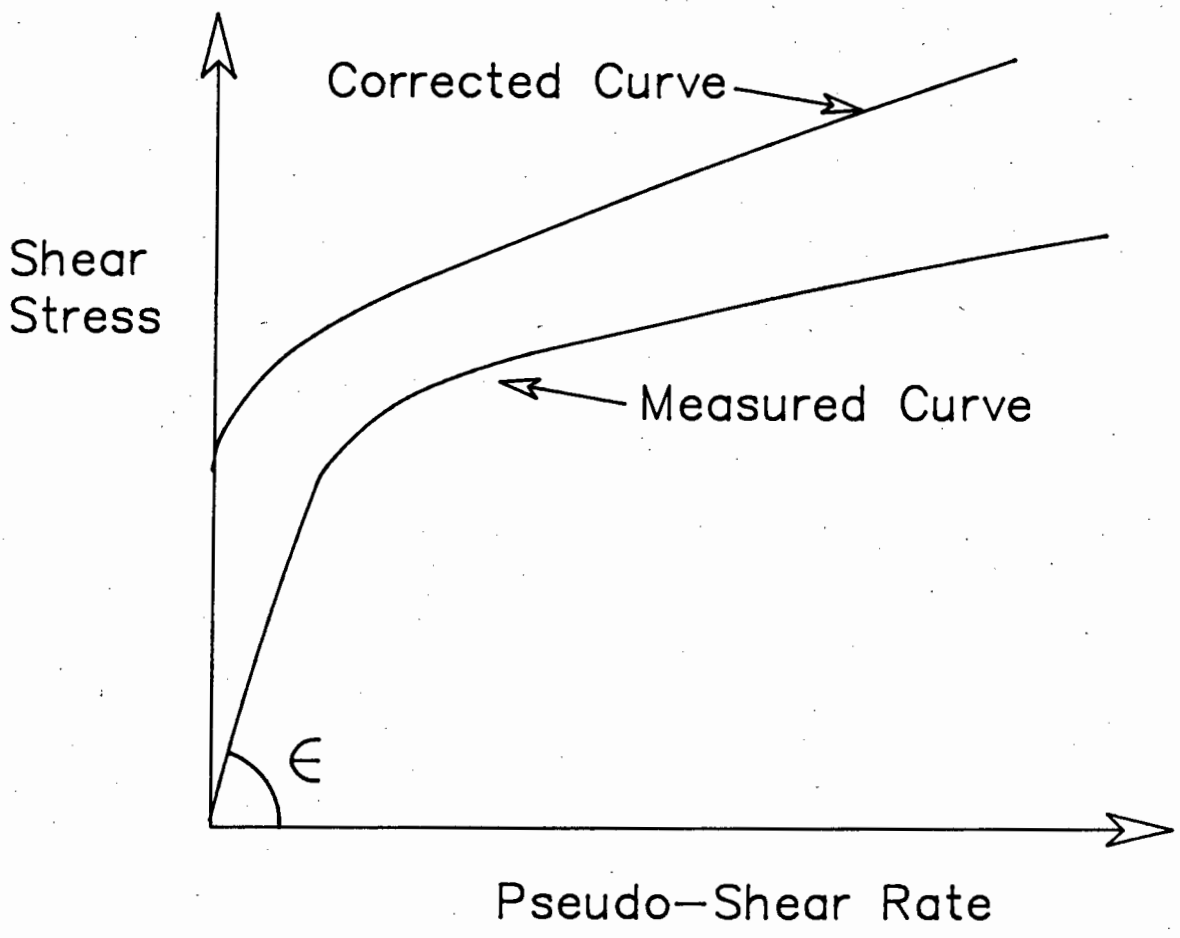

Fig. 2.15 Correction of a pseudo-shear diagram for the effect of a boundary-layer.

CHAPTER 3

RESEARCH APPARATUS

3.1 DESCRIPTION OF THE BALANCED BEAM TUBE VISCOMETER

The novel Balanced Beam Tube Viscometer, which has been developed at UCT is shown in Figs. 3.1 to 3.3. The viscometer consists of two pressure vessels (1 and 2) mounted on a steel joist and supported at two points L and F. A load cell is located at point L and point F is the system fulcrum (supported on a knife edge). Figs. 3.2 and 3.3 show that the pressure vessels are connected by three transparent PVC tubes with nominal internal diameters of 28 mm, 13 mm and 4 mm. Baker et al (1979) recommends that at least two tube diameters should be used to ensure time dependance and wall shear anomalies are detected. The precise internal diameters are 28.38 mm, 13.37 mm and 4.20 mm and were determined to this precision by weighing sections of the tubes with and without water. This precision is required since a rheogram point inherently contains the fourth power of the diameter.

Each tube has ball valves at either end and only one tube is used at a time. Each pressure vessel has a nest of stirrers (inside), driven by motors (on top) connected by shafts through seals in the vessel cover plate. Air pressure is supplied to either vessel using a 700 KPa air supply, a pressure regulator and a three-way valve. The necessary driving force to cause the slurry to flow between vessels is developed by pressurising one vessel and venting the other to the atmosphere. Velocities of up to 9 m/s can be achieved in this manner.

Pressure tappings shown in Fig. 3.4 are fitted to the tubes, allowing direct measurement of the differential pressure due to friction head loss. This avoids the inclusion of entrance and exit losses and hydraulic grade line curvature due to developing flow. The diameter of the pressure tapping holes is 2 mm. There are four pressure tappings in each tube, allowing the operator flexibility of

pressure range. The pressure tappings are water filled and connected to the differential pressure transducer (DP cell) via slurry isolation pods, and a flushing/bleeding facility shown in Fig. 3.4. The pressure tappings are located far enough from the tube entrances to ensure fully developed flow exists between them. The hydraulic effective length is thus equal to the physical distance between the tappings (L).

The primary output from the viscometer consists of successive voltage readings representing load cell input (power supply voltage), load cell output and DP cell output. These are converted into volumetric flow rate and differential pressure for analysis. The operator has the facility to manually reject the non-steady state flow readings taken during acceleration. These are distinguishable as non-linear differential pressures. A sample is taken for ancillary tests (S_s, S_m, pH and particle size distribution) described in Appendix C.

The viscometer is capable of rheologically characterising fluids such as water and slurries (Slatter 1986), (Lazarus and Sive 1985)). The viscometer is also a minature pipeline and is capable of collecting turbulent flow data and indicating the laminar-turbulent flow transition (Slatter 1986).

3.2 MEASUREMENT TECHNIQUES

A data acquisition system consisting of a computer, data acquisition unit and transducers is used to measure flow and differential pressure.

3.2.1 Flow Measurement

A load cell is located at point L (Fig. 3.1), to determine the slurry mass distribution between the two vessels. A typical flow measurement consists of 20 readings of mass and time shown in Fig. 3.5. A least squares linear regression on this data yields the mass flow rate (dm/dt). Q_m and V_m can be calculated from (dm/dt) as follows

$$Q_m = \frac{\frac{dm}{dt}}{\rho_m} \tag{3.1}$$

$$V_m = \frac{Q_m}{A} = \frac{\frac{dm}{dt}}{\rho_m A} \tag{3.2}$$

The load cell is designed and constructed at UCT and is shown in Fig. 3.6 and Fig. 3.7. It can operate in both tension and compression and has a resolution of 1N and a range of ± 1000N (accuracy of 0.1%).

Four strain gauges are bonded in the positions of maximum strain A, B, C, and D on the load cell (Fig. 3.7). The strain gauges are connected in a Wheatstone Bridge shown in Fig. 3.8.

A HP6214A power supply used for the input voltage and is set at a nominal 10V. The output voltage of the bridge varies linearly with applied force, and is proportional to the input voltage. The output voltage is divided by the input voltage, giving a non-dimensional load cell reading (v/v) which is independent of input voltage and temperature fluctuations.

A typical response characteristic is shown in Fig. 3.9.

3.2.2 Differential Pressure Measurement

A differental pressure transducer (DP cell) is used to measure the differential pressure between two pressure tappings on a selected tube. The differential pressure is calculated as the arithmetic mean of 20 differential pressure measurements shown in Fig. 3.5. The DP cell is located next to the viscometer fulchrum and is connected to the slurry isolation pods with flexible reinforced tubing with a low strain memory. Because the DP cell cannot read in reverse, high-low selectors shown in Figs. 3.10 and 3.11 are provided so that the pressure differential can be reversed.

A Gould PDH 3000 series differential pressure transducer is used and is shown in Fig. 3.12. The DP cell has an accuracy of 0.25% and a maximum range of 200 KPa and is connected to a 24V power supply as shown in Fig. 3.13. The output is 4-20 mA in the supply leads which is linear with pressure differential across the two halves of the cell. The current output is converted to a 40-200 mV voltage output by a 10 Ω series resistor.

The range and the span are adjustable. A typical response characteristic is shown in Fig. 3.14.

3.2.3 Computer Hardware

The computer hardware is used for high speed data acquisition and processing.

The computer hardware consists of a HP-87C computer, HP82901M double flexible disc drive, HP82905A printer, HP7470A plotter and a HP3421A data acquisition unit (analogue to digital converter) shown in Fig. 3.15. These are located opposite the fulchrum of the viscometer in a cooled computer box.

The HP-87C is a 128k RAM basic computer with I/O and Advanced Programming ROM's and an interface loop (IL) peripheral.

The data acquisition unit (DAU) equipped with a 10 channel multiplexer is used as a software controlled digital voltmeter to read various analogue input channels.

The computer is connected to the data acquisition unit by an interface loop and to the other three peripheral devices by an interface bus as shown in Fig. 3.16.

To facilitate operation the following device codes are listed:

Interface	Peripheral Device	Code
Interface Loop :	Data Acquisition Unit	901
Interface Bus :	Disc Drive 0	700
	Disc Drive 1	701
	Printer	701
	Plotter	705

3.2.4 Experimental Error

Fluctuations of the analogue outputs of the transducers occur in any measurement system. The discrete readings of the data acquisition unit may be taken at an extreme analogue value. This can be accounted for using statistical techniques.

In general if a measured parameter is given by

$$X = fn\ (\ a,\ b,\ c,\ \ldots\ldots\ ,n\ ) \tag{3.3}$$

then the error in X due to an error in n is given by (Brinkworth (1968))

$$\frac{(\Delta X)_n}{X} = \left(\frac{\partial X}{\partial n}\ \frac{\Delta n}{X}\right)$$

$$= \left(\frac{\partial X}{\partial n}\ \frac{n}{X}\ \frac{\Delta n}{n}\right)$$

and the maximum error is given by

$$\left(\frac{(\Delta X)_n}{X}\right) = \sum \sqrt{\left(\frac{\partial X}{\partial n}\ \frac{n}{X}\ \frac{\Delta n}{n}\right)^2} \tag{3.5}$$

Error in Internal Tube Diameter Measurement

The internal tube diameter is determined by measuring the mass of water that fills a section of tube of length L using the equation given by

$$D = \sqrt{\frac{4\ m_w}{\rho_w\ \pi\ L}} \tag{3.6}$$

The maximum error is given by

$$\left(\frac{\Delta D}{D}\right) = \sqrt{\left(\frac{1}{2}\sqrt{\frac{4}{\rho_w\ m_w\ \pi\ L}}\ \frac{m_w}{D}\ \frac{\Delta m_w}{m_w}\right)^2 + \left(-\frac{1}{2}\sqrt{\frac{4\ m_w}{\rho_w\ \pi\ L^2}}\ \frac{L}{D}\ \frac{\Delta L}{L}\right)^2} \tag{3.7}$$

and presented in Table 3.1.

Table 3.1 Maximum error in diameter.

Nominal Diameter (mm)	L(m) ±0,001	m_w (kg) ±0,001	Actual Diameter (mm)	Error in Diameter (mm)	Percentage Error (%)
28	5	3,163	28.38	± 0.007	0.0026
13	5	0,702	13.37	± 0.0022	0.0034
4	5	0,0693	4.20	± 0.0034	0.0815

Error in Velocity Measurement

Velocities between 0.1 and 10 m/s are measured using the equation

$$V_m = \frac{4\,Q_m}{\pi\,D^2}$$

$$= \frac{4\,M_m}{\rho_m\,\pi\,D^2}$$

$$= \frac{2\,F}{t\,\rho_m\,\pi\,D^2\,g} \qquad (3.8)$$

The mass distribution between the two vessels is measured using the load cell. The load cell is calibrated using the equation given by

$$F = m\,(v/v) + c \qquad (3.9)$$

The slope of the calibration curve is determined by a least squares linear regression shown in Fig. 3.9. The slope is given by

$$m = \frac{F}{v/v} \qquad (3.10)$$

and the maximum error may be approximated as

$$\left(\frac{\Delta m}{m}\right) = \sqrt{\left(-\frac{F}{(v/v)^2}\,\frac{v/v}{m}\,\frac{\Delta v/v}{v/v}\right)^2} + \sqrt{\left(\frac{1}{v/v}\,\frac{F}{m}\,\frac{\Delta F}{F}\right)^2} \qquad (3.11)$$

The largest error in the measurement of the dimensionless load cell output is estimated at 0,5%. The largest error in the measurement of applied force $\Delta F/F$ is 0,06%. Therefore the maximum error in slope $\Delta m/m$ is 0,56%.

The maximum error in F is given by

$$\left(\frac{\Delta F}{F}\right) = \sqrt{\left(\frac{v}{v}\,\frac{m}{F}\,\frac{\Delta m}{m}\right)^2} + \sqrt{\left(m\,\frac{v/v}{F}\,\frac{\Delta v/v}{v/v}\right)^2} \qquad (3.12)$$

which is calculated to be 1,06%.

The maximum error in V_m calculated using the slope of the graph of mass versus time is approximated by

$$\begin{aligned}\left(\frac{\Delta V_m}{V_m}\right) = &\sqrt{\left(\frac{2}{t\,\rho_m\,\pi\,D^2\,g}\,\frac{F}{V_m}\,\frac{\Delta F}{F}\right)^2} \\ &+ \sqrt{\left(\frac{-2F}{t^2\,\rho_m\,\pi\,D^2\,g}\,\frac{t}{V_m}\,\frac{\Delta t}{t}\right)^2} \\ &+ \sqrt{\left(\frac{-4F}{t\,\rho_m\,\pi\,D^3\,g}\,\frac{D}{V_m}\,\frac{\Delta D}{D}\right)^2} \\ &+ \sqrt{\left(\frac{-2F}{t\,\rho_m^2\,\pi\,D^2\,g}\,\frac{\rho_m}{V_m}\,\frac{\Delta\rho_m}{\rho_m}\right)^2}\end{aligned} \qquad (3.13)$$

The largest error in the measurement of force $\Delta F/F$ is 1,06%. The largest error in the measurement of time $\Delta t/t$ is 0,1%. The largest error in the measurement of mixture density $\Delta\rho_m/\rho_m$ is 0,3%. The maximum errors in velocity are presented in Table 3.2.

Table 3.2 Maximum error in velocity.

Nominal Diameter (mm)	Percentage Error in Velocity (%)
28	1.46
13	1.47
4	1.62

Error in Shear Stress Measurement

Shear stresses between 1 and 600 (Pa) are measured. This involves the measurement of differential pressure between 1 and 250 (kPa). The calibration curve for the DP cell is given by

$$p = m\,v + C \tag{3.14}$$

The errors in the measurement of differential pressure are calculated in the same way as for the load cell. The accuracy of the DP cell is 0,25%. The largest error in the measurement of applied pressure is 0,1%. The maximum error in the calibration slope $\Delta m/m$ is calculated to be 0,35%. The maximum error in the measurement of pressure is calculated to be 0,6%.

The equation used to calculate the shear stress at the wall is given by

$$\tau_o = \frac{D\,\Delta\,p}{4\,L} \tag{3.15}$$

The maximum error in τ_o is given by

$$\left(\frac{\Delta\tau_o}{\tau_o}\right) = \sqrt{\left(\frac{\Delta p}{4L}\,\frac{D}{\tau_o}\,\frac{\Delta D}{D}\right)^2} + \sqrt{\left(\frac{D}{4L}\,\frac{\Delta p}{\tau_o}\,\frac{\Delta\Delta p}{\Delta p}\right)^2} + \sqrt{\left(\frac{-D\Delta p}{4L^2}\,\frac{L}{\tau_o}\,\frac{\Delta L}{L}\right)^2} \tag{3.16}$$

The largest error in the measurement of the length between pressure tappings $\Delta L/L$ is 0.2%. The maximum errors in shear stress are presented in Table 3.3.

Table 3.3 Maximum error in shear stress

Nominal Diameter (mm)	Percentage Error in Shear Stress (Pa)
28	0.803
13	0.803
4	0.882

The maximum error in the above experimental measurements is within acceptable limits.

3.3 OPERATING PROCEDURE

The operating program called "VISCO" must be loaded from the programs disc in drive 0 onto the HP-87 computer and run to start up the system. The main menu will then display the available software functions. The menu tree is shown in Fig. 3.17 to facilitate operation. The following definitions shall apply:

A READING consists of one transducer output.

A RUN consists of 20 consecutive BBTV transducer outputs (load cell, DP cell and time) representing one pseudo-shear diagram point.

A TEST consists of up to 100 readings from each tube representing one pseudo-shear diagram as shown in Fig. 3.19 and 3.20. This may be rheologically characterised to yield the values for τ_y, K and n.

The load cell is a sensitive device and should be replaced with a blank when not in use. To install the load cell the BBTV must have equal amounts of slurry in each vessel so that it balances on its knife edge.

Details of the functions are given below.

3.3.1 Log On

This function sets the date on the computer clock which is used at several stages in the program. The computer clock is zeroed each time the system is switched on, and if it is not set a date of "00/00/00" will used.

3.3.2 Readchannel

This function reads one of the three input channels namely: load cell input voltage and load cell output voltage and DP cell output voltage. It is used to check that the transducers are operating properly.

3.3.3 Calibration

The CALIBRATE LOAD CELL and CALIBRATE DP CELL options are used to calibrate the load cell and the DP cell respectively. The LOAD CELL CALIB PLOT and DP CELL CALIB PLOT options are used to plot the respective calibration graphs. After the calibration the data is stored on the data disc in drive 1, so that the calibration constants can be recalled at any time. A calibration of each transducer must be done before a test.

The following steps are executed for load cell calibration:

1. Standard weights are placed above the centroids of each vessel (ie. on top of the stirrer motors). A downward force on the LH vessel is considered positive and a downward force on the RH vessel is considered negative.

2. The slurry levels in the vessels must be approximately the same.

3. Select the CALIBRATION function and the CALIBRATE LOAD CELL option to start the calibration. The computer will prompt the operator for the force value in newtons after which it takes the average of ten load cell input and output readings.

4. Readings are taken for a range of approximately ten different load values, noting that a zero load is valid and desirable for calibration purposes.

5. At the end the computer will do a least squares linear regression on the data which yields the calibration constants

   m = gradient of the calibration line
   c = ordinate intercept of the calibration line

   from the equation

   (Applied load) = m x (Transducer output) + c

A typical load cell calibration output is shown in Fig. 3.9.

The following steps are followed for DP cell calibration:

1. Connect the pods to the mercury/water manometer as shown in Fig. 3.18.

2. Open the manometer relief valve.

3. Bleed the DP cell system and the manometer of all air and solids by flushing supply water via the bleed valve through the various components.

4. Close the manometer relief valve.

5. Using the manometer relief valve and a low mains flow, a pressure differential is set up. The pressure differential can be reduced by releasing some water with the manometer relief valve. The high-low selectors must be set to run from LHS to RHS.

6. Select the CALIBRATION function and the CALIBRATE DP CELL option to start the calibration. The computer will prompt the operator for the levels of the mercury in mm, after which it will take the average of ten DP cell output readings.

7. This is repeated for a range of approximately ten different differential pressures, noting that a zero pressure differential is valid and desirable for calibration purposes.

8. At the end the computer will do a least squares linear regression on the data points which will yield calibration constants m and c.

A typical DP cell calibration output is shown in Fig. 3.14.

3.3.4 Visco Run

During a test the data is continously stored in two workfiles on the programs disc called "WORKFILE" and "NOPTS". There is also an option of viewing the partially complete pseudo-shear diagram after each run. The results shown in Fig. 3.19 will be printed out if the printer is ON LINE.

The test data is given a name of the form AABXXDDMM where:

AA is an identity code
B is the tube size (L, M or S)
XX is the volumetric concentration as a percent
DDMM is the date.

The following steps are executed to run a test:

1. The power supplies located in the computer hut must be turned on and allowed to warm up (about 10 minutes).

2. Half fill each vessel through the filling ports, and replace port lids and insert the load cell.

3. Pump the slurry from one vessel to the other several times to mix it thoroughly by using steps 8 to 15 without using the computer. The operator should begin to get a qualitative "feel" for the slurry rheology.

4. A one litre sample should be taken for record purposes and ancillary tests (S_m, S_s, pH and particle size distribution) described in Appendix C, using a sample valve.

5. Flush any solids from the pods and bleed the pressure system of air. Connect the pods to the required tappings and open respective tapping valves.

6. Insert the load cell. Ensure calibrations of the transducers are available. Select the VISCORUN function to start the test.

7. The computer will prompt the user for several parameters and ancillary test results namely: tube diameter, tapping width, calibration codes, pH, temperature, solids relative density (S_s), mixture relative density (S_m) and the identity code AA.

8. Close the vent valve on the full vessel side and close the tube valve on that side.

9. Open the vent valve and open the tube valve on the empty vessel side.

10. Select the correct direction on the high-low selectors (see Figs. 3.10 amd 3.11).

11. Set the pressure regulator to the desired pressure.

12. Switch the 3-way valve so that the full vessel is pressurized (see Fig. 3.3).

13. Open the tube valve on the pressurized side.

14. Press the appropriate time key to specify the time interval between each of the 20 readings and to start the data acquisition.

15. At the end of the run close the tube valve slowly to prevent water hammer.

16. The accumulated data will be displayed on two graphs, the upper one a graph of mass versus time and the lower one a graph of pressure versus time similar to Fig. 3.5. The operator is prompted to select the time span over which the results are relevant. Key in 0,0 to discard the data.

17. Steps 8 to 16 are repeated over a range of pressures.

18. The operator will be prompted to store the data which transfers the test data from the workfile to the data disk.

The time key selection should be chosen so that at least 15 of the 20 readings are evenly spaced over the flow time.

The stirrer motors should be used when the slurry particles have a high settling velocity.

3.3.5 Store Data

If a fatal error should occur during the test the accumulated data can be recovered by using the STORE DATA function.

3.3.6 Utilities

This function provides access to several useful programs on the programs disc. The programs and their functions are listed below:

Program name	Key label and Description
GRAPH 1	PLOT ONE P-S GRAPH - plots the results from one test in the form of a pseudo-shear diagram shown in Fig. 3.20.
GRAPH 2	PLOT MANY P-S GRAPHS - plots numerous test results on one pseudo-shear diagram.
LS SOLVE	FIT YPP CURVE - fits a yield pseudo-plastic curve a set of test data.
FITDRAWU	PLOT YPP CURVE & DATA - plots data from several files and the fitted YPP curve.
FILE PRINT	FILE PRINT - prints the contents of any data file on to the screen or the printer.

3.3.7 Operating Notes

- The A/G key may be used at any time to view the most recent graph
- The right hand vessel is on a cantilever and may be set into oscillatory motion when bumped or during a run. This will show up as an inclined sine wave on the mass versus time graph and the data should be discarded.
- Make sure that no slurry leaks through the tubes that are not being used.
- At the end of a run air may be sucked into the tube. This should be avoided because it airates the slurry and sets the viscometer into oscillatory motion.
- Allow a short time for the flow to stabilize before reading data.
- If the slurry isolation pods fill up with slurry they must be disconnected and flushed.
- At high concentrations the pressure tappings block causing an error message in the pressure reading.

3.4 CONCLUSIONS

The Balanced Beam Tube Viscometer is a versatile instrument that is capable of producing reliable rheological and pipeline data.

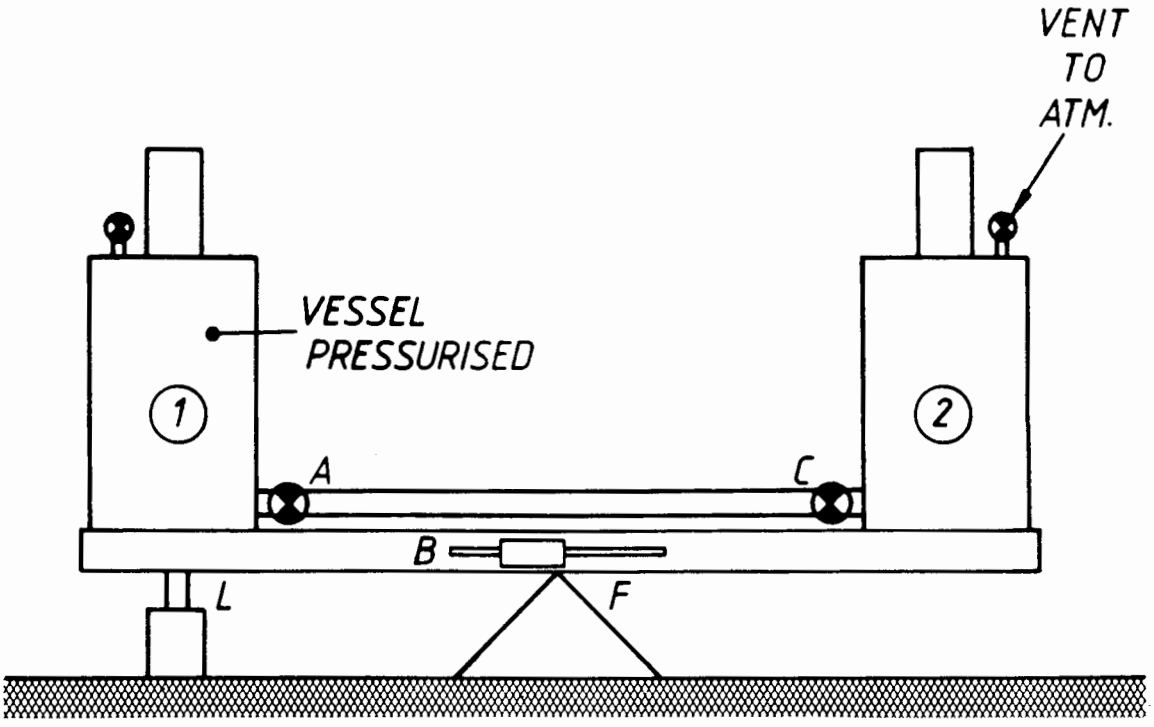

Fig. 3.1 Diagramatic layout of BBTV.

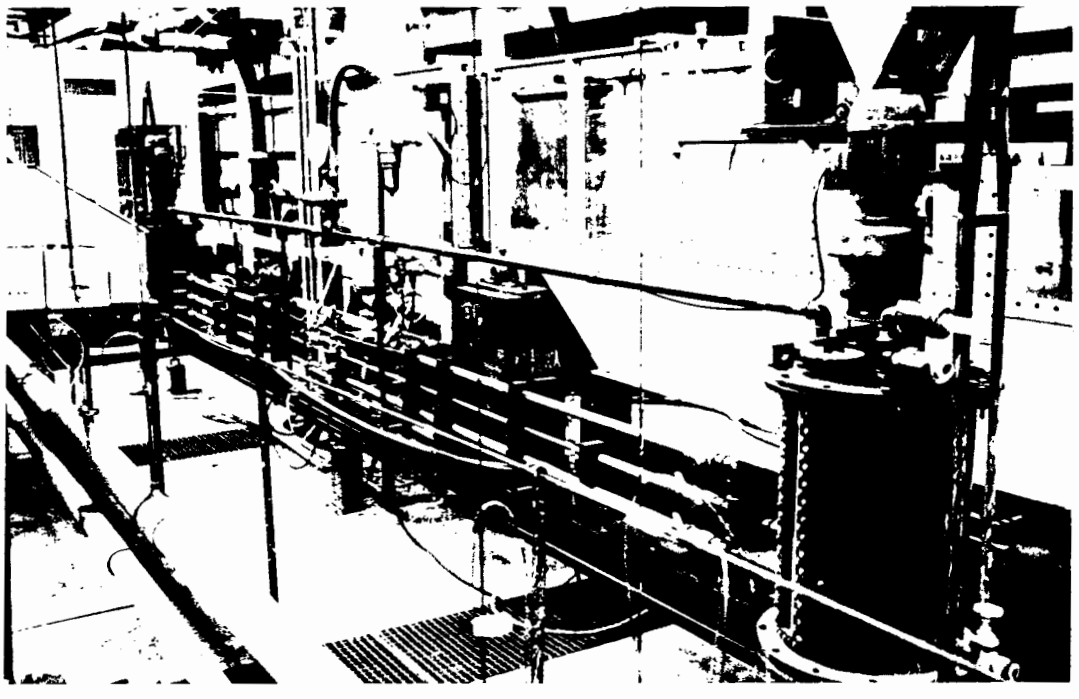

Fig. 3.2 Photograph of BBTV.

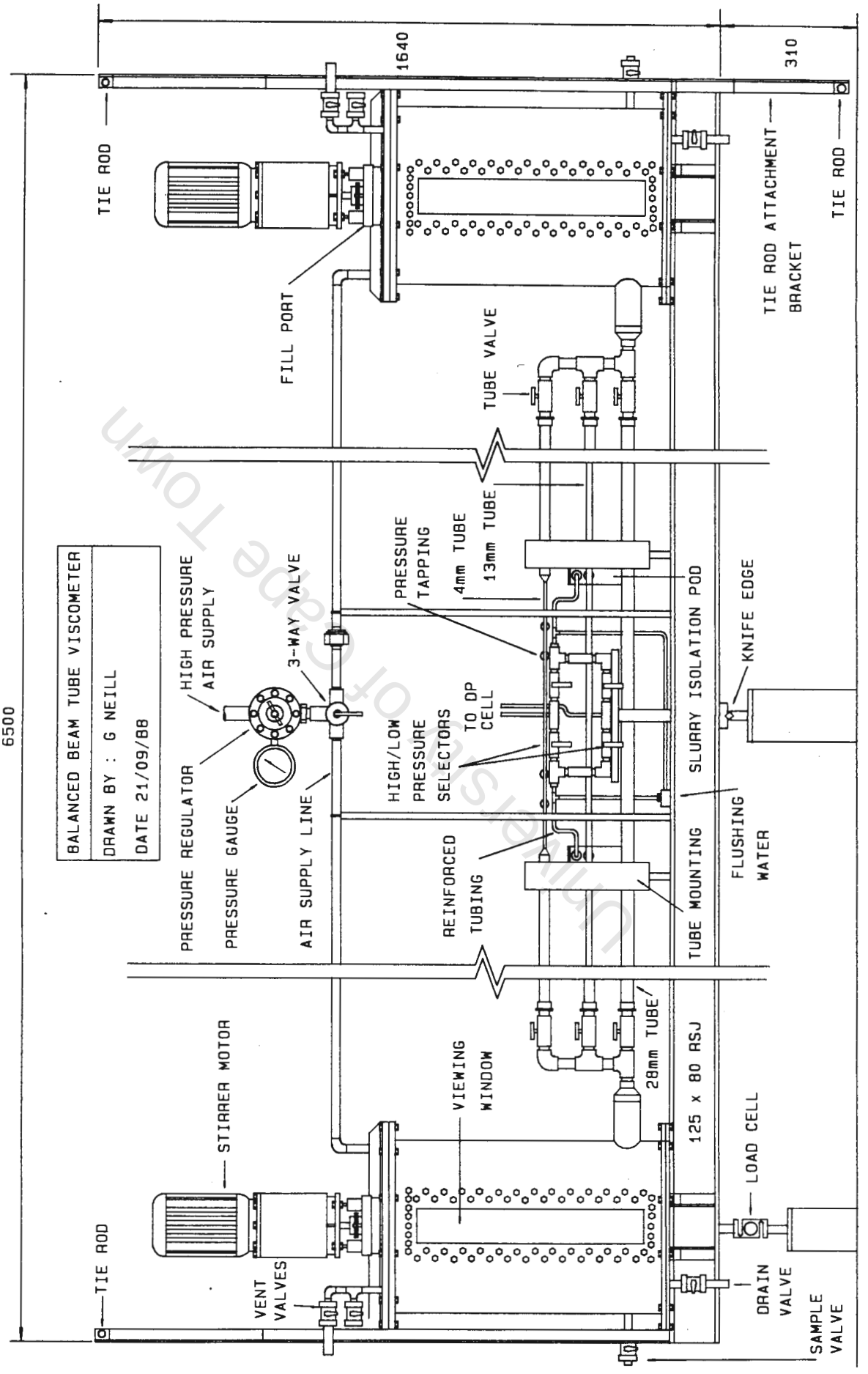

Fig. 3.3 Assembly drawing of BBTV.

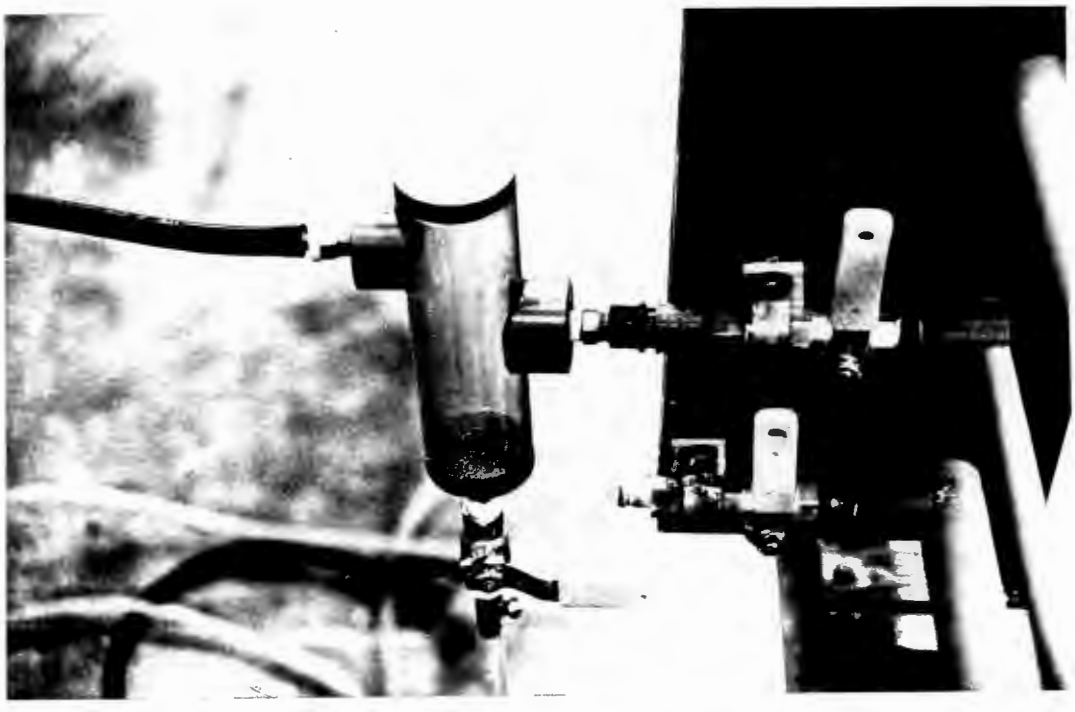

Fig. 3.4 Photograph of pressure tapping and slurry isolation pod.

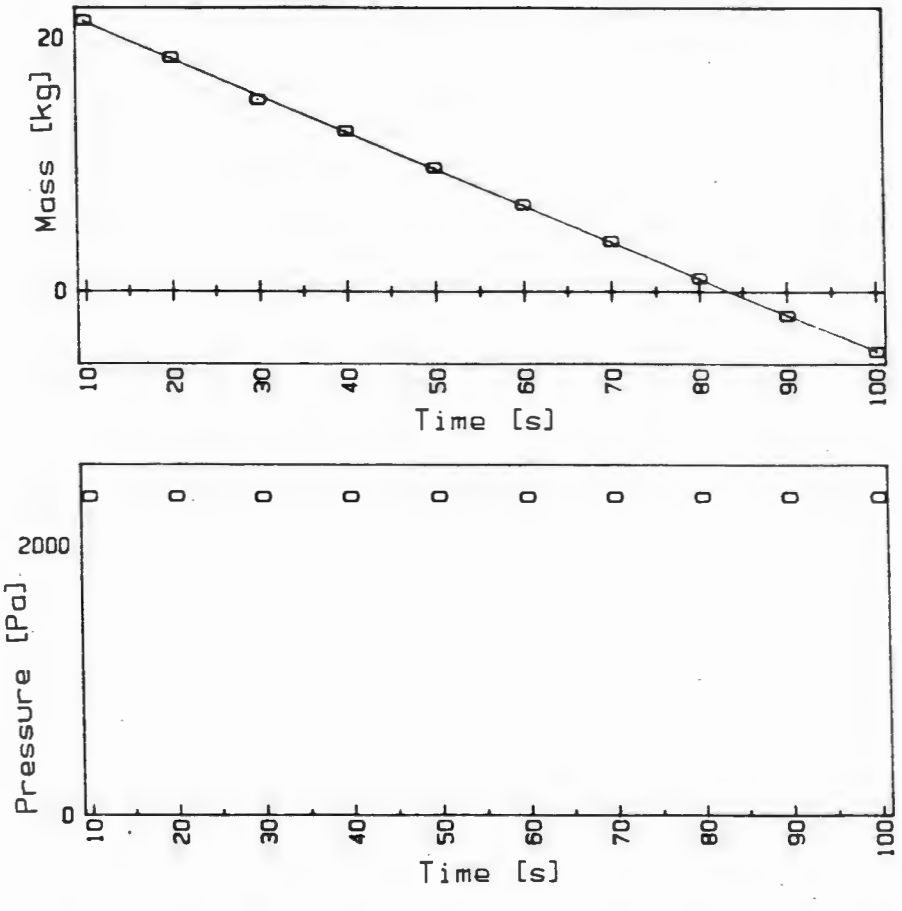

Fig. 3.5 A run in graphical form (Slatter (1986)).

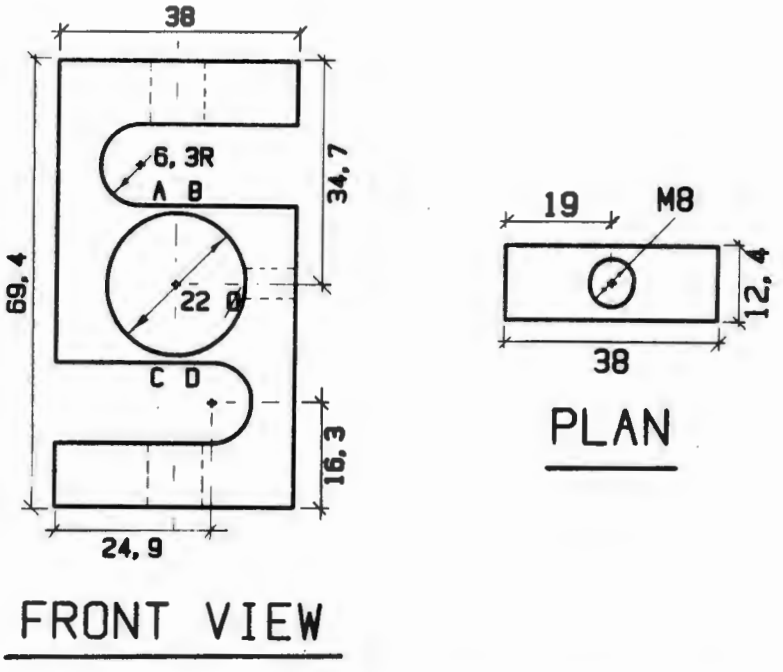

Fig. 3.6 Load cell (Slatter (1986)).

Fig. 3.7 Photograph of load cell.

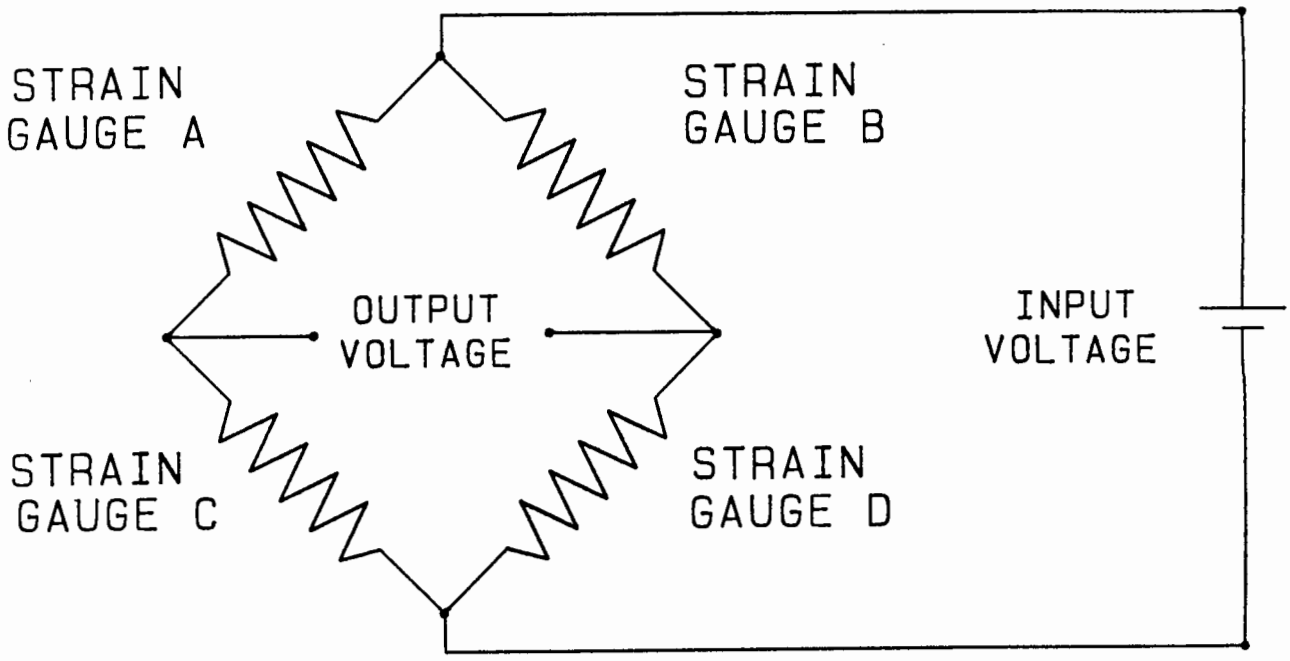

Fig. 3.8 Wheatstone bridge circuit.

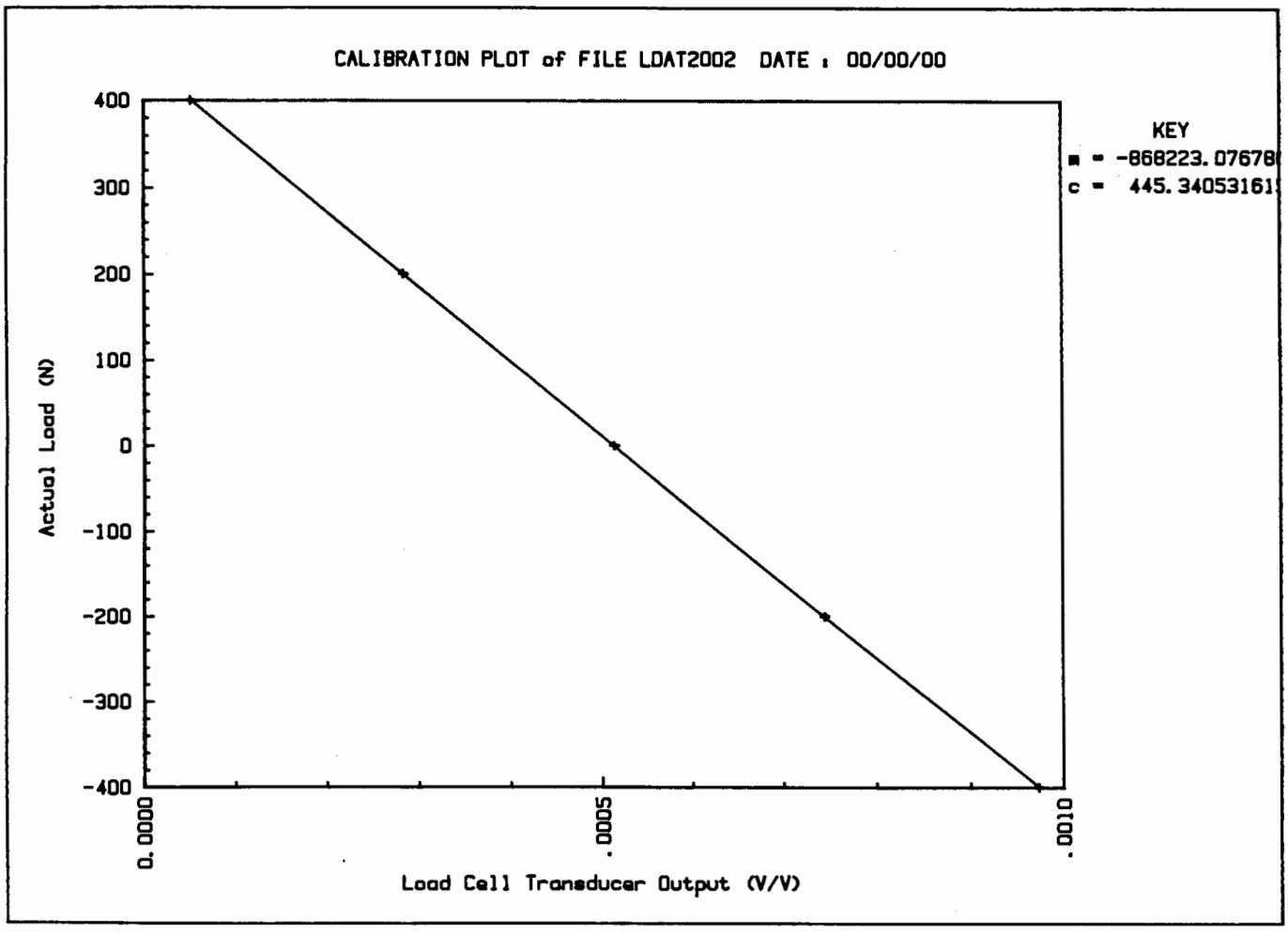

Fig. 3.9 Load cell response characteristic.

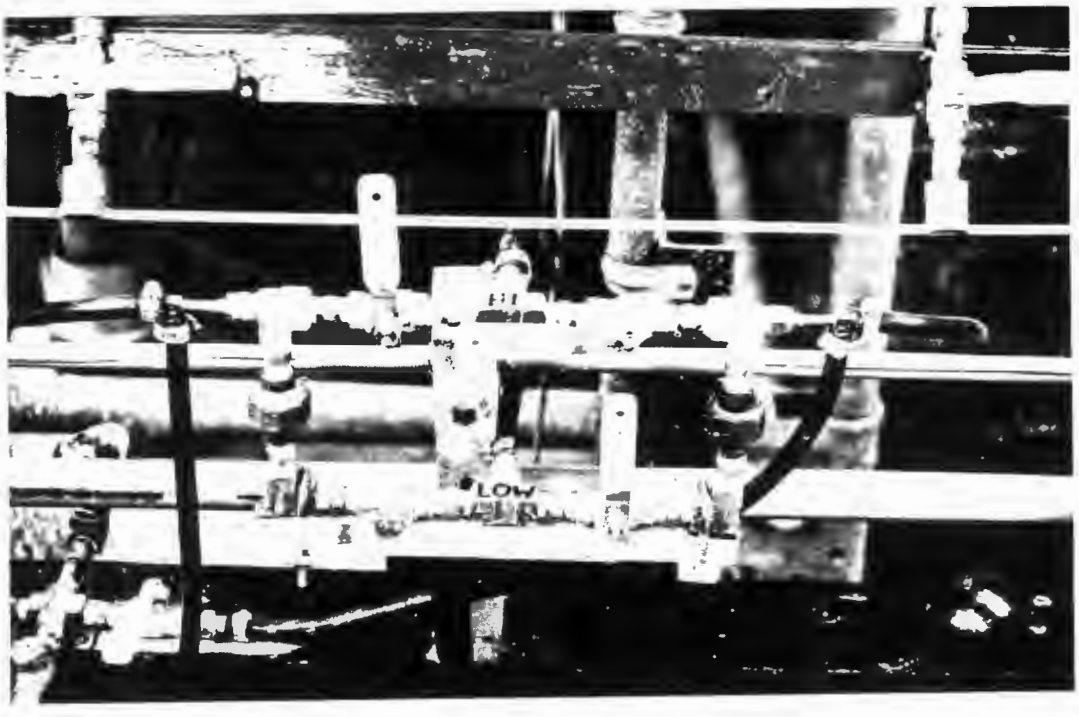

Fig. 3.10 Photograph of high/low pressure selectors.

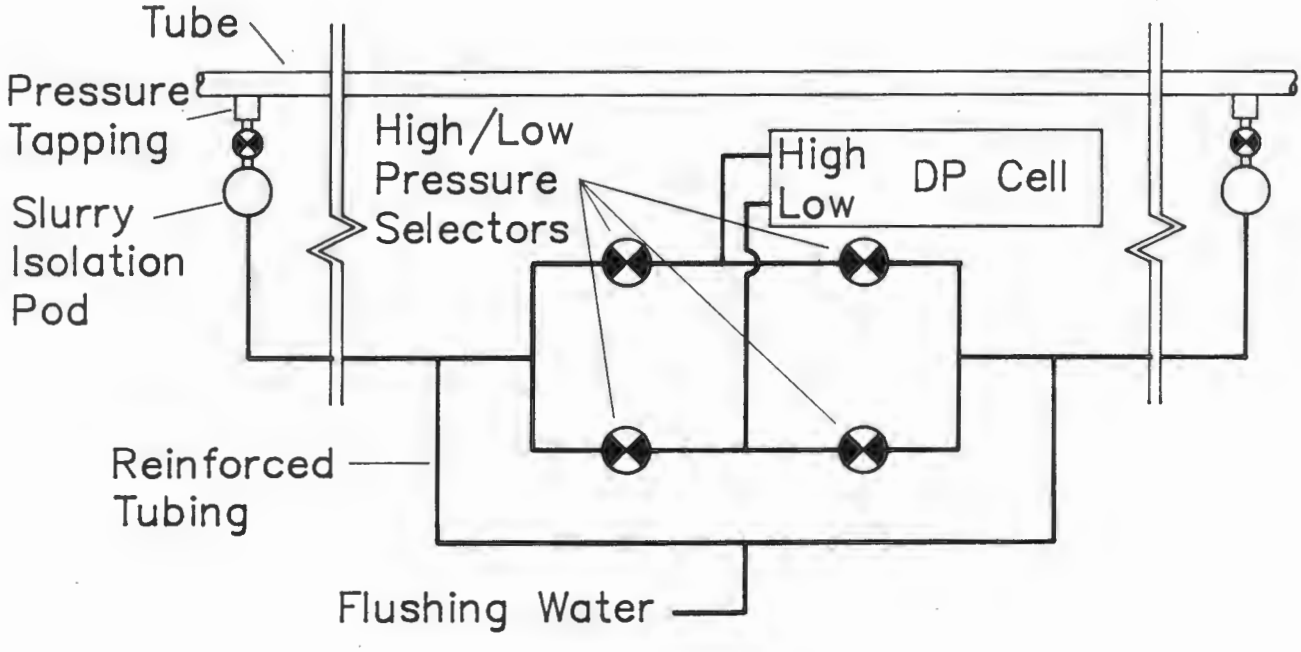

Fig. 3.11 Digram of high/low pressure selectors.

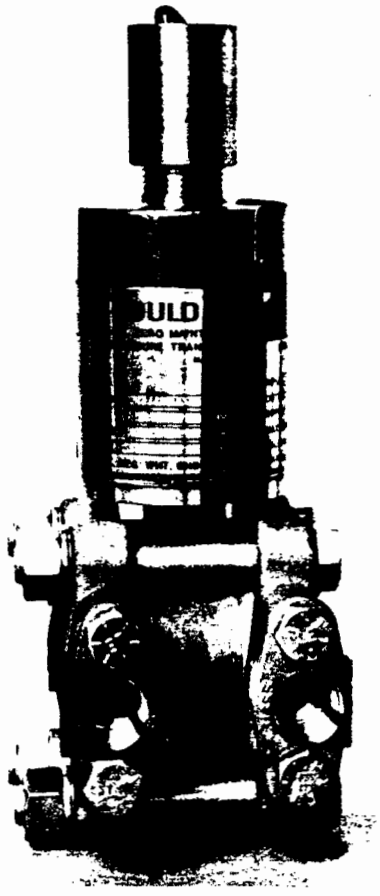

Fig. 3.12 Differential pressure transducer (DP cell) (Gould (1980)).

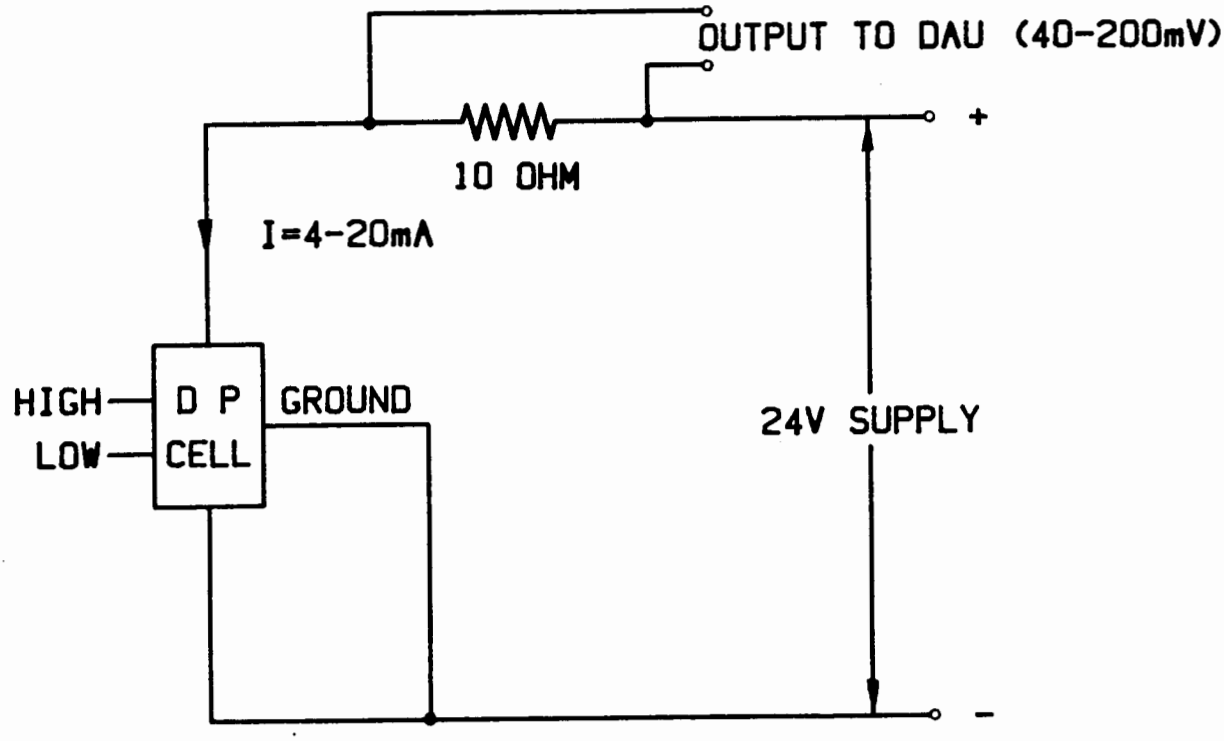

Fig. 3.13 DP cell circuit diagram (Slatter (1986)).

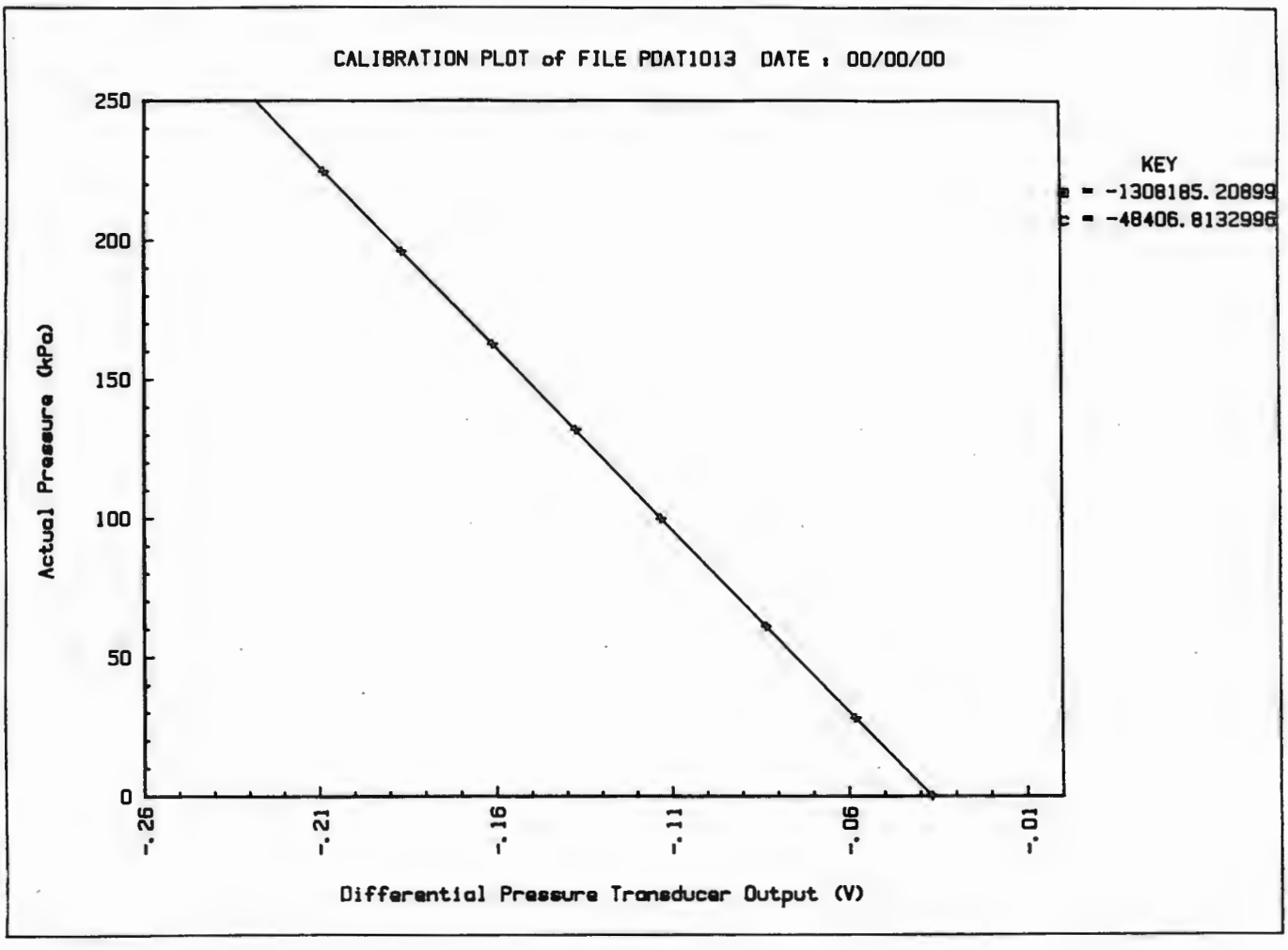

Fig. 3.14 DP cell response characteristic.

Fig. 3.15 Photograph of the computer hardware.

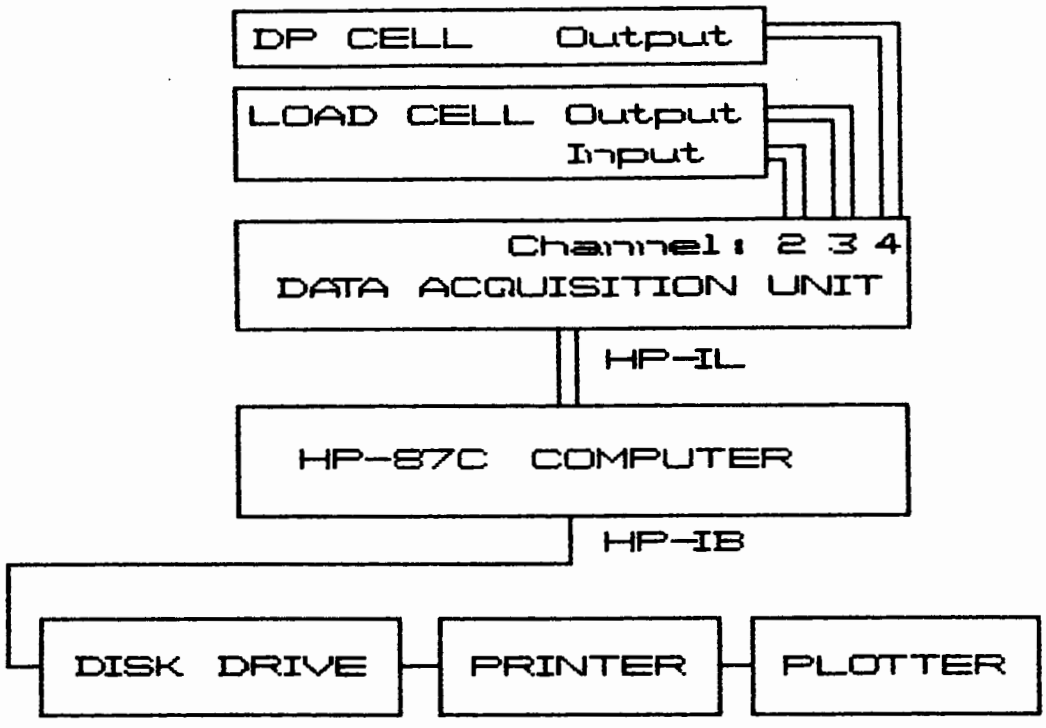

Fig. 3.16 Computer hardware connection diagram.

MENU TREE

MAIN MENU:	OPTIONS:	DESCRIPTION:
LOGON		(Sets date on the computer clock)
READ CHANNEL	LOAD IN V	(Load cell input voltage)
	LOAD OUT V	(Load cell output voltage)
	DP OUTPUT	(DP cell output voltage)
	MAIN MENU	(Returns to the main menu)
CALIBRATE	CALIBRATE LOAD CELL	(Calibrates the load cell)
	CALIBRATE DP CELL	(Calibrates the DP cell)
	LOAD CELL CALIB PLOT	(Plots the load cell calibration)
	DP CELL CALIB PLOT	(Plots the DP cell calibration)
	MAIN MENU	(Returns to the main menu)
VISCORUN		(Operating program)
STOREDATA		(Stores data on data disc after fatal error)
UTILITIES	PLOT ONE P-S GRAPH	(Plots one test on a pseudo-shear diagram)
	PLOT MANY P-S GRAPHS	(Plots many tests on one pseudo-shear diagram)
	FILE PRINT	(Prints a file to the screen or printer)
	FIT YPP CURVE	(Fits yield-pseudoplastic curve to data)
	PLOT YPP CURVE & DATA	(Plots the yield-pseudoplastic curve and data)
	MAIN MENU	(Returns to the main menu)

Fig. 3.17 Software menu tree.

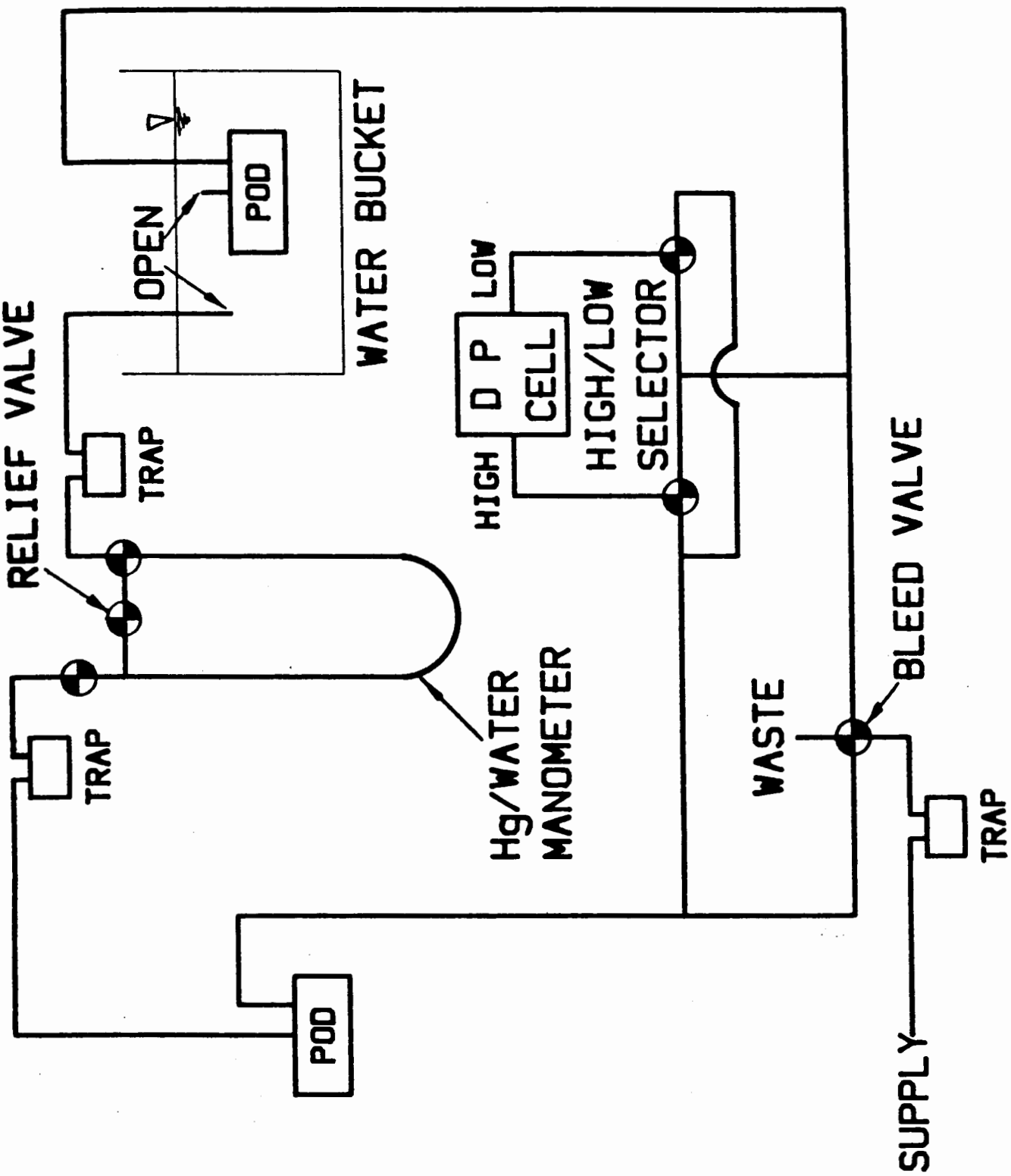

Fig. 3.18 DP cell calibration connections.

BBTV TEST: FTM400905

DIAM .01337
TEMP 20
Ss 2.7468
Sm 1.7038
Cv .4029
LOAD CELL CALIBRATION SLOPE -868223.08 CONST 445.34
D P CELL CALIBRATION SLOPE -1334155.02 CONST -42569.55
pH 7.00
LENGTH BETWEEN TAPPINGS 1.478 m

No	v (m/s)	p (Pa)	DP/4L (Pa)	8V/D (1/s)
1	.014	11087	25.1	8.2
2	.019	17024	38.5	11.4
3	.017	22553	51.0	10.3
4	.050	29299	66.3	29.9
5	.107	36390	82.3	64.0
6	.235	44499	100.6	140.8
7	.480	52430	118.6	287.4
8	.860	60667	137.2	514.6
9	1.364	68171	154.2	816.3
10	1.902	75885	171.6	1138.2
11	2.651	88565	200.3	1586.4
12	3.003	94958	214.8	1796.7
13	3.750	100885	228.2	2243.6
14	4.252	107728	243.6	2544.3
15	4.854	114601	259.2	2904.0
16	5.285	121769	275.4	3162.0
17	5.661	127156	287.6	3386.7
18	6.368	135548	306.6	3809.9
19	7.004	143132	323.7	4190.4

Fig. 3.19 Computer printout of a test.

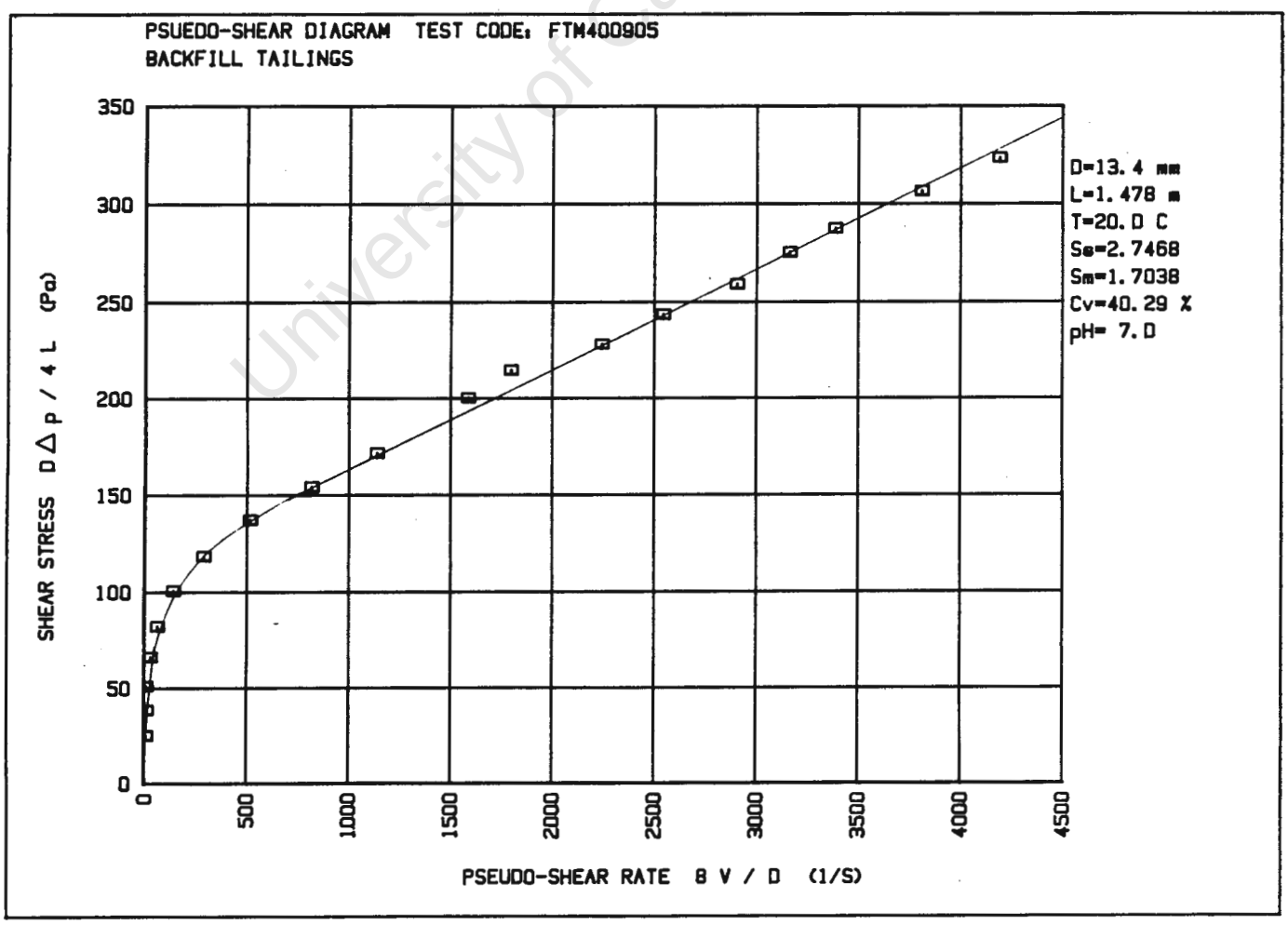

Fig. 3.20 Pseudo-shear diagram of a test.

CHAPTER 4

EXPERIMENTAL PROCEDURE

4.1 PRELIMINARY TESTS

The data logging and processing programs were checked by hand and found to have no significant arithmetical errors.

4.1.1 Comparative Tests between Full Plant Tailings and Belt Filtered Tailings

Two types of tailings are used for backfilling in the mining industry namely Full Plant Tailings and Belt Filtered Tailings. These tailings were obtained from the Chamber of Mines and may vary in origin. Tests detailed in Appendix E were performed to determine their similarity. These tests showed that solids relative density and particle size distribution of the tailings are identical. The -106 μm and -62 μm fractions of each of the tailings were rheologically characterized at various concentrations. The pseudo-shear diagrams of the tailings for each concentration and particle size distribution are coincident. This indicates that the variables other than particle size distribution and concentration affecting the rheology are the same. Due to their similarity the Full Plant Tailings hereafter referred to as backfill tailings are taken as being representative of both tailings.

4.1.2 Flow at High Concentrations

A test was conducted to establish the highest concentration at which the backfill tailings are fluid. The upper limit of fluidity is taken when the tailings are able to wet a smooth surface completely. Mixtures at various concentrations were made up and checked for fluidity. The fluidity

at each concentration is shown in Fig. 4.1. At S_m = 2.2 the tailings form granules and the fluidity is zero. At S_m = 2.0 the tailings form a single ball which can be broken up and show the first signs of fluidity. At this concentration the consistency is too high for it to be tested in the viscometer. At S_m < 1.9 the tailings are flowable and the rheology can be determined.

4.1.3 *In Situ* and Delivered Concentrations

A test was conducted to detect differences between *in situ* concentration (C_{vt}) and delivered concentration (C_{vd}). A sample of the -42 μm fraction of the backfill tailings was prepared at C_v = 34.50% (S_m = 1.62). The delivered concentration of the sample was measured through four different tube diameters at a roughly constant shear rate. The results are presented in Table 4.1.

Table 4.1 Delivered concentrations through different tube diameters.

Tube Diameter (mm)	Diameter Ratio (d_{50}/D)	Delivered Concentration (C_{vd}) (%)
14	0.0005	34.58
8	0.001	34.44
4	0.002	34.49
2	0.004	34.52

The results suggest that there is no difference between the *in situ* concentration and the delivered concentration at this concentration. Therefore the slurry is homogeneous.

4.1.4 Developing Flow

Pseudo-shear diagrams of the -60 μm fraction of the backfill tailings at S_m = 1.7 were obtained from differential pressures measured at the initial and final sections of the 28 mm diameter tube. The two pseudo-shear diagrams are superimposed for comparison and shown in Fig. 4.2. Similar tests were done on the other two tube diameters. The two curves for each diameter coincide indicating that the flow becomes fully developed before the first pressure tapping. These results also indicate that the tailings are not time dependent.

4.2 EXPERIMENTAL PROCEDURE

In order to evaluate the available methods of analysis, the backfill tailings were tested in various size fractions and at various concentrations. These results will also be used for the prediction of friction headloss for the design and optimization of backfill systems using combinations of backfill material that include the tailings. A summary of the slurries tested is presented in Table 4.2.

Table 4.2 Summary of tests done.

Particle Size (μm)	Mixture Relative Density (S_m)	Volumetric Concentration (C_{vt}) (%)	Concentration by Weight (C_{wt}) (%)
-500	1.902	51.71	74.5
	1.846	48.50	72.2
	1.812	46.58	70.4
	1.754	43.27	67.4
	1.703	40.32	64.7
	1.651	37.35	62.0
-106	1.804	46.03	70.08
	1.748	42.81	67.23
	1.704	40.29	64.95
	1.651	37.26	61.99
	1.599	34.30	56.72
	1.551	31.53	55.85
-62	1.683	38.89	63.69
	1.650	36.91	61.68
	1.607	34.58	59.30
	1.553	31.68	56.22
	1.514	29.28	53.29
-42	1.675	38.06	63.02
	1.649	36.57	61.53
	1.603	34.03	58.86
	1.551	31.10	55.59
	1.501	28.23	52.15

The -500 μm fraction was tested in nominal internal tube diameters of 32 and 13mm. The viscometer was then modified and the remaining particle sizes were tested in nominal internal tube diameters of 28, 13 and 4mm as detailed in Chapter 3.

Samples were taken before each test for ancillary tests described in Appendix D.

4.3 SAMPLE PREPARATION

A 18" Sweco Vibro-Energy Separator shown in Fig. 4.3 was used in conjunction with a Bornemann EH250 eccentric helical rotor pump shown in Fig. 4.4 to scalp the slurry at various particle sizes. Three sieve sizes were used namely 106 μm (150 mesh), 62 μm (250 mesh) and 42 μm (325 mesh).

After scalping, the slurry concentration was increased by allowing it to settle and siphoning off the clear supernatant. The highest concentration obtained by settling was at all times below the concentration described in Section 4.1.2 at which the tailings become fluid. The tailings were tested at this concentration and then diluted and retested in decrements of $S_m = 0.05$.

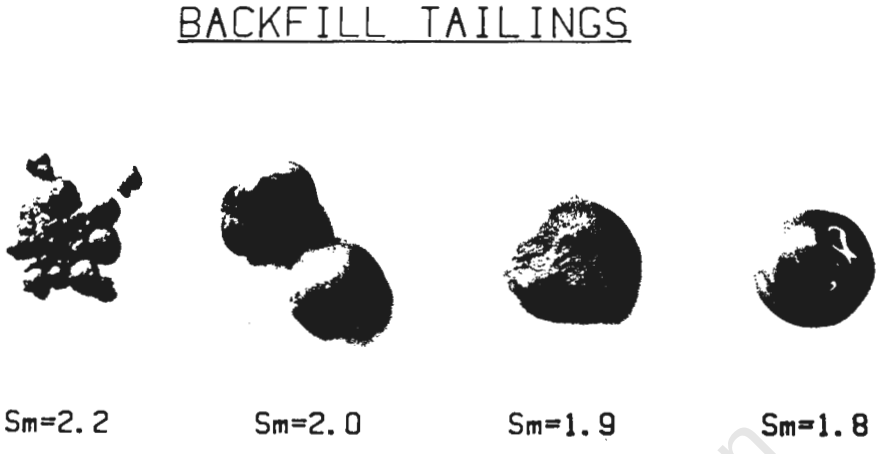

Fig. 4.1 Appearance of the backfill tailings at various high mixture relative densities.

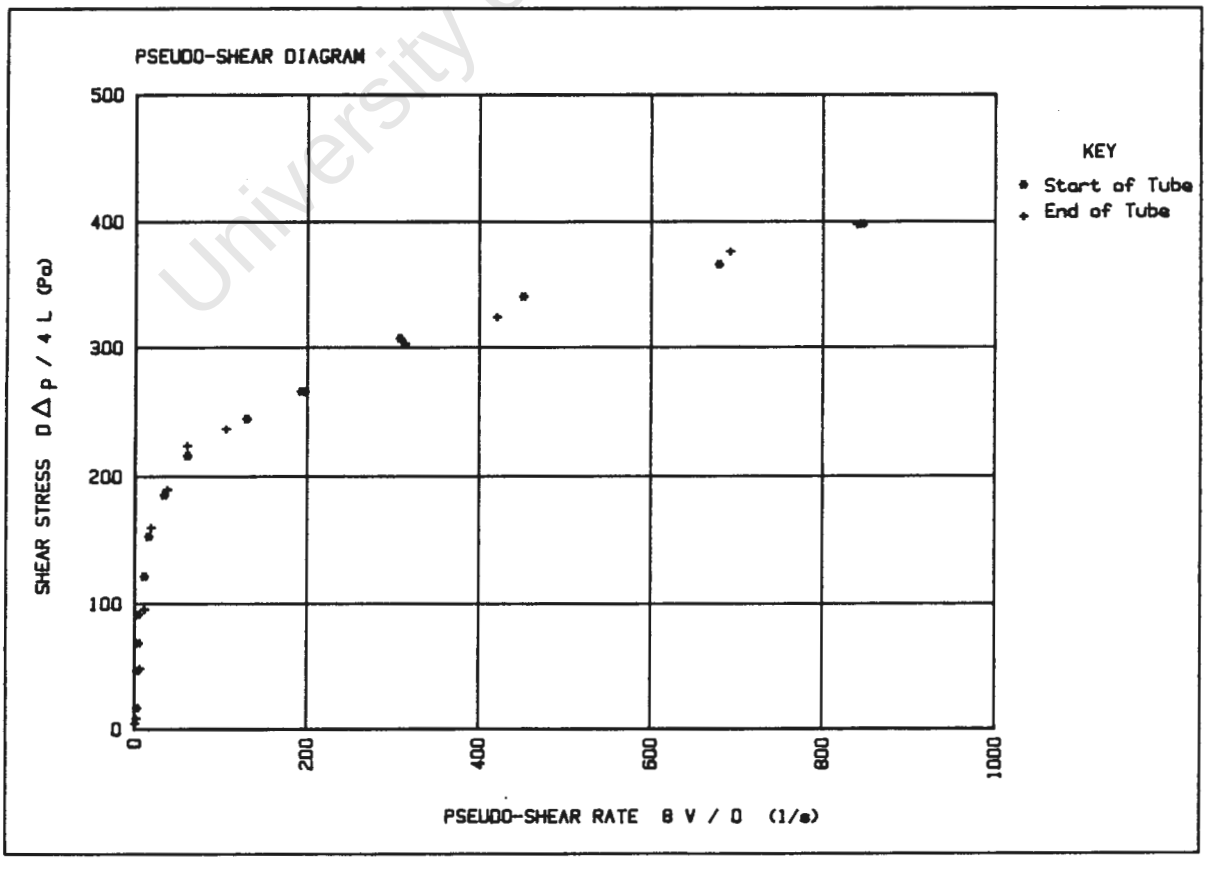

Fig. 4.2 The results of a preliminary test to check that fully developed flow exists between the pressure tappings.

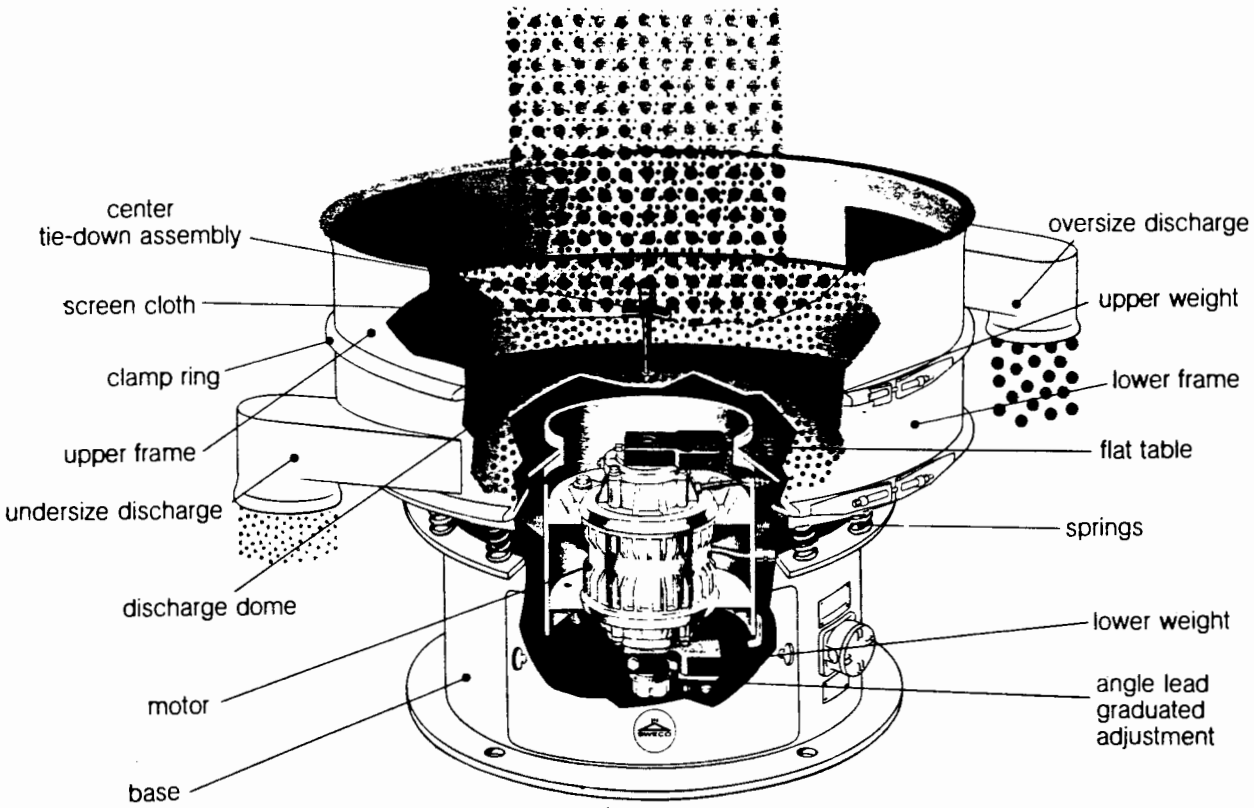

Fig. 4.3 Sweco Vibro-Energy Separator used for scalping (Sweco (1986).

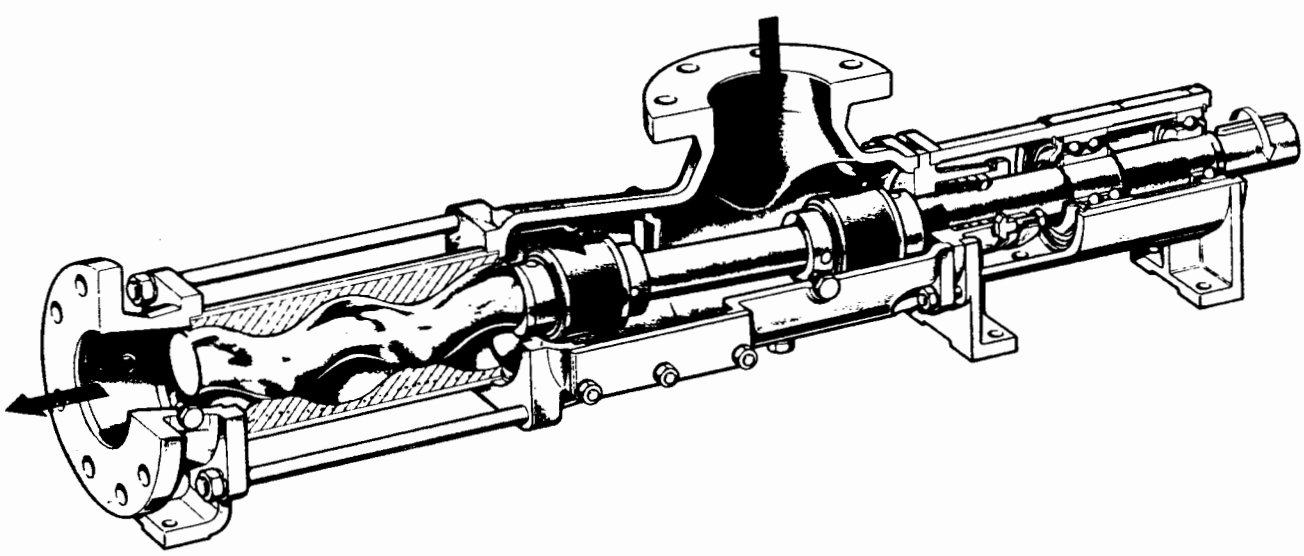

Fig. 4.4 Bornemann EH250 eccentric helical rotor pump used for scalping (Bornemann (1986)).

CHAPTER 5

MATERIAL DESCRIPTION

5.1 INTRODUCTION

Backfill refers to hydraulically placed particulate material in slurry form used as an underground support medium. This technique is used in the deep gold mines on the Witwatersrand. In order to get the optimal properties the backfill material is made up of various combinations of:

Aggregate - coarse crushed rock
Tailings - fine material that is left after the extraction process
Binder - cementatious material used to add strength

The material tested in this thesis falls under the tailings category.

5.2 PARTICLE SIZE DISTRIBUTIONS

The four particle size distributions were determined using a Malvern Particle Sizer described in Appendix D. The particle size distributions are shown in Figs. 5.1 to 5.4. The d_{10}, d_{50}, and d_{90} values for each of the slurries are presented in Table 5.1.

Table 5.1 Summary of d_{10}, d_{50} and d_{90} values

Particle Size (μm)	d_{10} (μm)	d_{50} (μm)	d_{90} (μm)
-500	6.0	12.0	20.5
-106	-	10.5	16.0
-62	-	10.0	12.3
-42	-	9.5	11.8

5.3 SOLIDS RELATIVE DENSITIES

The solids relative densities were determined using the procedure outlined in Appendix D. The results of the tests are presented in Table 5.2.

Table 5.2 Solids relative densities.

Particle Size (μm)	Solids Relative Density (S_g)
-500	2.743
-106	2.747
-62	2.757
-42	2.773

5.4 MIXTURE RELATIVE DENSITY

The mixture relative densities were determined using the procedure outlined in Appendix D. The results of the tests are presented in Table 4.1.

5.5 pH VALUES

The pH of each particle size distribution was measured using the instrument described in Appendix D. The results are presented in Table 5.3.

Table 5.3 pH Values

Particle Size (μm)	pH Value
-500	7.63
-106	7.67
-62	7.63
-42	7.85

5.6 TEMPERATURE

The temperature of the slurry during testing varied between 15 and 20°C. A minimal increase in temperature due to frictional heating was measured during testing.

5.7 MICROGRAPHS

Micrographs of the tailings were taken using an optical microscope. The micrographs are shown in Figs. 5.5 to 5.8. The angularities of a range of solid particles sizes are clearly visible under different magnifications.

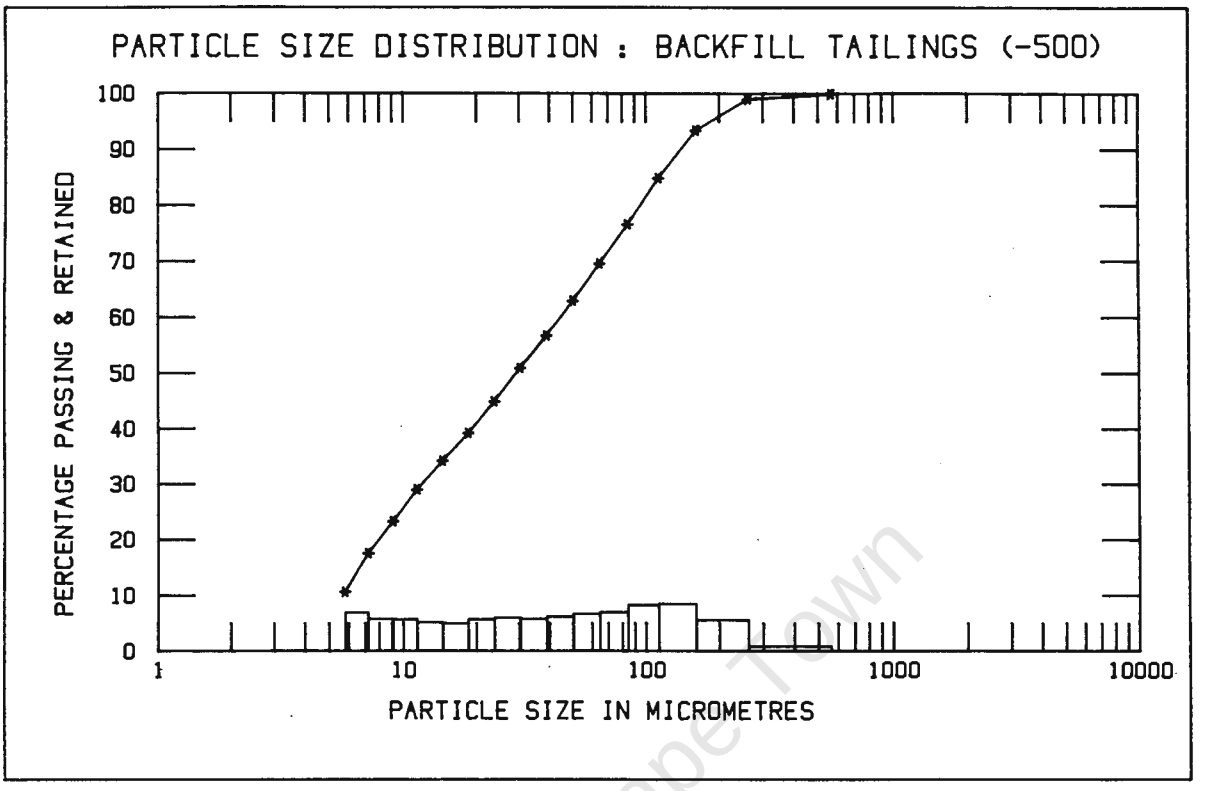

Fig. 5.1 Particle size distribution for the -500 μm fraction of the backfill tailings.

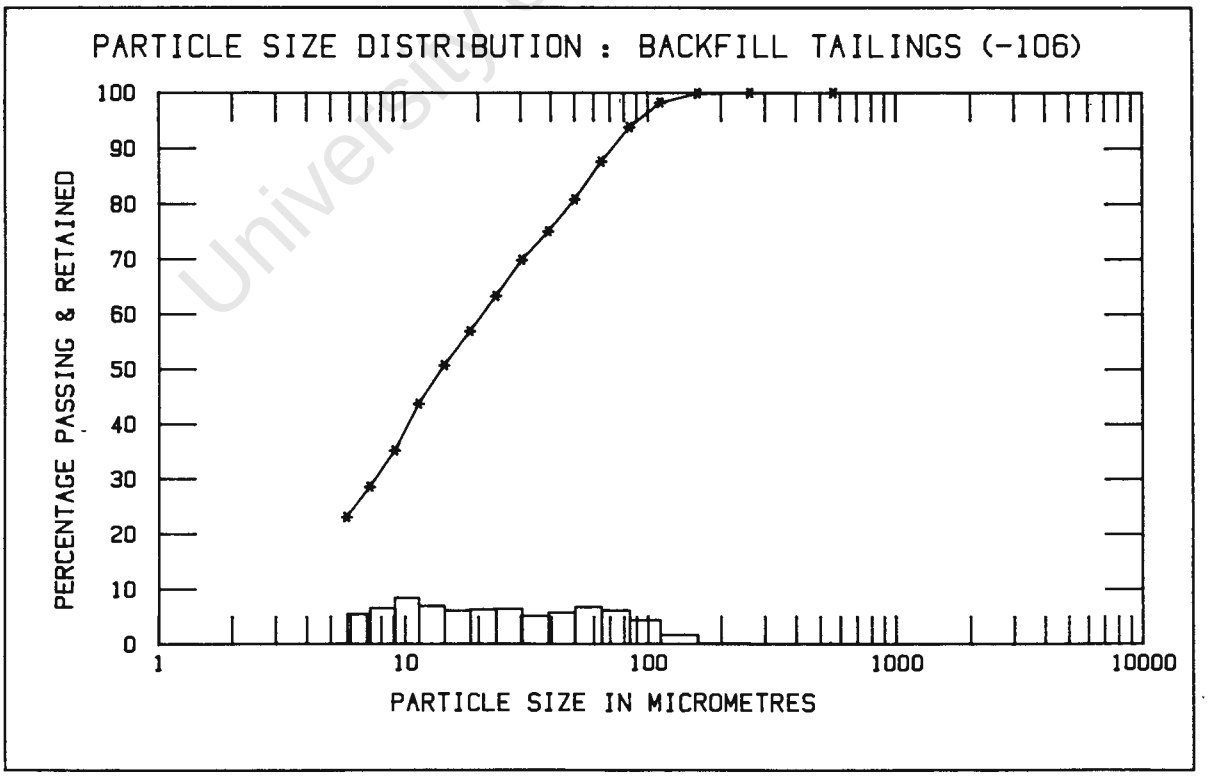

Fig. 5.2 Particle size distribution for the -106 μm fraction of the backfill tailings.

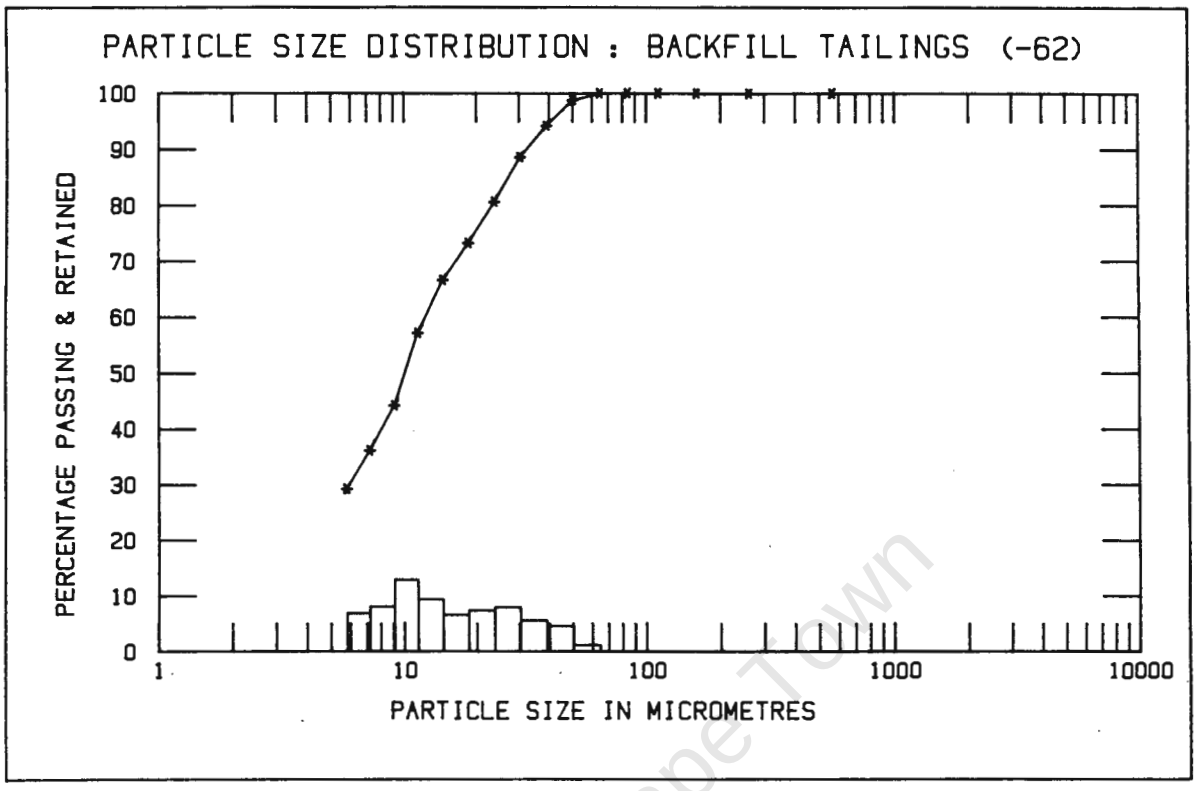

Fig. 5.3 Particle size distribution for the -62 μm fraction of the backfill tailings.

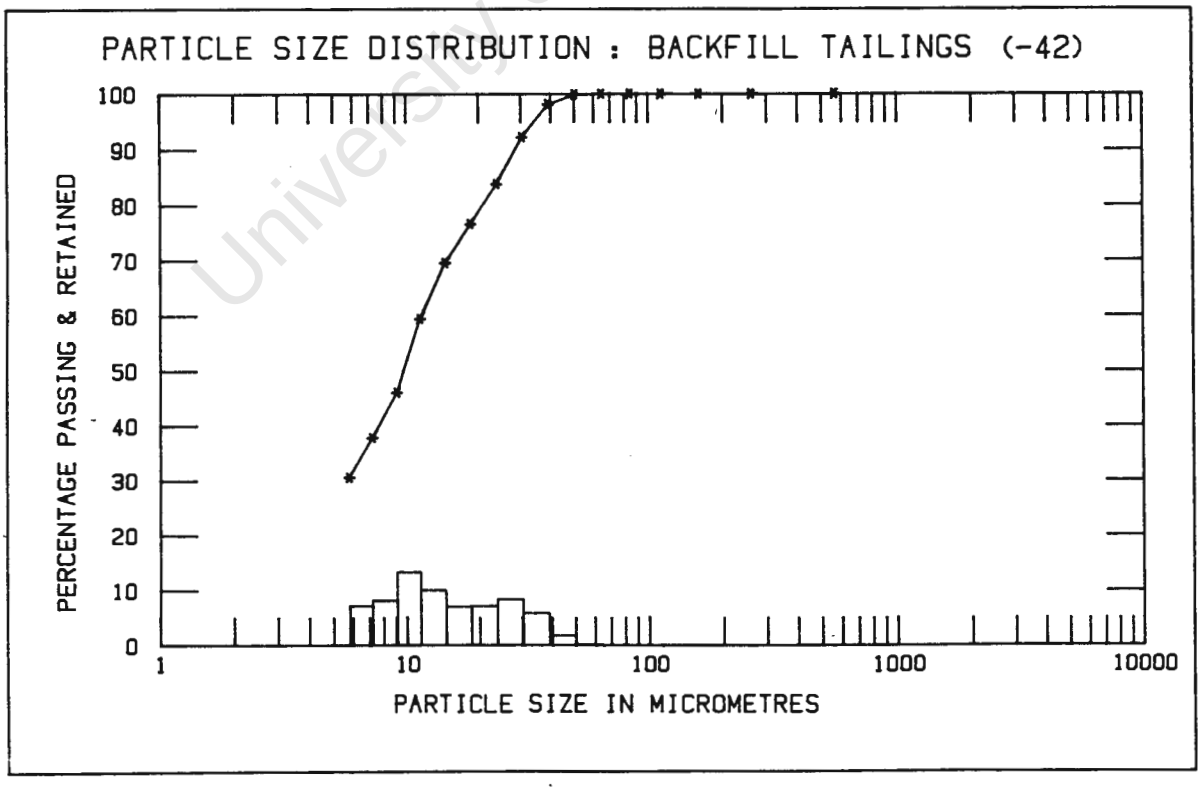

Fig. 5.4 Particle size distribution for the -42 μm fraction of the backfill tailings.

Fig. 5.5 Micrograph of 75 - 100 μm solid particles under a magnification of 10x.

Fig. 5.6 Micrograph of 20 - 90 μm solid particles under a magnification of 16x.

Fig. 5.7 Micrograph of 10 - 20 μm solid particles under a magnification of 40x.

Fig. 5.8 Micrograph of 2 - 10 μm solid particles under a magnification of 40x.

CHAPTER 6

EXPERIMENTAL RESULTS AND ANALYSIS

6.1 OBSERVATIONS DURING TESTING

The flow through the clear PVC tubes is clearly visible. Although the slurry is opaque, the motion of the solid particles near the tube wall are visible at low velocities. These solid particles were observed to move along rectilinear paths. The solid particles close to the tube wall moved slower than the solid particles further from the tube wall. The existence of a wall layer was not established due to transparency and optical distortion through the clear PVC. At the visual onset of turbulence the differential pressure reading oscillated at a frequency of approximately 2 Hz. Settling of the solid particles was not observed at any of the concentrations.

6.2 PSEUDO-SHEAR DIAGRAMS

The pseudo-shear diagrams for each of the tests detailed in Table 4.1 are presented in Figs. 6.1. Combined pseudo-shear diagrams for the laminar flow region of each particle size distributions are presented in Fig. 6.2 to Fig. 6.5 for comparison.

6.3 FRICTION FACTOR REYNOLDS NUMBER DIAGRAMS

Friction factor Reynolds number diagrams for each of the particle size distributions are presented in Fig. 6.6 to Fig 6.9. The Reynolds number used is based on the a Reynolds number of water at the mean mixture velocity.

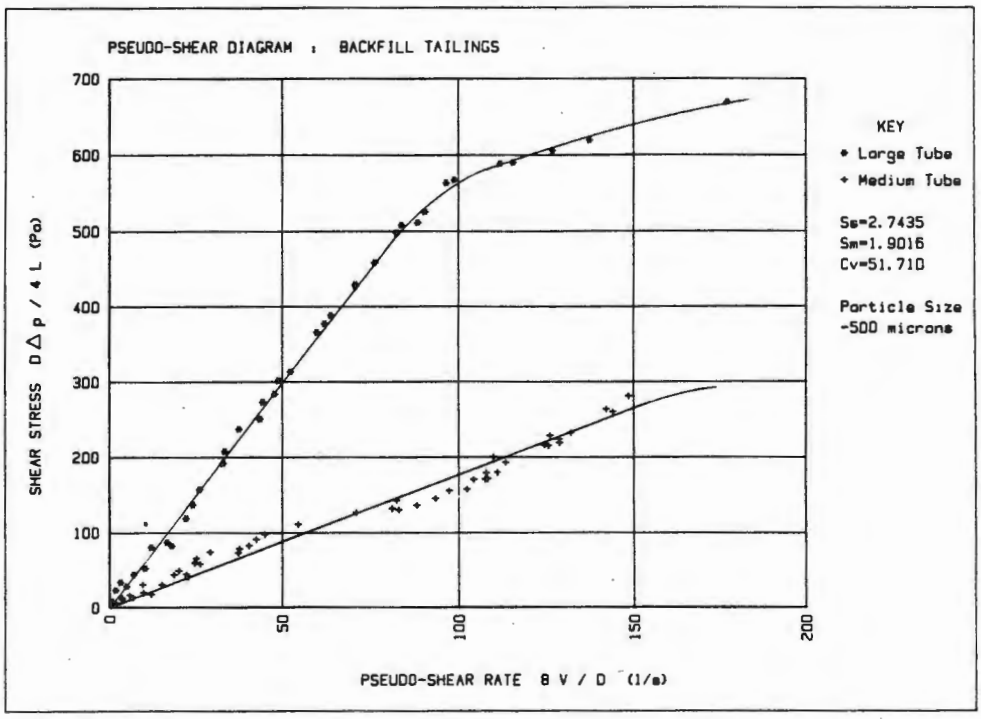

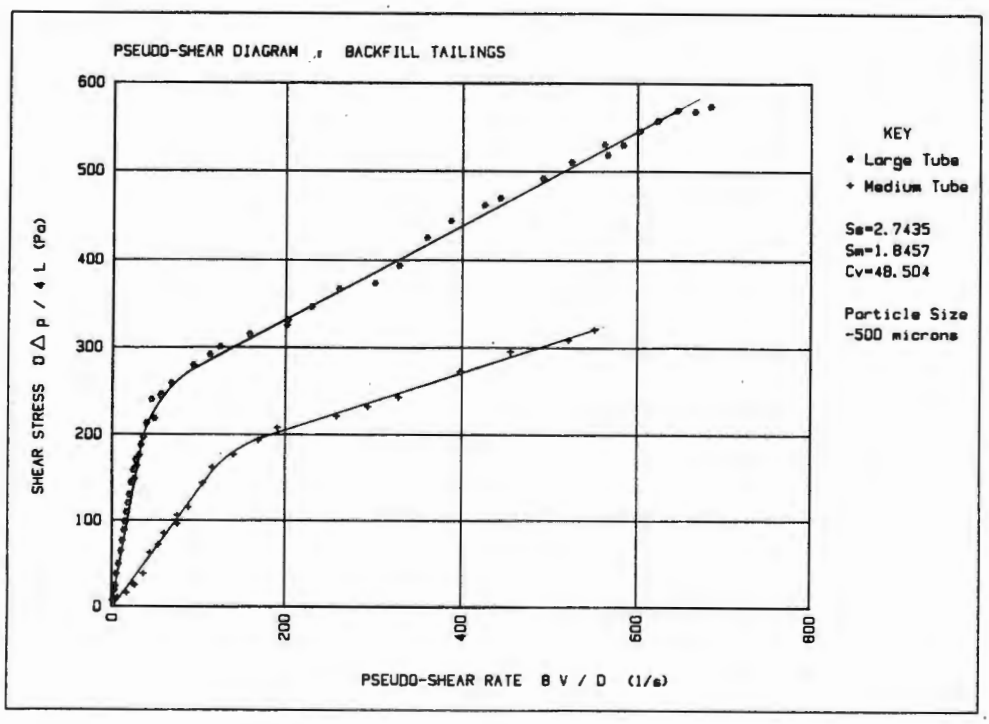

Fig. 6.1 Pseudo-shear diagrams for all the tests on backfill tailings are presented. The results of the tests done on the -500, -106, -62 and -42 μm fractions are presented sequentially starting at the highest and ending with the lowest concentration for each particle size.

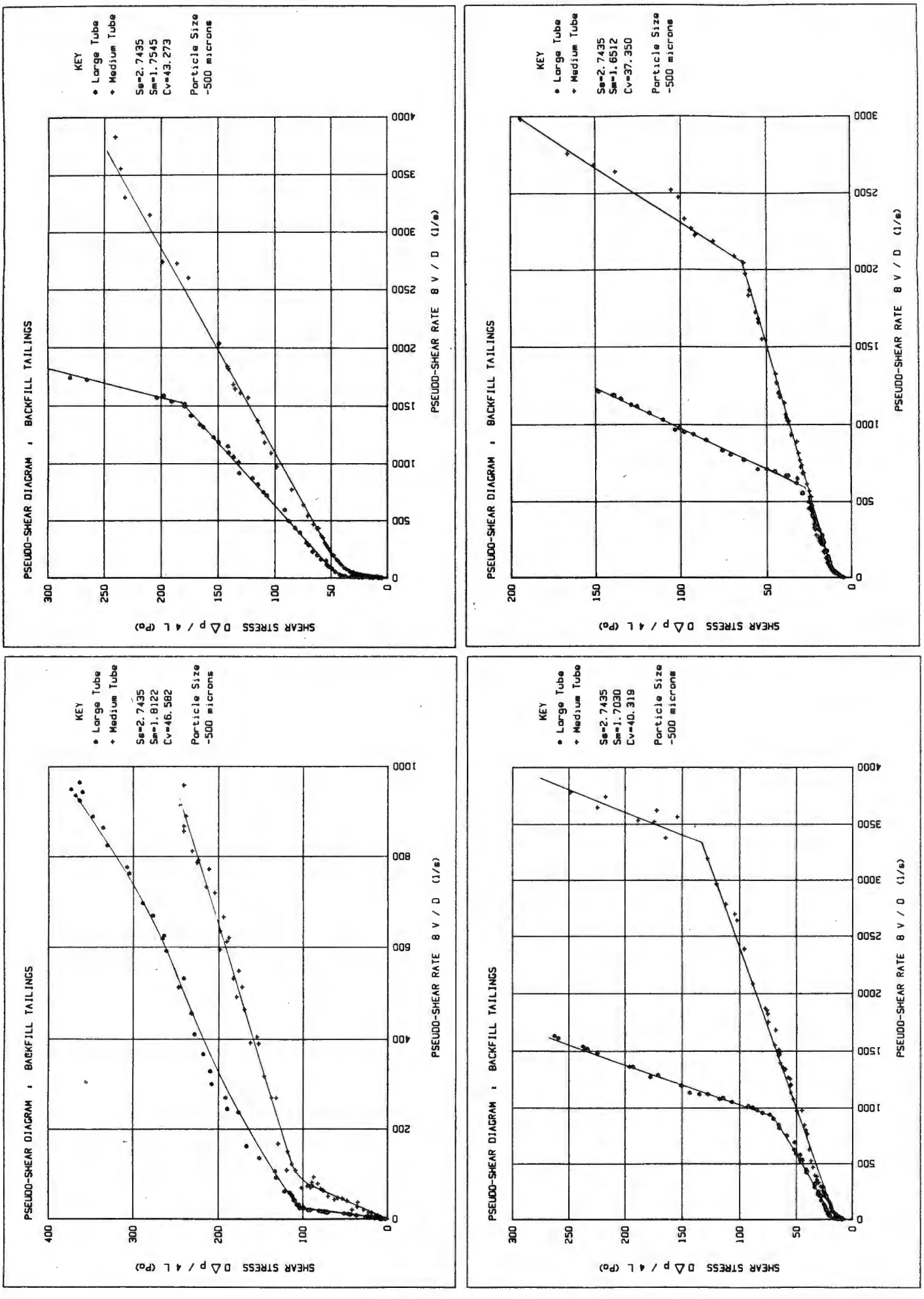

Fig. 6.1 continued

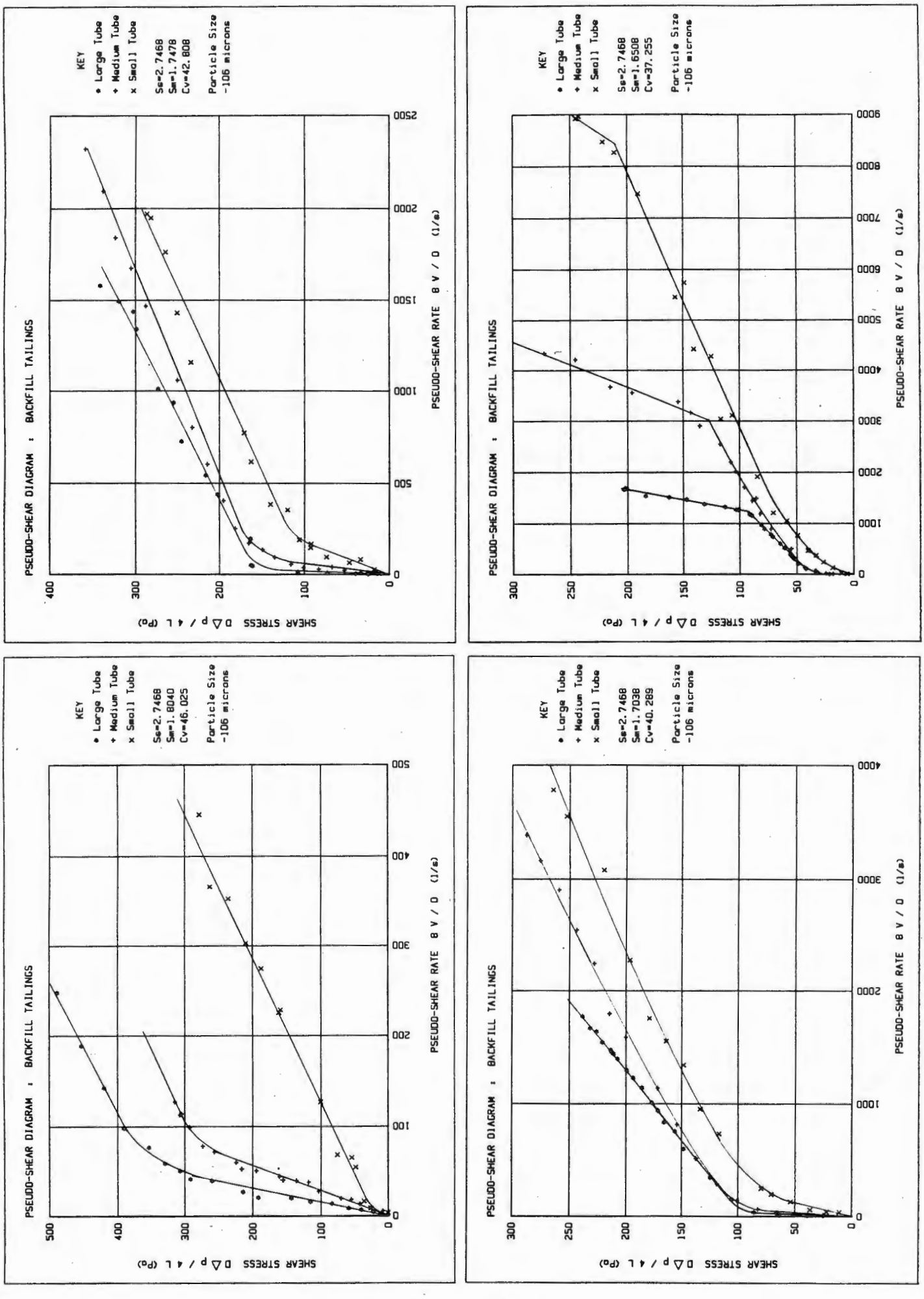

Fig. 6.1 continued

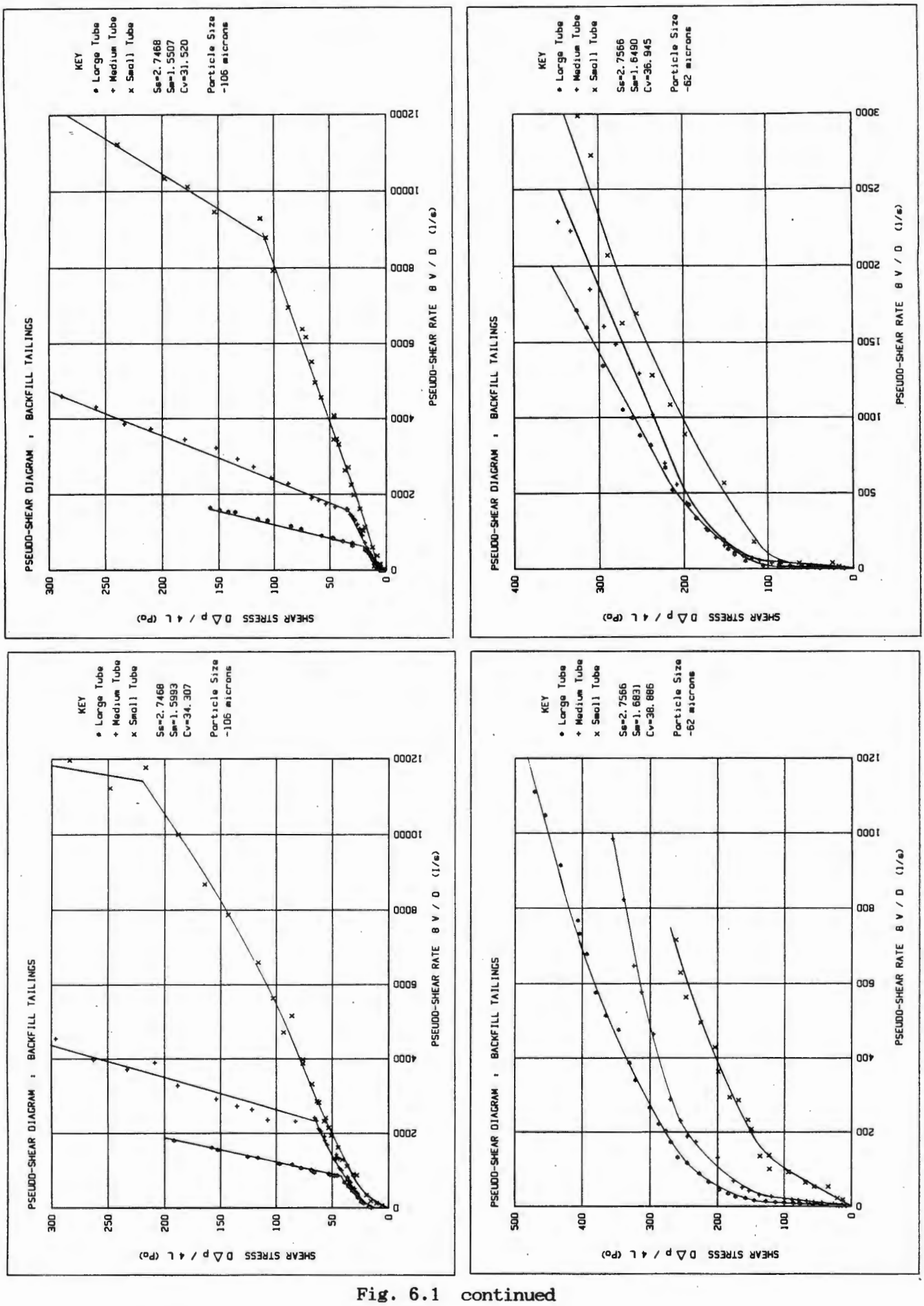

Fig. 6.1 continued

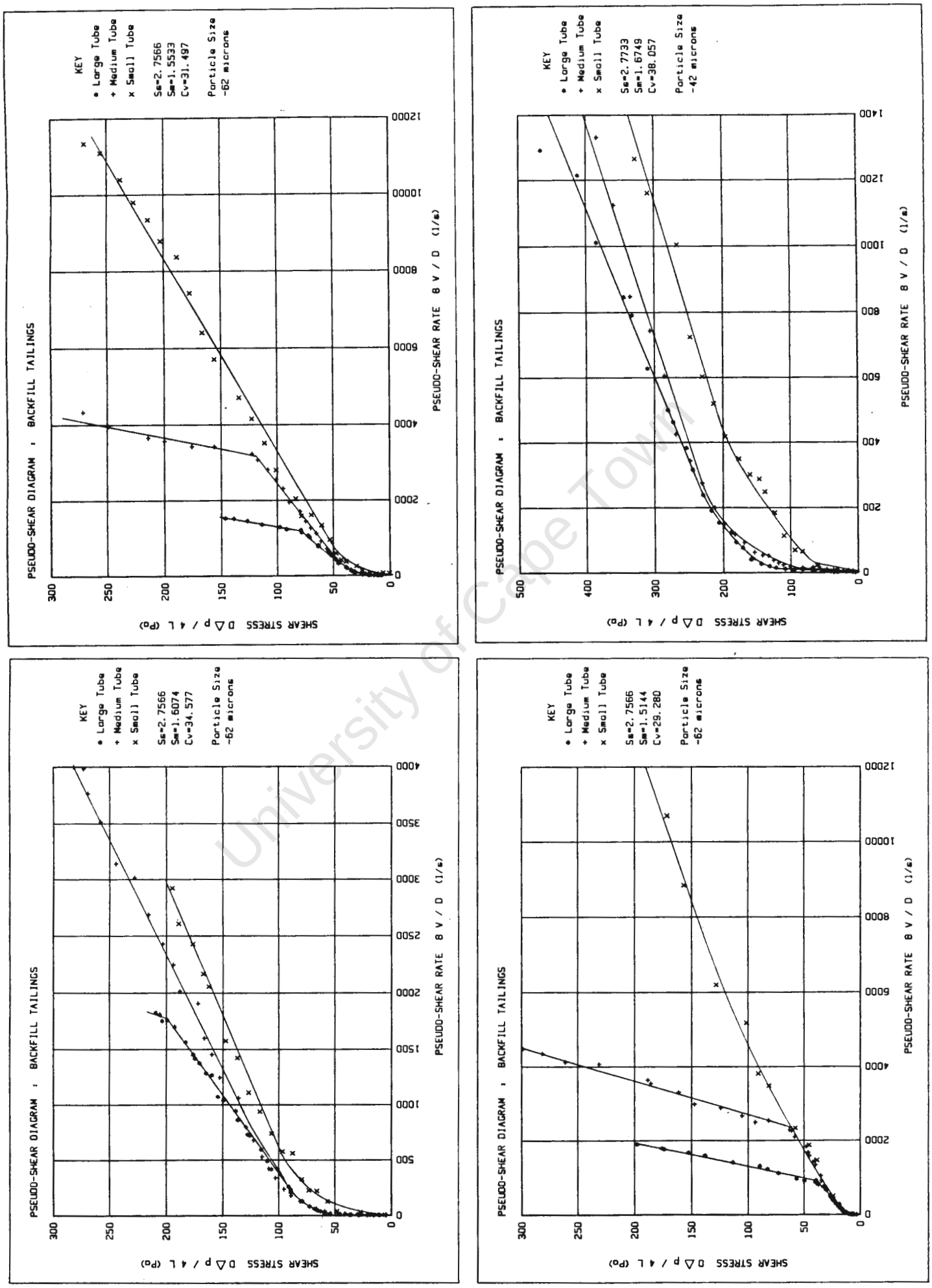

Fig. 6.1 continued

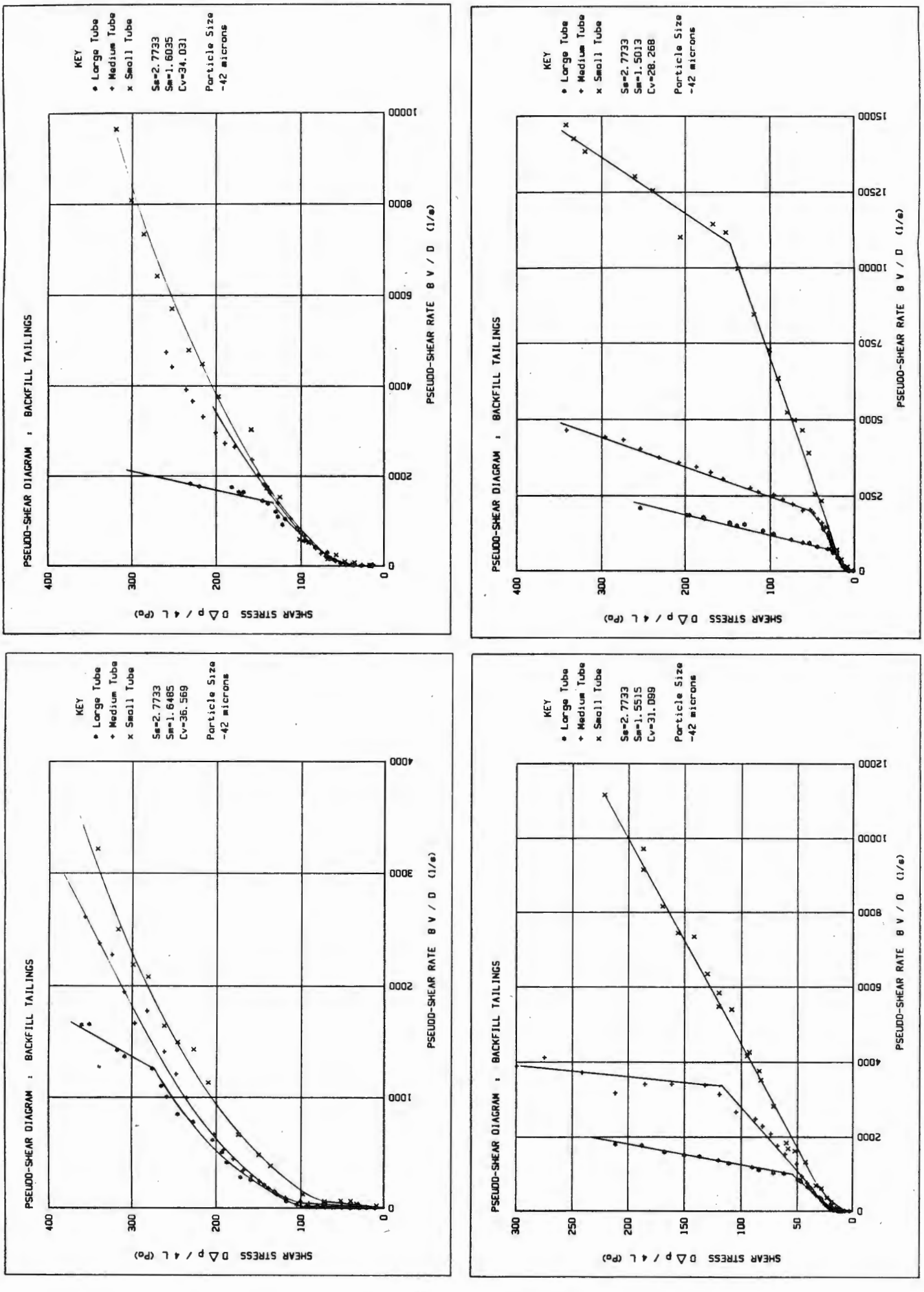

Fig. 6.1 continued

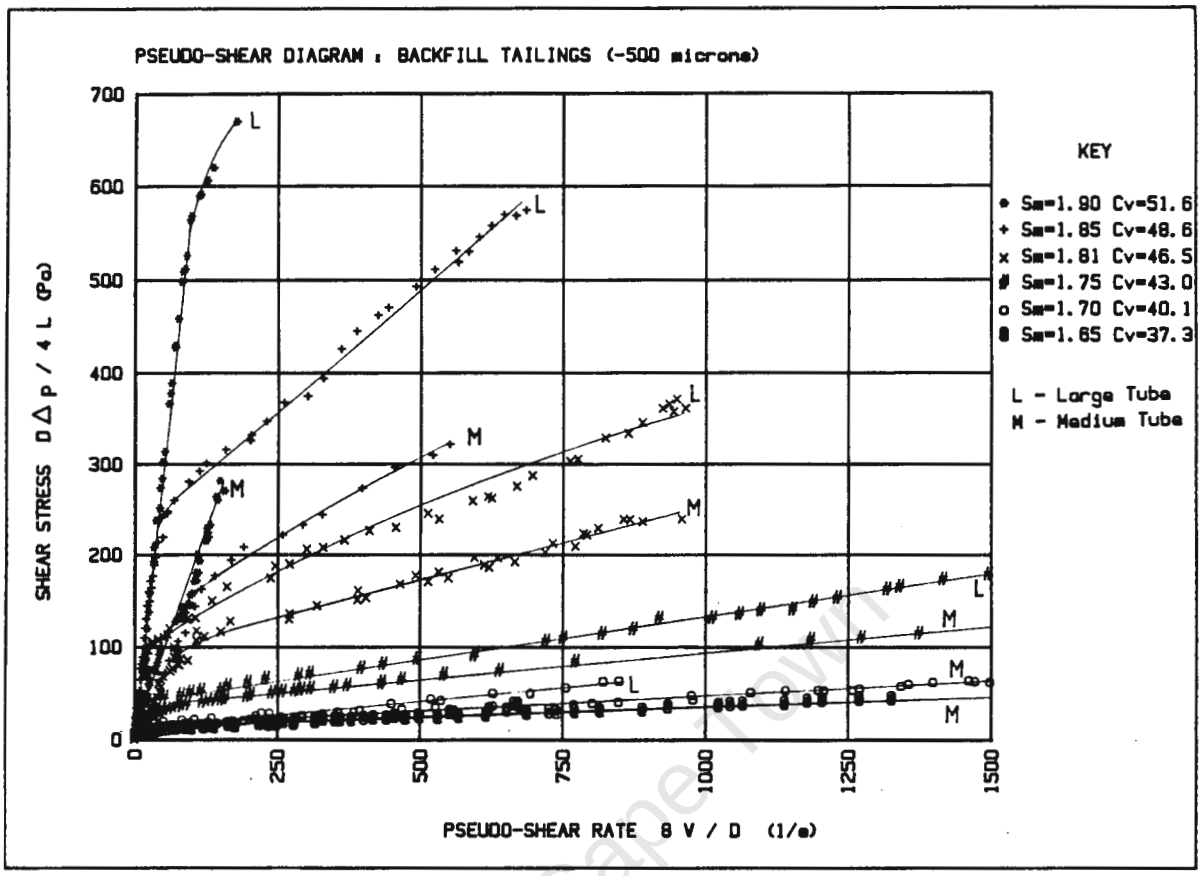

Fig. 6.2 Combined pseudo-shear diagrams for the -500 μm fraction of the backfill tailings.

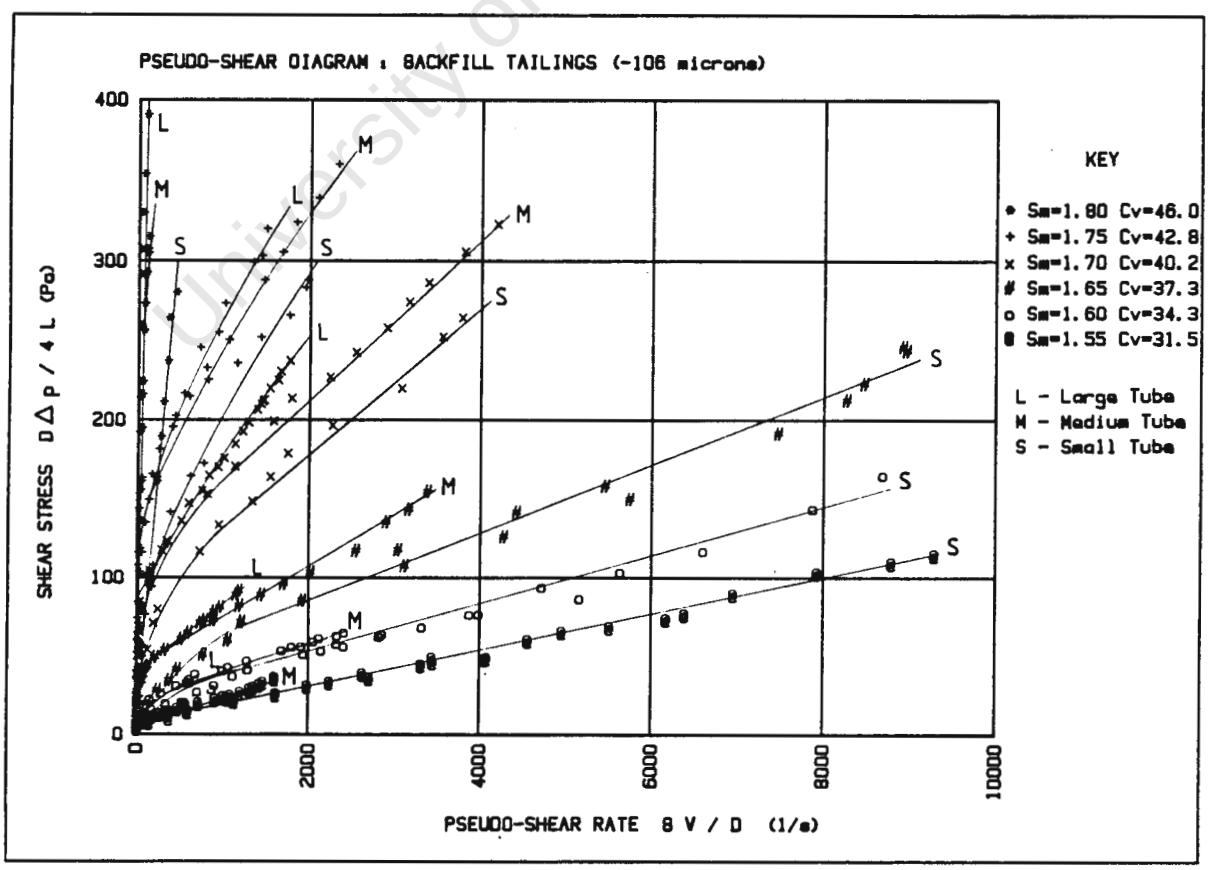

Fig. 6.3 Combined pseudo-shear diagrams for the -106 μm fraction of the backfill tailings.

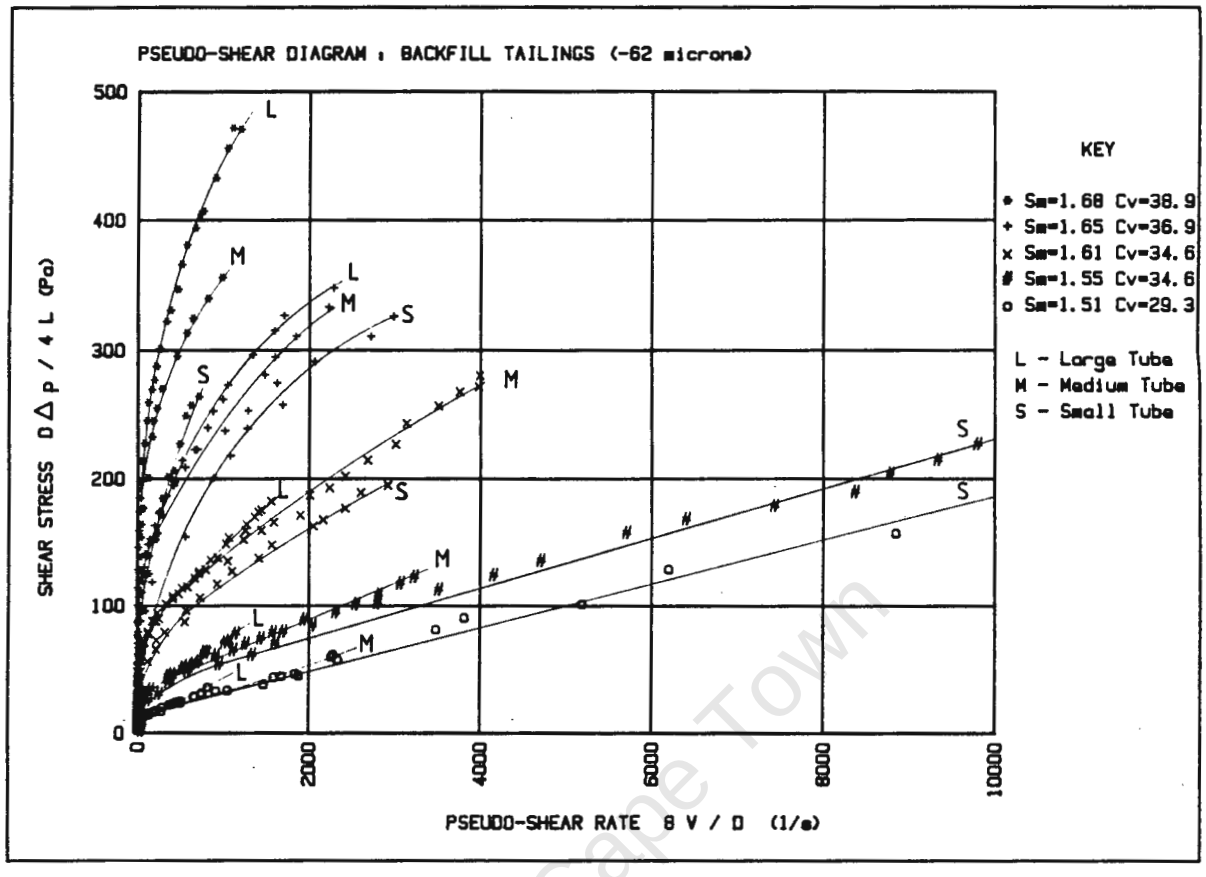

Fig. 6.4 Combined pseudo-shear diagrams for the -62 μm fraction of the backfill tailings.

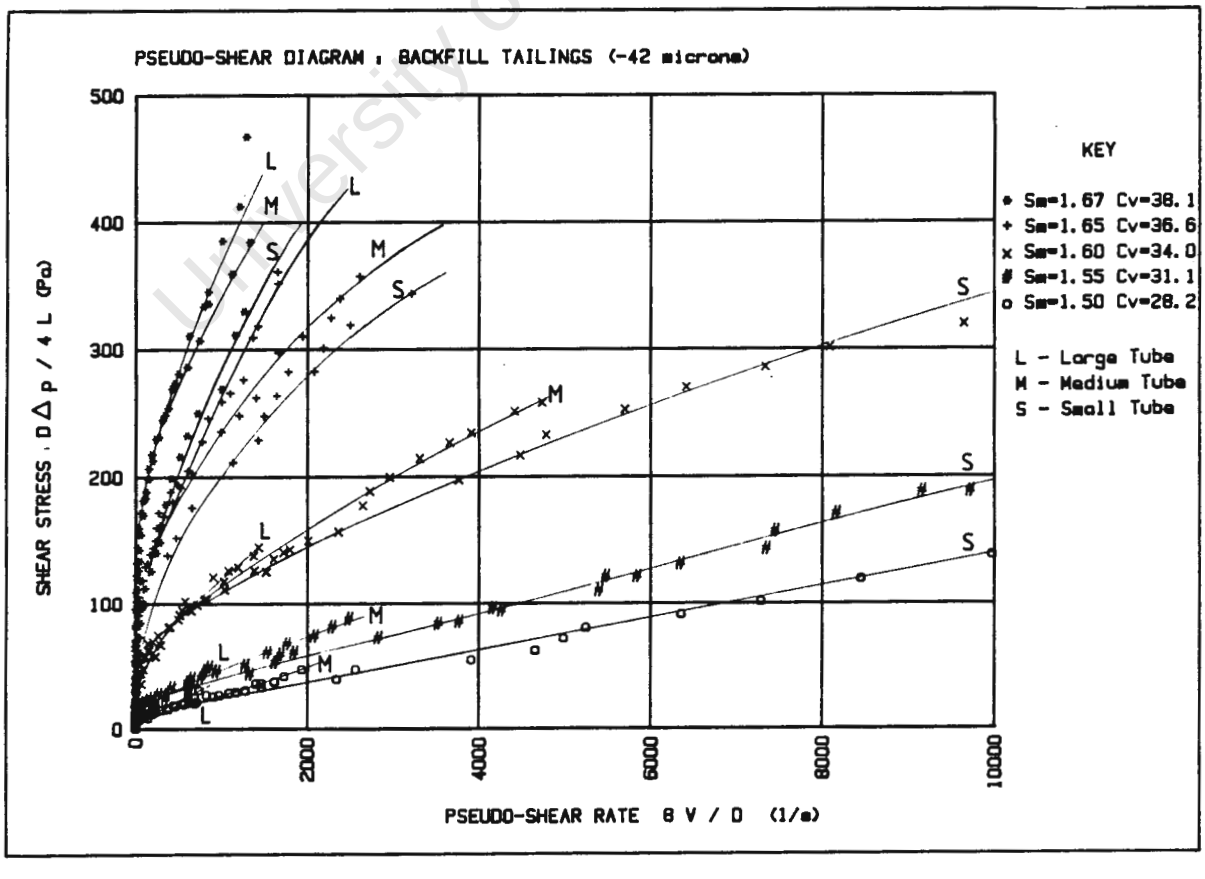

Fig. 6.5 Combined pseudo-shear diagrams for the -42 μm fraction of the backfill tailings.

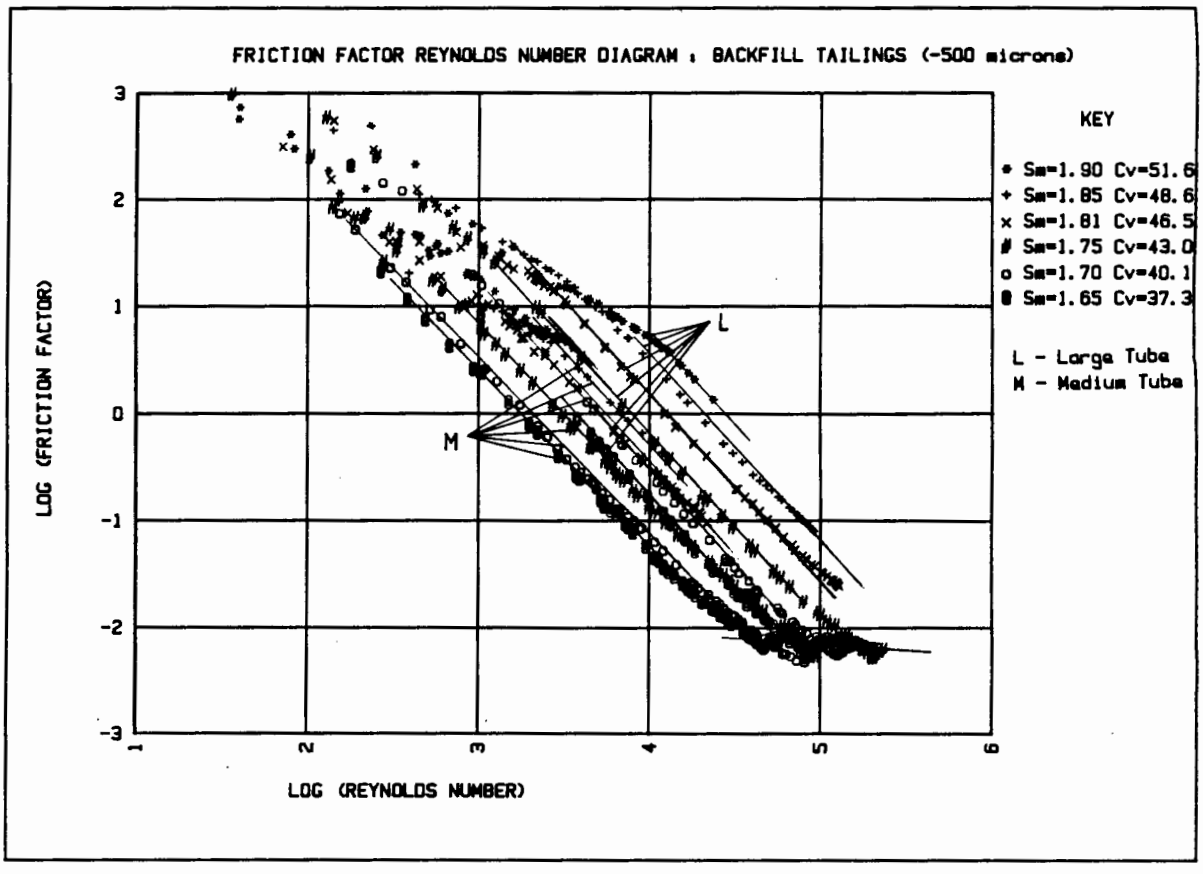

Fig. 6.6 Friction factor Reynolds number diagram for the -500 μm fraction of the backfill tailings.

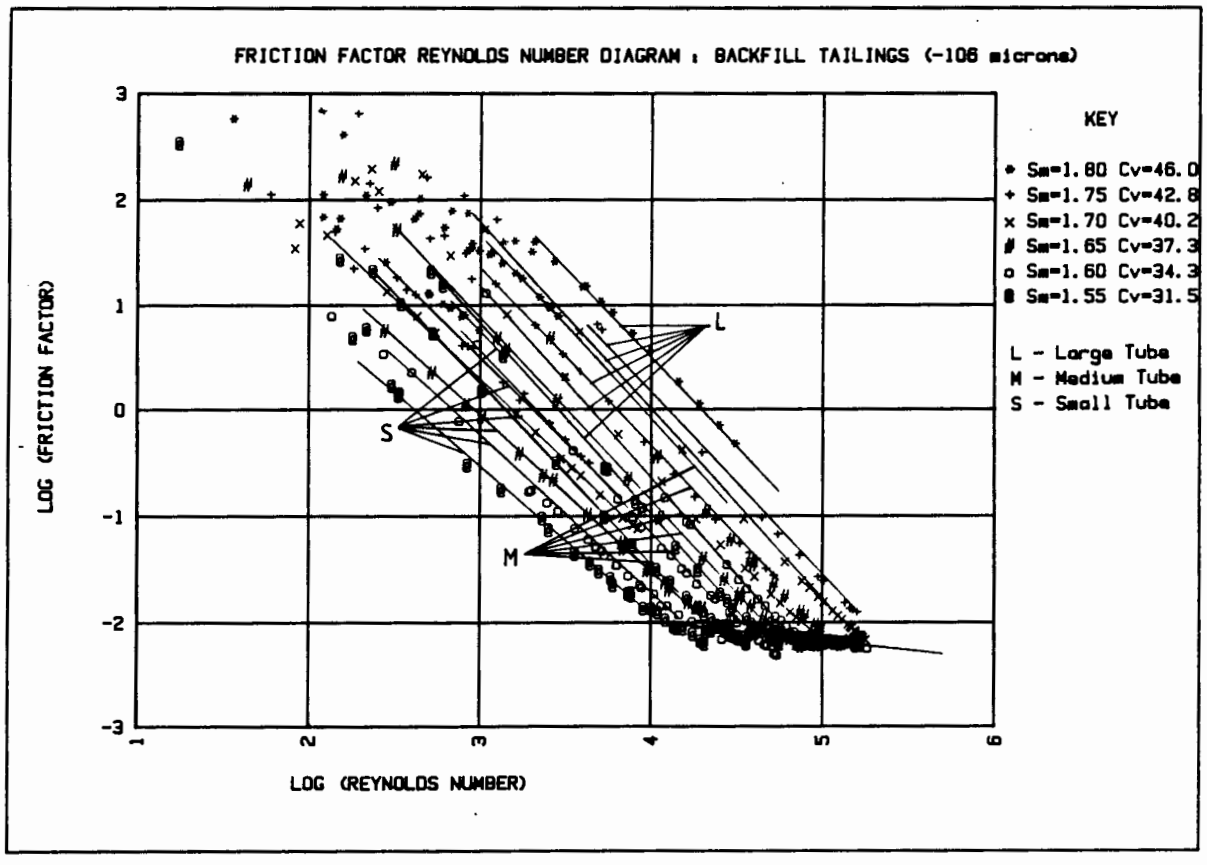

Fig. 6.7 Friction factor Reynolds number diagram for the -106 μm fraction of the backfill tailings.

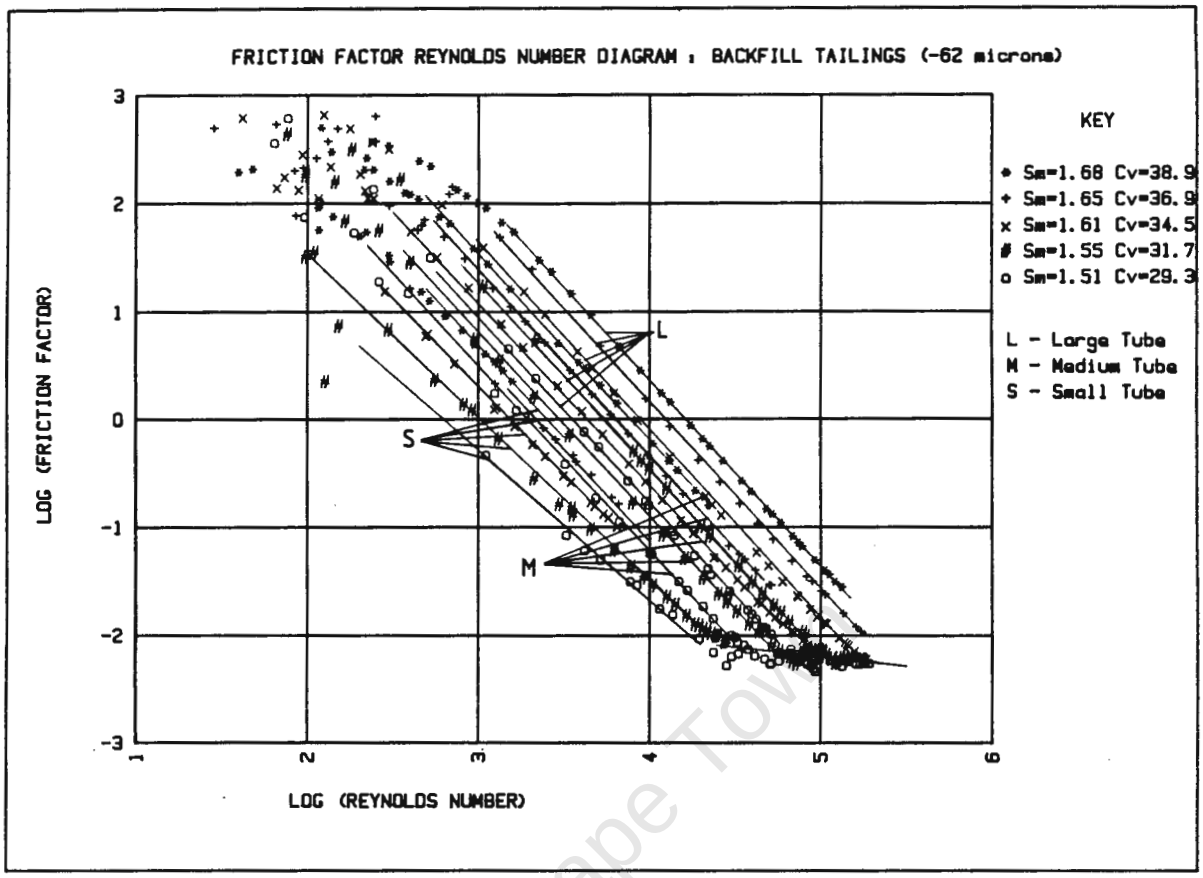

Fig. 6.8 Friction factor Reynolds number diagram for the -62 μm fraction of the backfill tailings.

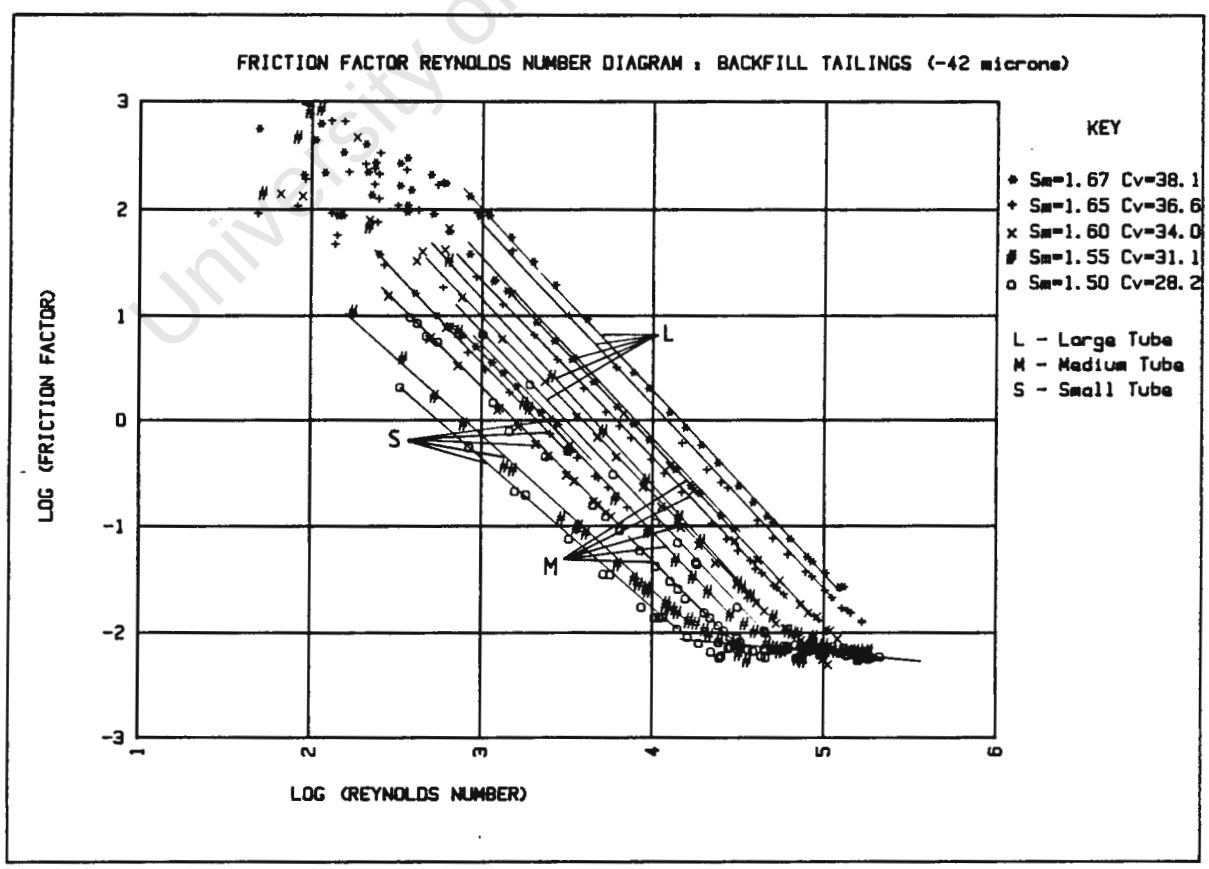

Fig. 6.9 Friction factor Reynolds number diagram for the -42 μm fraction of the backfill tailings.

CHAPTER 7

ANALYSIS OF EXPERIMENTAL RESULTS

7.1 INTRODUCTION

The author is confident that the measurements taken are an accurate representation of the intended quantities. It is assumed that the variations in pH and temperature are not significant enough to affect the rheology.

The pseudo-shear diagrams presented in Chapter 6 consist of clearly defined laminar and turbulent flow curves. The transition from laminar to turbulent flow is distinguishable as a sharp increase in the slope of the pseudo-shear diagrams. Instability in differential pressure measurements was recorded at these times.

The low concentration results are discussed in Section 7.2 and the high concentration results are discussed in Section 7.3.

7.2 TUBE FLOW THEORY

At low concentrations (C_v < 30%, S_m < ± 1.55) the pseudo-shear diagrams do not exhibit tube diameter dependence in the laminar flow region. At these concentrations the slurry behaves as a single phase fluid and is analysed using tube flow theory. The rheology of the lowest concentration of each particle size distribution is characterized using equation 2.13, the procedure described in Section 2.8.2 and the program described in Appendix C. The results of this procedure are presented in Table 7.1.

Table 7.1 Results of the rheological characterization of low concentration backfill tailings.

Particle Size (μm)	Slurry Relative Density (S_m)	Yield Stress (T_y)	Fluid Consistency Index K	Flow Behaviour Index n	Error in 8V/D per point
-500	1.651	6	0.09424	0.8309	5.8
-106	1.551	5	0.02687	0.8955	38.7
- 62	1.514	12	0.04179	0.8902	31.3
- 42	1.501	8	0.03708	0.8791	42.8

The fitted curves are plotted with the original data in Fig 7.1 to Fig. 7.4. The rheology is characterized using the yield-pseudoplastic model (shear thinning).

These results show that the rheology changes continuously with an increase in maximum particle size. Duckworth et al (1983) found that rheology changed significantly with the addition of coarser particles. The hypothesis made by Hanks and Hanks (1982) that a rheologically active fraction of the solid particles exists is contradictory to these findings and therefore unrealistic.

The friction head loss of low concentration backfill tailings in laminar flow can be predicted using equation 2.13 and the results in Table 7.1.

7.3 ANOMALOUS BEHAVIOUR

At high concentrations (C_v > 30%, S_m > ± 1.55) the pseudo-shear diagrams exhibit anomalous behaviour in the form of a tube diameter dependence that becomes more substantial with concentration.

The particle alignment near the tube wall documented by Bain and Bonnington (1979) is not the cause of the anomalous behaviour because the shapes of the solid particles shown in the micrographs are not elongated.

It has been established that the anomalous behaviour is not caused by settling of the solid particles, time dependency or undeveloped flow. Experimental errors are insignificant because the low concentration results are consistent with the theory.

The -60 μm fraction of backfill tailings at S_m = 1.68 shown in Fig. 7.5 is taken as a representative sample of the high concentration results. This representative test is evaluated in the following subsections using the theories outlined in Section 2.10 to 2.14.

7.3.1 Effective slip

The representative test results are analysed using effective slip theory described in section 2.9. A verification of the programs used for this analysis by hand showed no significant arithmetical errors.

The first step of the procedure is to plot a graph of τ_o versus $Q/\pi R^3 \tau_o$ shown in Fig. 7.6. From this a graph of $Q/\pi R^3 \tau_o$ versus 1/R at various fixed values of τ_o is plotted and shown in Fig. 7.7. The slopes of these lines which correspond to the effective slip coefficients β are calculated at each value of τ_o. At high velocities the slope of the graphs begin to vary and are approximated by straight lines. A graph of the slip velocity versus shear stress is then plotted and is shown in Fig. 7.8. Using this graph the measured data is corrected for effective slip shown in Fig. 7.9. The results of this analysis for other high concentration tests yield similar results.

It is evident that the measured data is overcorrected for slip yielding negative velocities which are clearly erroneous. A possible cause of this outcome may be that instead of a reduction in concentration near the wall which occurs in monodisperse mixtures, a gradual change in particle size distribution occurs near the wall which is expected if the mixture is polydisperse.

7.3.2 Dense-phase model

At high concentrations the applicability of rheology is questionable because at these concentrations the rheology, a property of the slurry becomes dependent on tube diameter. It is possible that the backfill tailings flow as a plug with sliding friction due to the solid particles forming the largest part of the overall head loss as proposed by Streat (1986). The representative test results are plotted on a graph of hydraulic gradient (i_m) versus mean mixture velocity (V_m) shown in Fig. 7.10. The equation proposed by Streat (1986) is plotted on this graph for comparison using a random value for the coefficient of sliding friction. Variation of the coefficient of sliding friction results in a vertical shift of the theoretical curve.

The predicted hydraulic gradient has a substantially different shape to the data. This may be due to a coefficient of sliding friction that is dependent on velocity. Variations in the coefficient of sliding friction with mean mixture velocity may be be examined by making it the subject of equation 2.27. The test results shown in Fig. 7.10 are then used to plot a graph of the coefficient of sliding friction versus mean mixture velocity shown in Fig. 7.11. It is clear from Fig. 7.11 that the coefficient of sliding friction is dependent on velocity and is different for each tube diameter.

A fundamental assumption for dense-phase flow theory is that the submerged weights of the solid particles are transferred to the tube invert by particle-particle interactions. The backfill tailings are non-settling therefore assumption is not correct.

It may be concluded that the flow is not dense-phase and that the overall head loss is not due to sliding friction caused by the solid particles.

7.3.3 Wall effect

The pseudo-shear diagrams presented in Section 6 appear less viscous in the smaller diameter tubes. This may be caused by a wall effect described in Section 2.12.

A test described in Section 4.1.3 was conducted to detect differences between *in situ* concentration (C_{vt}) and delivered concentration (C_{vd}) in different tube diameters. If a wall effect occurs the difference between the *in situ* concentration and the delivered concentration will vary with tube diameter. The concentration tested was high enough for the diameter dependence to be significant. No difference between the *in situ* concentration and the delivered concentration was observed.

A reduction in *in situ* concentration is therefore not responsible for the anomalous behaviour as recorded by Maude and Whitmore (1955). This may be ascribed to the substantial difference in diameter ratio (d_{50}/D) between these tests and the tests conducted by Maude and Whitmore (1955). The redistribution of solid particles away from the tube wall will reduce the *in situ* concentration compounded with a change in the velocity profile which would affect the measured rheology contrary to the proposed theory.

7.3.4 Boundary-layer effect

The initial sections of the pseudo-shear diagrams for each diameter and particle size distribution have the same slope shown in Fig. 7.12. This is confirmation that a boundary-layer may exist. The representative test results are analysed using the boundary-layer theory described in Section 2.13. The slopes (ϵ) of the initial sections of the pseudo-shear diagrams shown in Fig. 7.13 are measured. The viscosity of water is used for the boundary-layer. The thicknesses of the boundary-layers in each tube diameter that would produce these results are calculated using equation 2.33 and presented in Table 7.2.

Table 7.2 Boundary-layer thickness in each tube diameter.

Nominal Tube Diameter (mm)	Slope (ϵ) (Pa s)	Boundary-Layer Thickness (δ) (μm)
28	8	0.43
13	4	0.42
4	1	0.52

The measured velocity is corrected using this data and plotted on a graph shown in Fig. 7.14. The corrected data for this and other high concentration tests exhibit a substantially higher yield stress and marginally increased consistency.

The existence of a boundary-layer is credible however it has not yet been proven. The diameter dependence in the corrected data is still not accounted for.

7.3.5 Modified friction factors

The data plotted on log friction factor log Reynolds number diagrams in Chapter 6 have a constant slope. The data is expected to lie on a single curve just as the data for a Newtonian fluid is expected to lie on the laminar flow curve $f = 16/Re$. The spread of data may be due to anomalous behaviour or the use of an inappropriate Reynolds number. The use of a viscous term in the Reynolds number that is derived from the pseudo-shear diagram such as the apparent viscosity would result in a graph of the friction factors versus its inverse. Therefore the Reynolds number of water at the mean mixture velocity is used as an approximation.

The representative test results are plotted on a friction factor Reynolds number diagram shown in Fig. 7.15. The equation proposed by Shook (1985) and the effect of the dimensionless coefficients K and m are shown for comparison in Fig. 7.15. The slope of the data is significantly different from the slope of the equation proposed by Shook (1985). The turbulent flow data appear to lie on a distinctive line.

The slurry's behaviour is therefore not governed by partial hydrodynamic lubrication if it occurs at all. The equation proposed by Shook (1986) does however theoretically account for some form of diameter dependence.

7.4 CONCLUSIONS

The theories presented in the literature and theory chapter have been evaluated using extensive test results on backfill tailings obtained in the Balanced Beam Tube Viscometer.

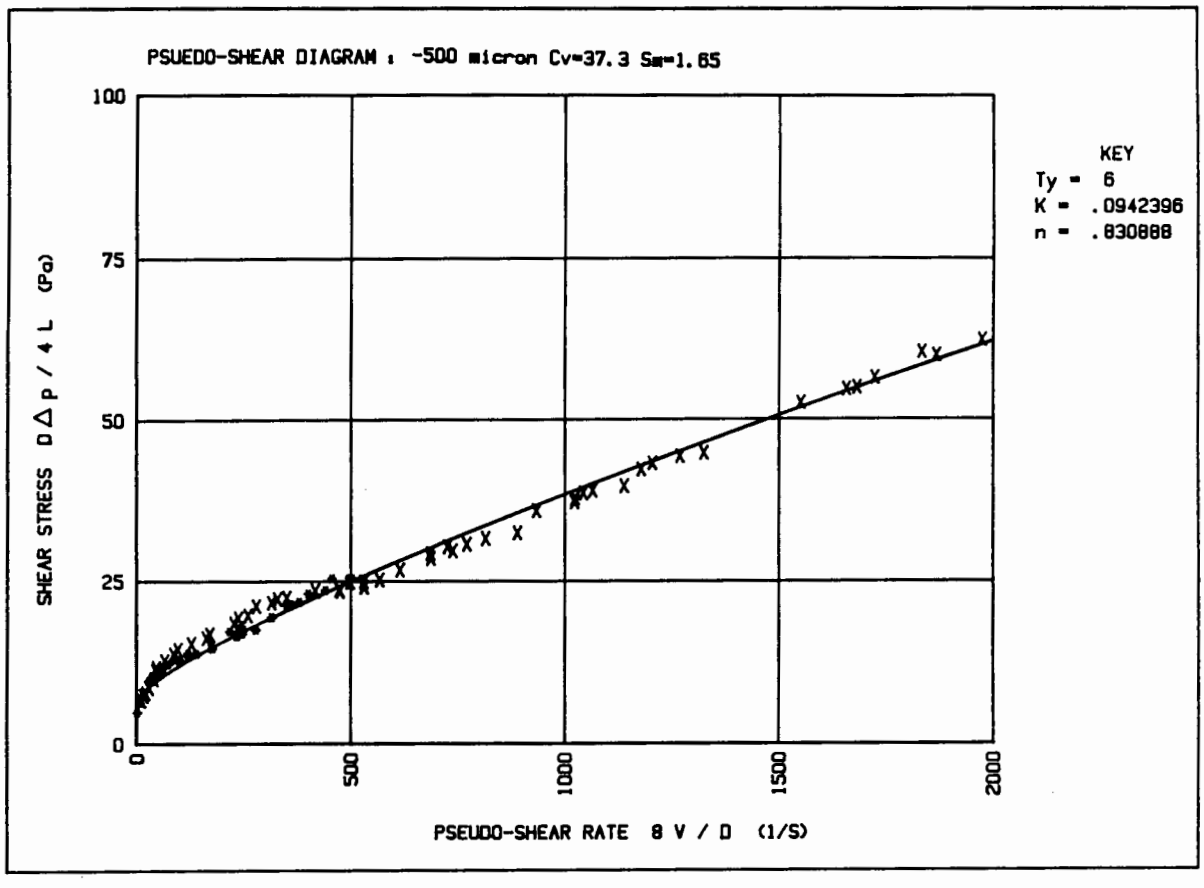

Fig. 7.1 Rheological characterization of the -500 μm fraction of the backfill tailings at the lowest concentration tested.

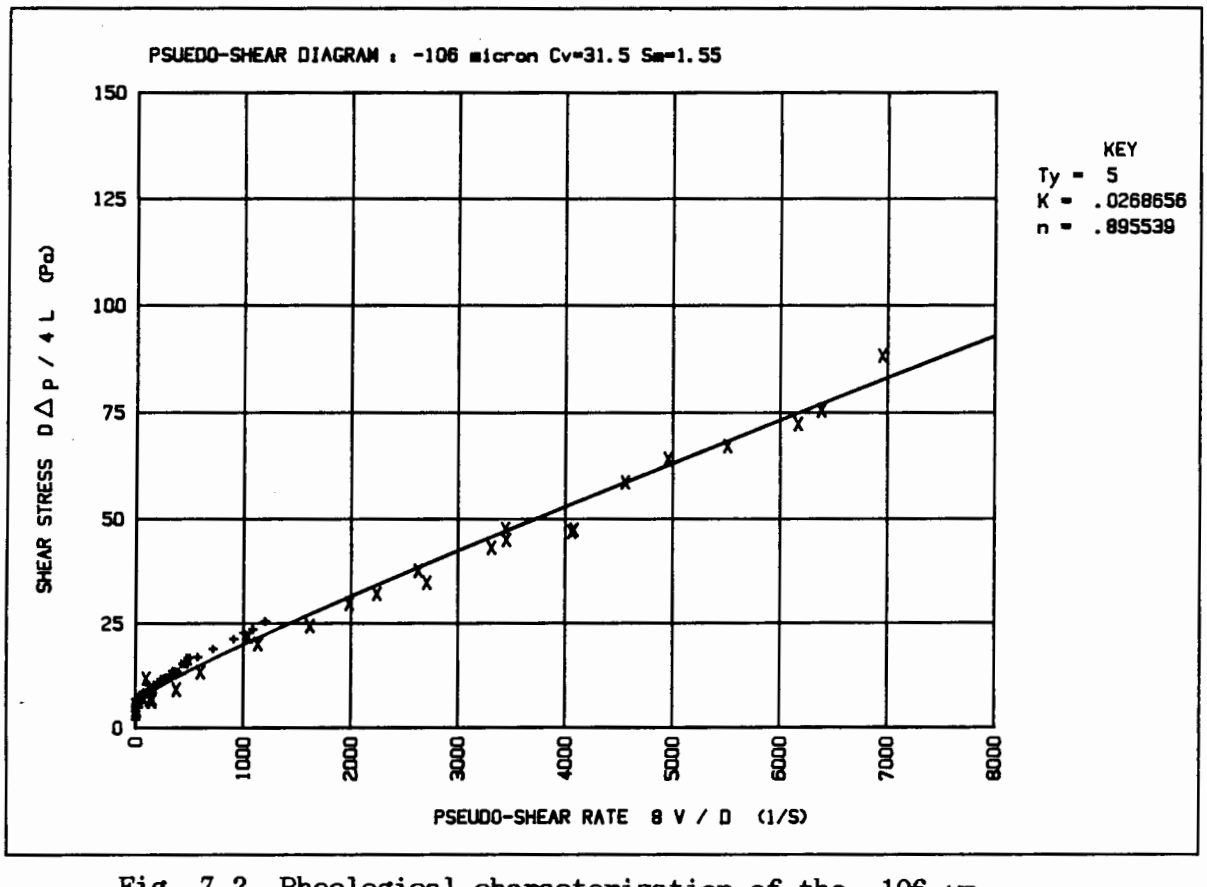

Fig. 7.2 Rheological characterization of the -106 μm fraction of the backfill tailings at the lowest concentration tested.

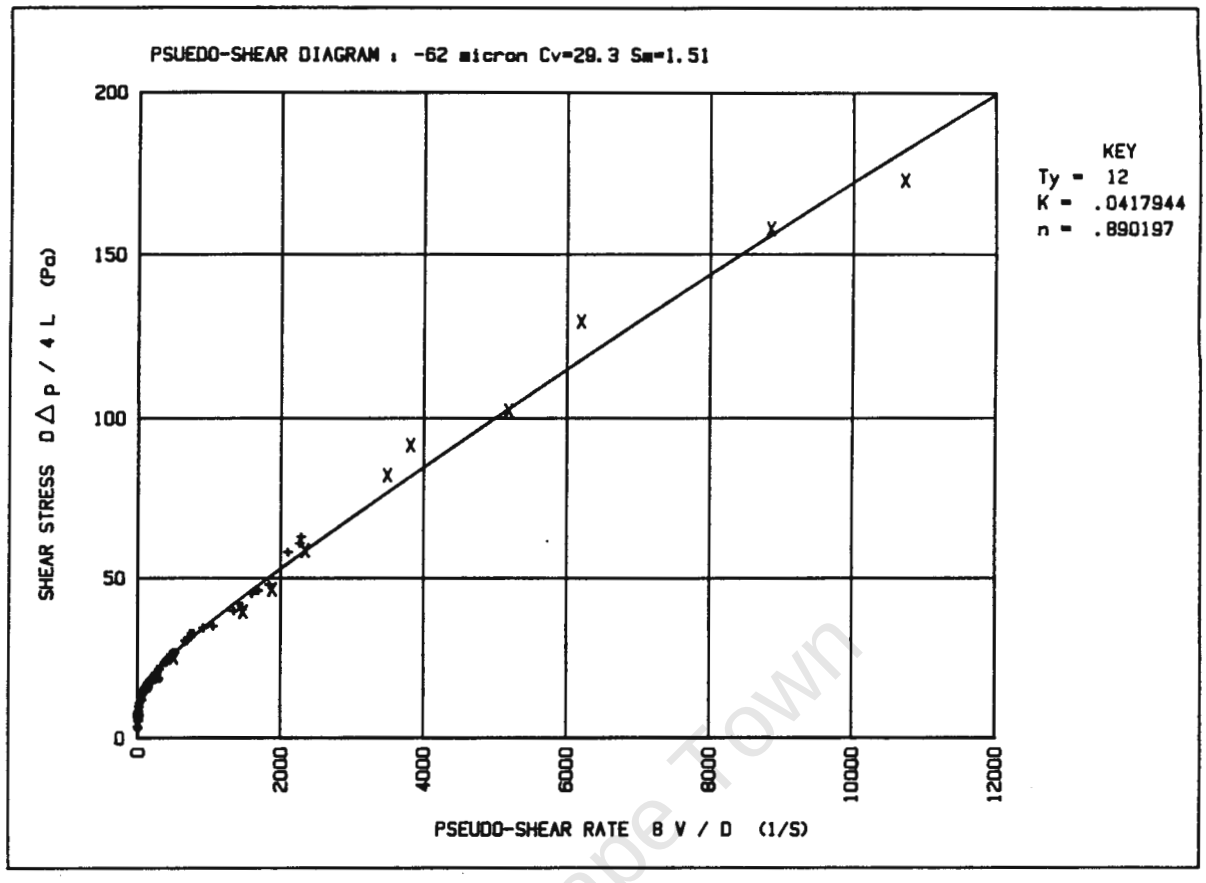

Fig. 7.3 Rheological characterization of the -62 μm fraction of the backfill tailings at the lowest concentration tested.

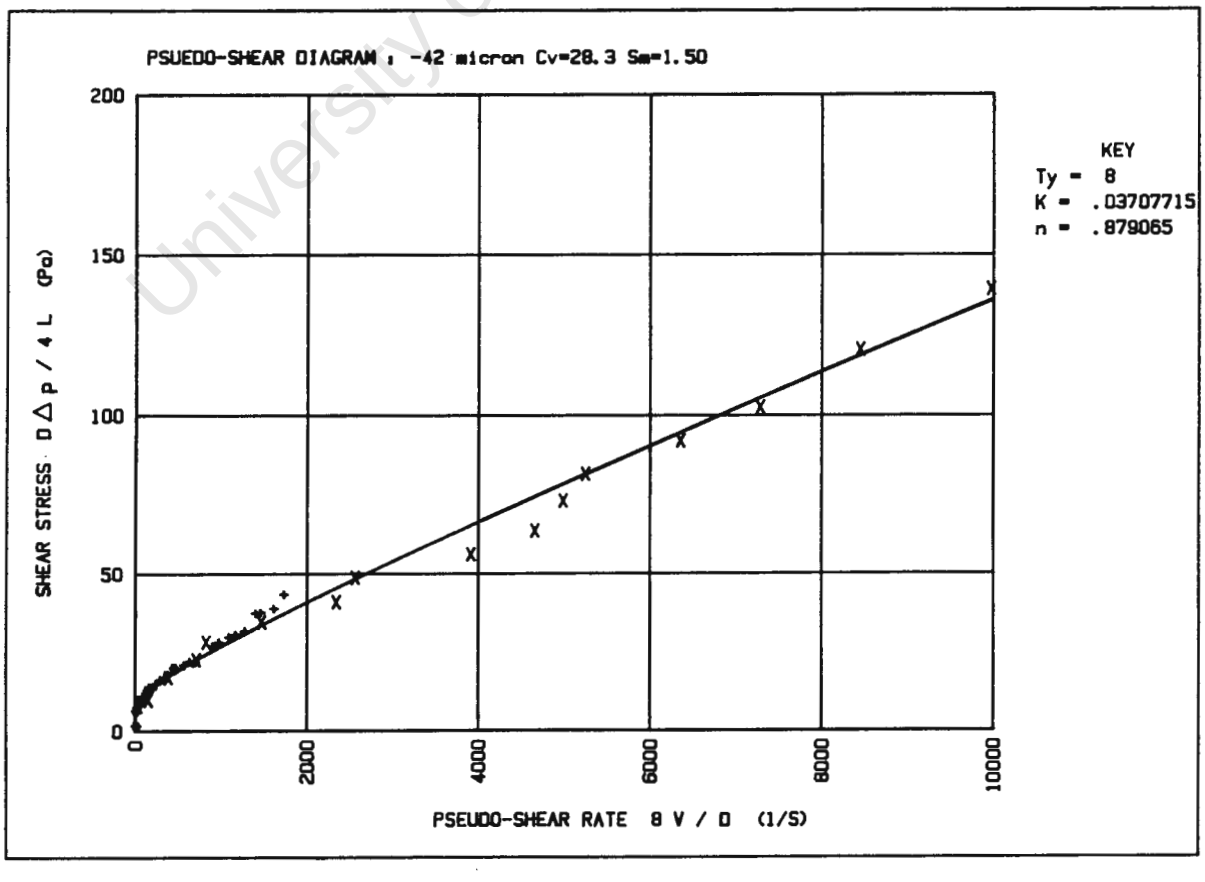

Fig. 7.4 Rheological characterization of the -42 μm fraction of the backfill tailings at the lowest concentration tested.

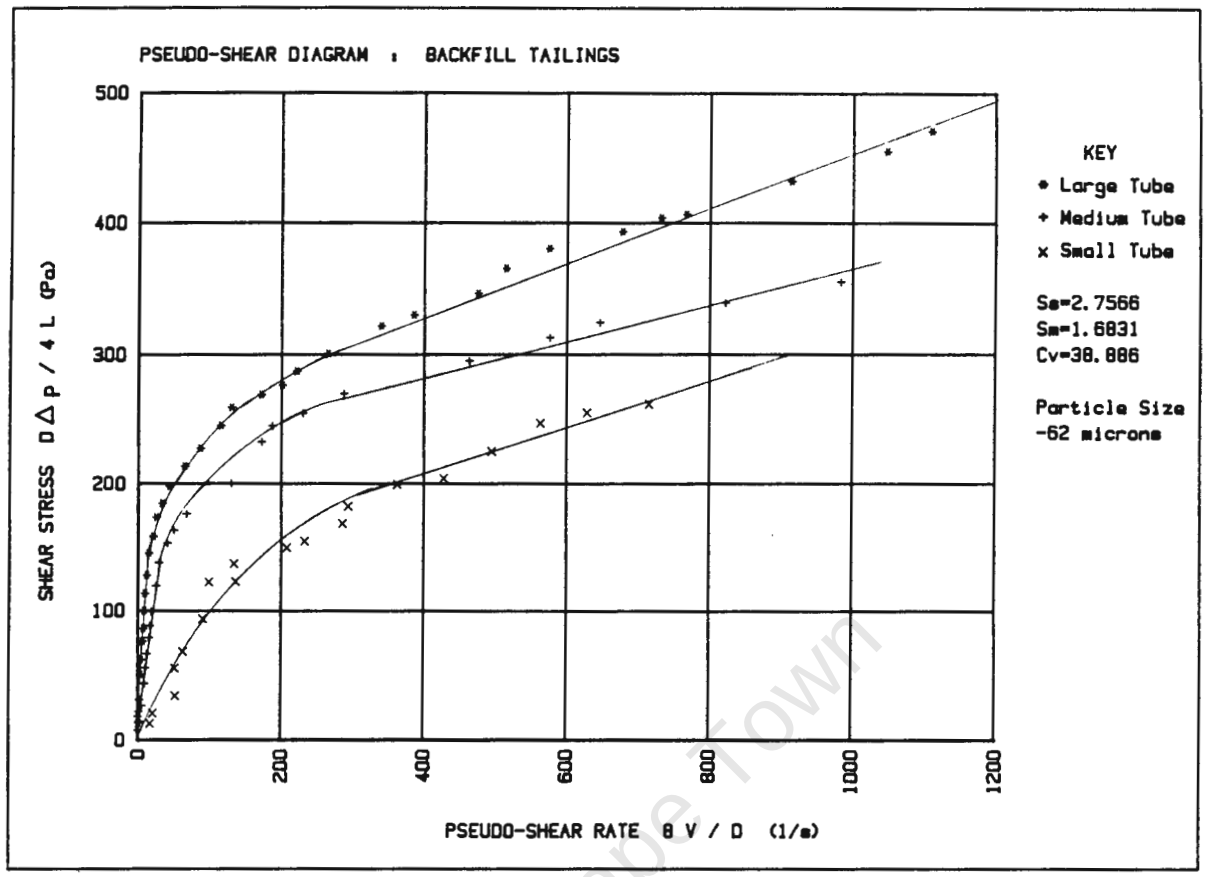

Fig. 7.5 Representative sample of high concentration anomalous behaviour used for analysis.

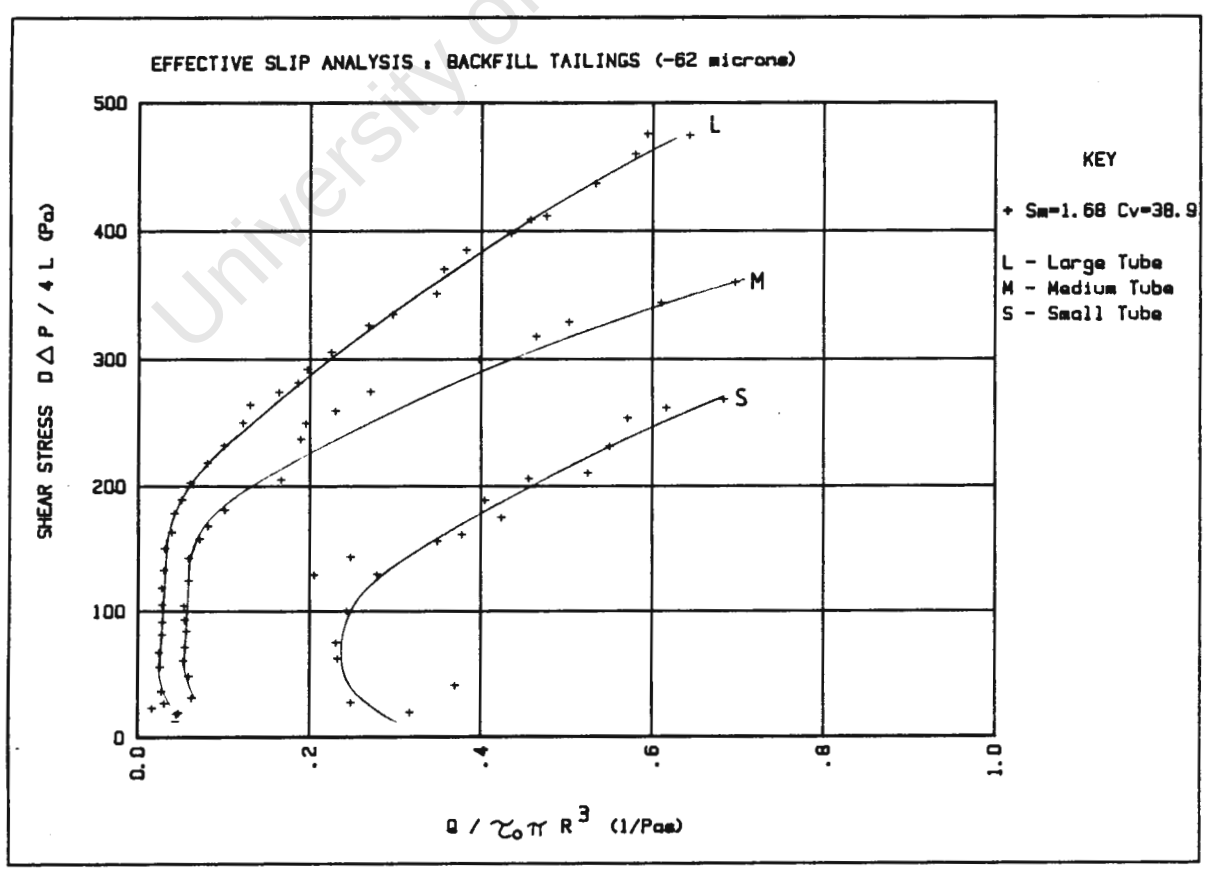

Fig. 7.6 Effective slip analysis - intermediate graph.

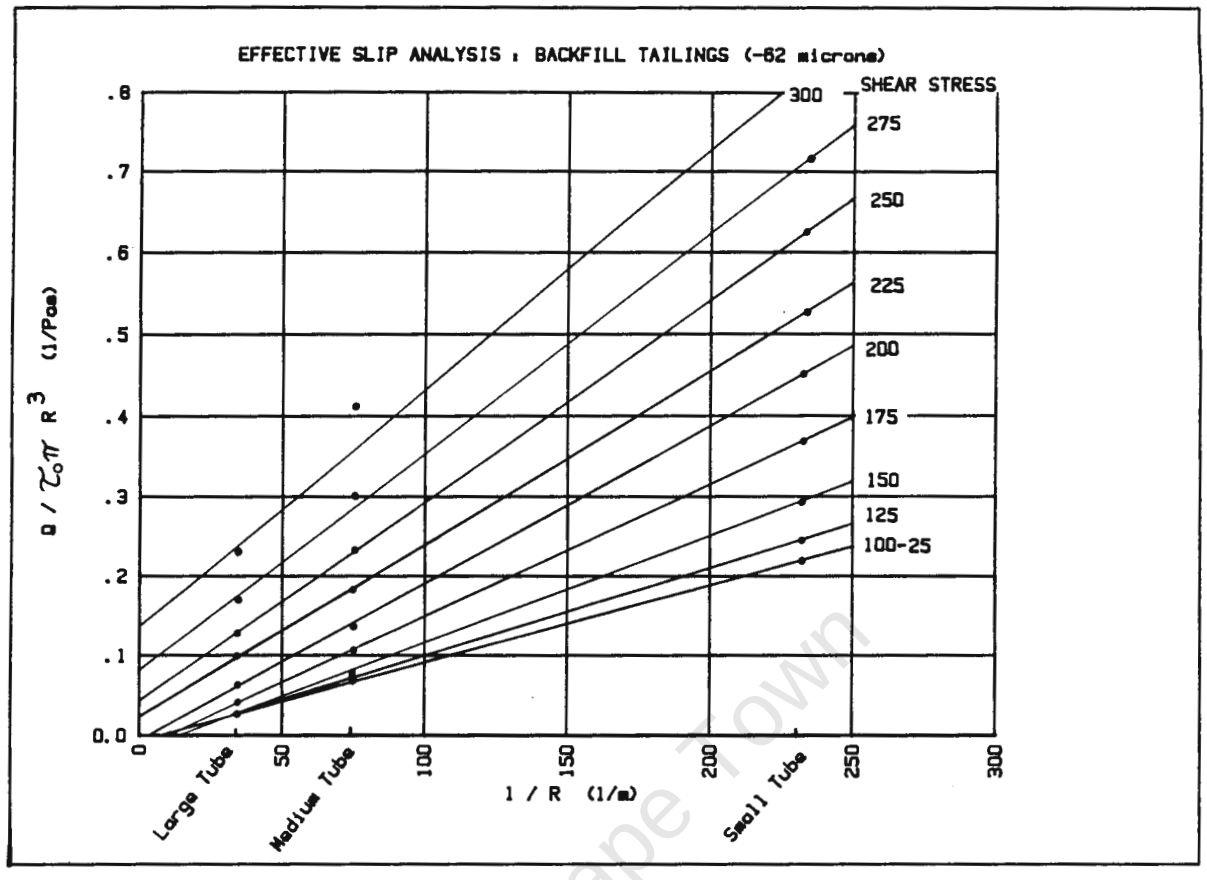

Fig. 7.7 Effective slip analysis - graph used to determine β.

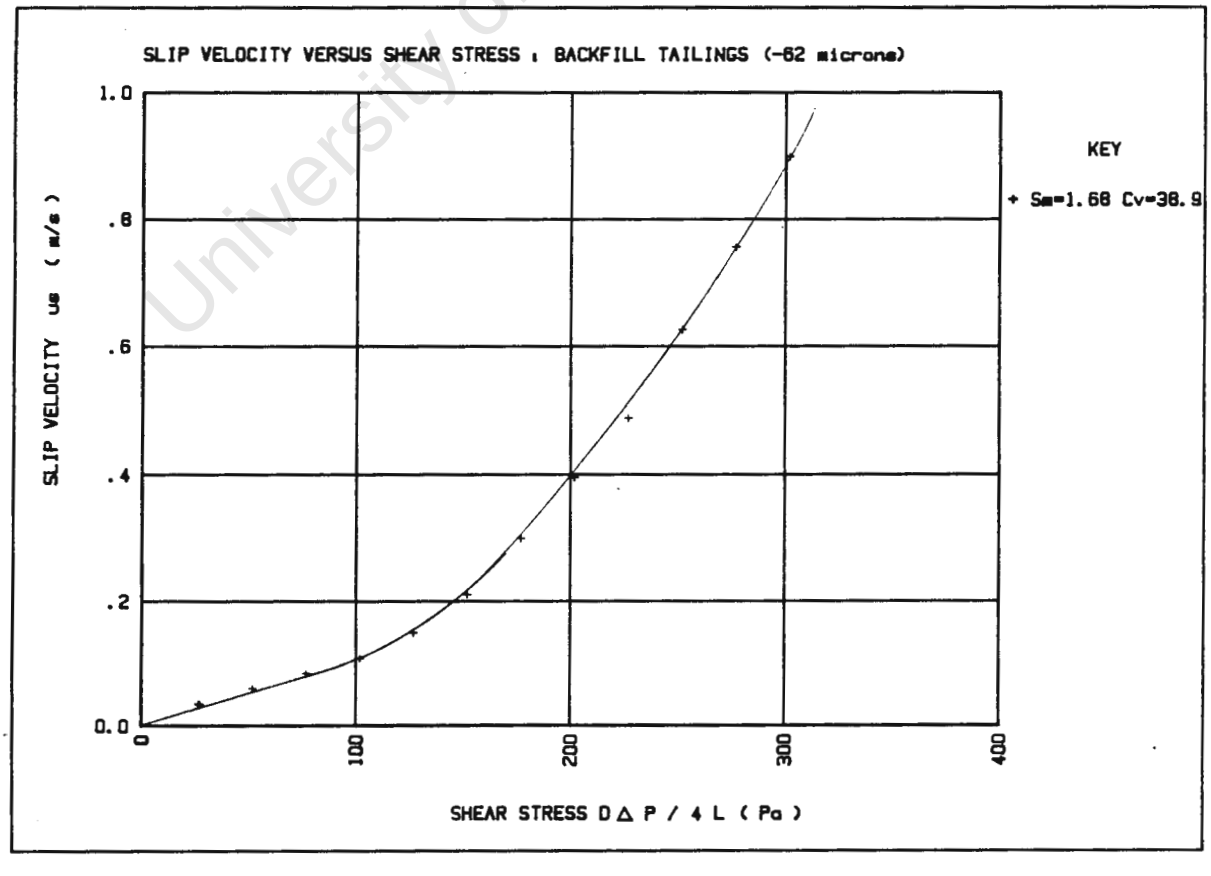

Fig. 7.8 Effective slip analysis - variation of slip velocity with shear stress.

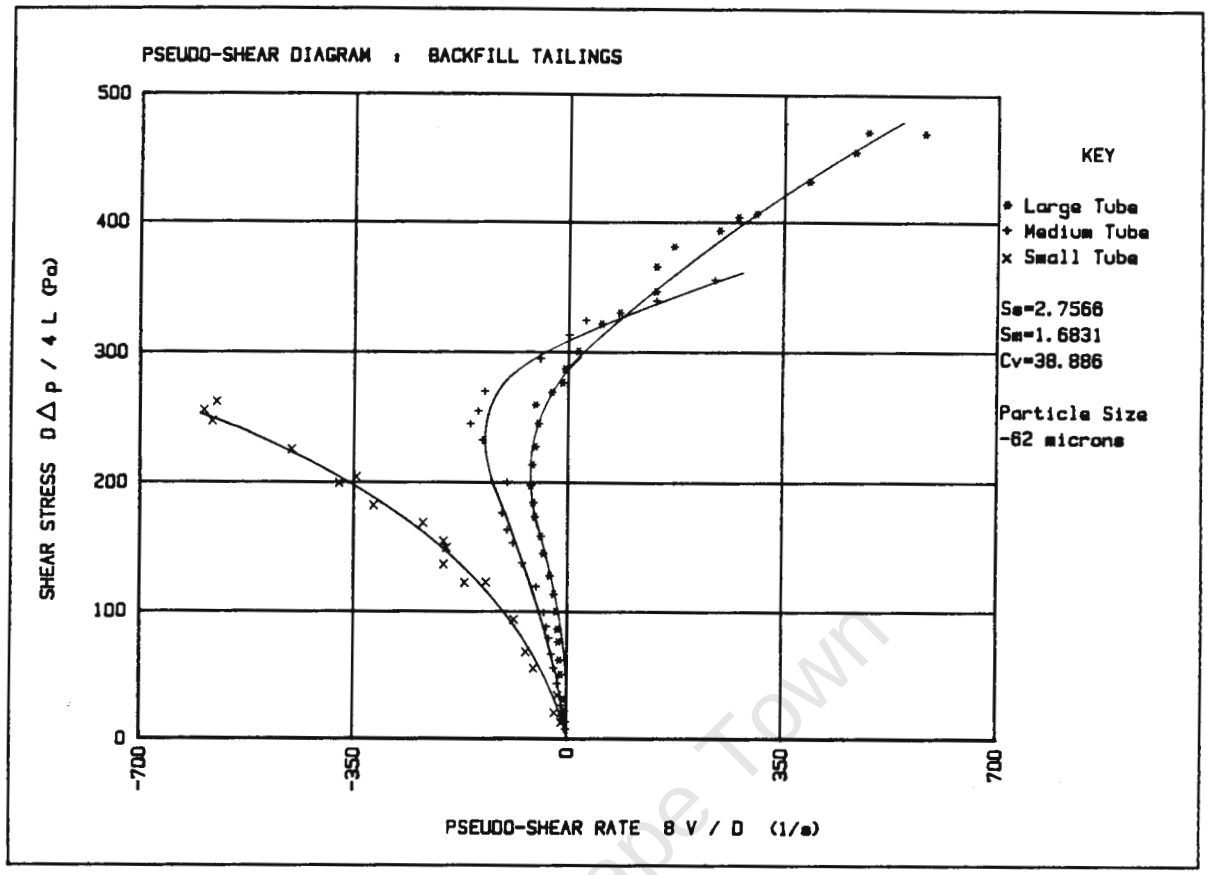

Fig. 7.9 Effective slip analysis - corrected pseudo-shear diagram.

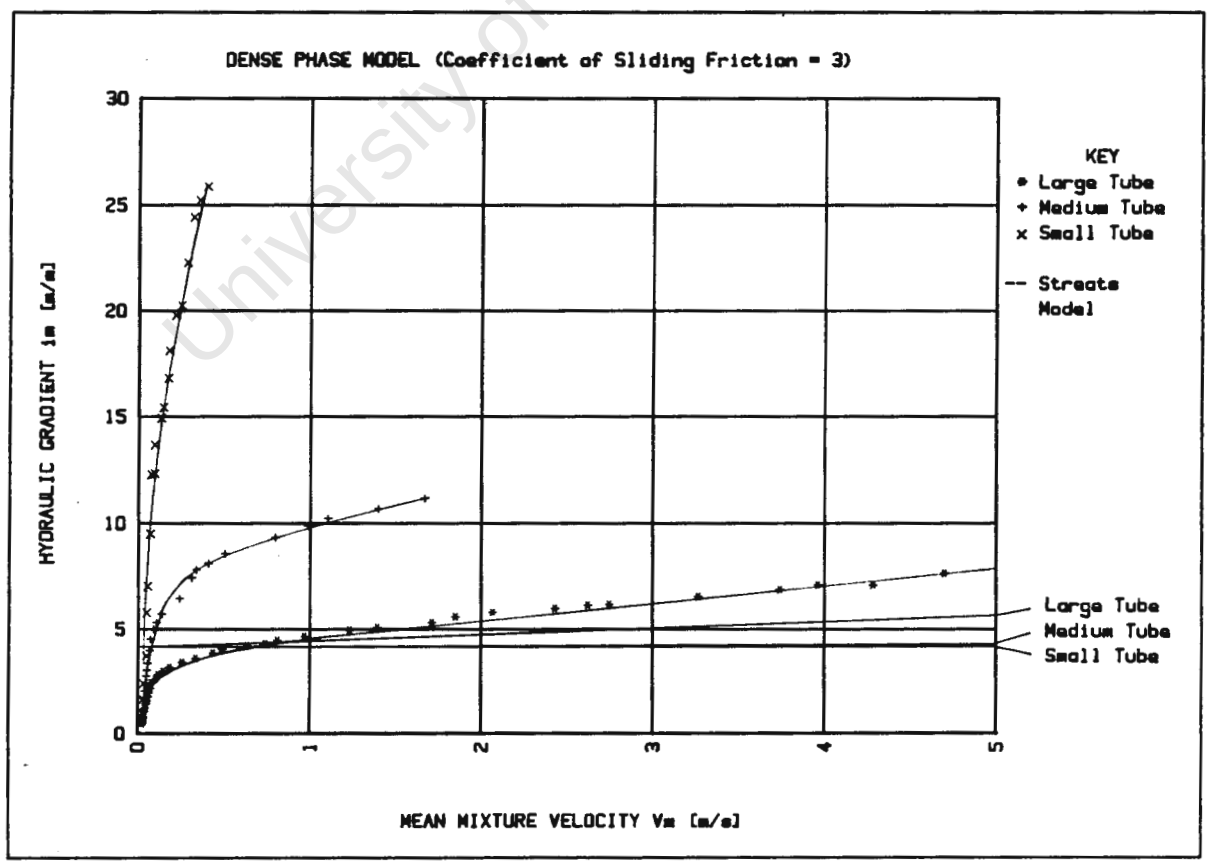

Fig. 7.10 Dense-phase model - experimental and theoretical hydraulic gradients.

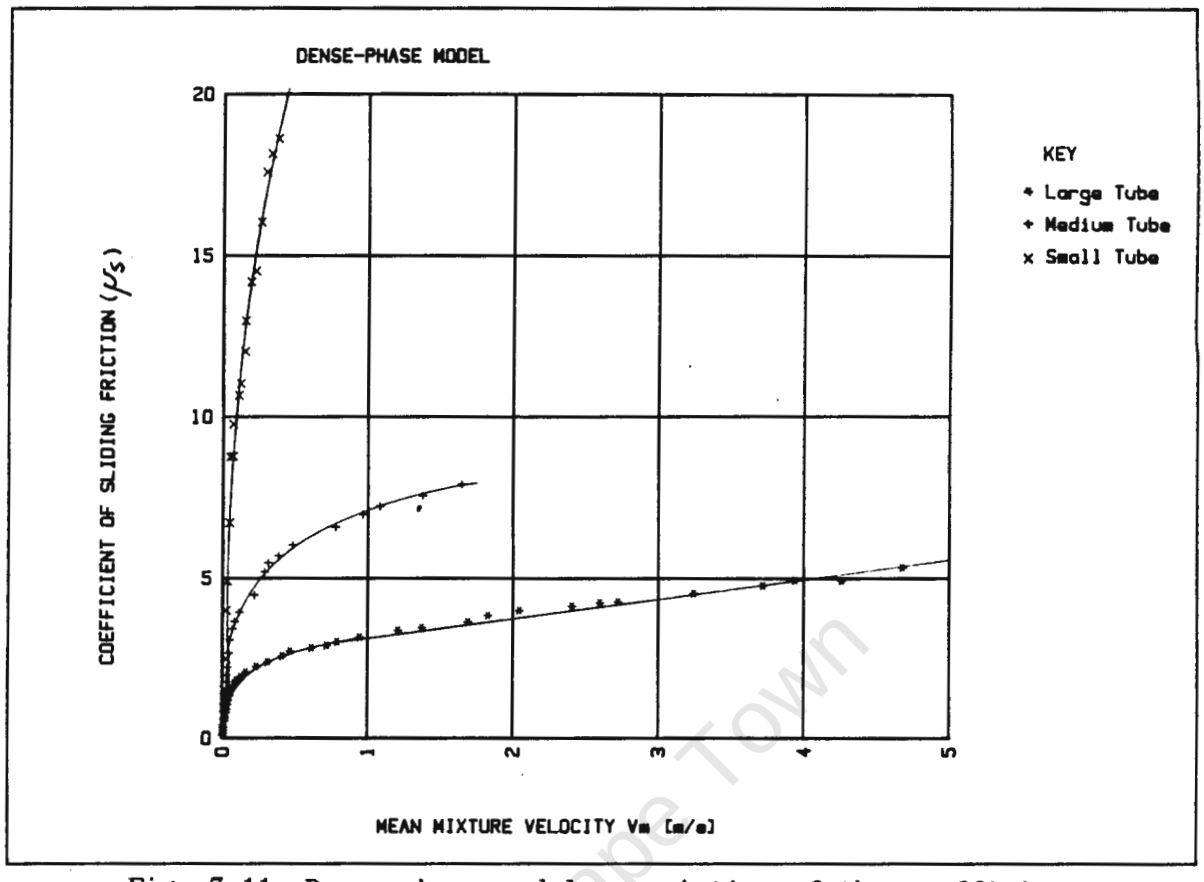

Fig. 7.11 Dense-phase model - variation of the coefficient of sliding friction with velocity.

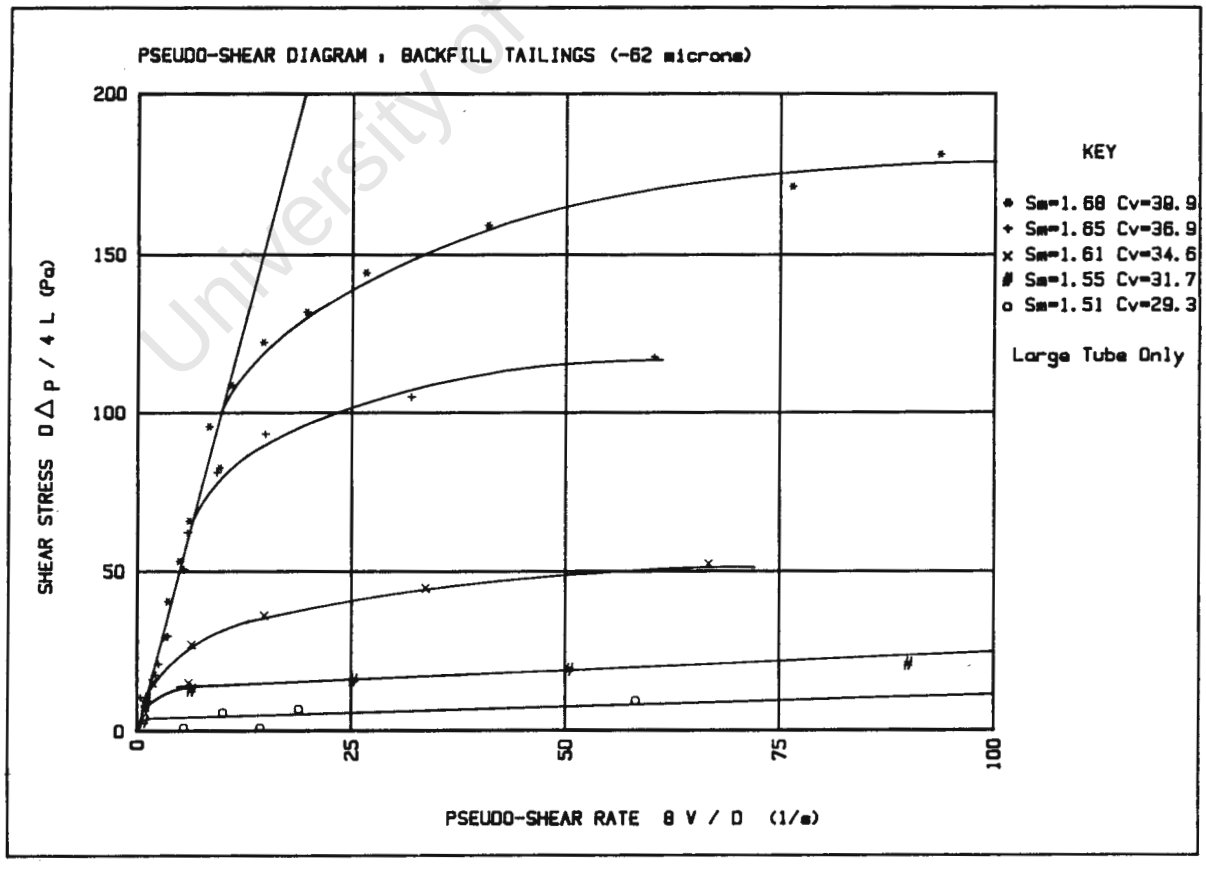

Fig. 7.12 Boundary-layer effect - coincidence of the initial sections of the pseudo-shear diagrams for a fixed particle size distribution and tube diameter.

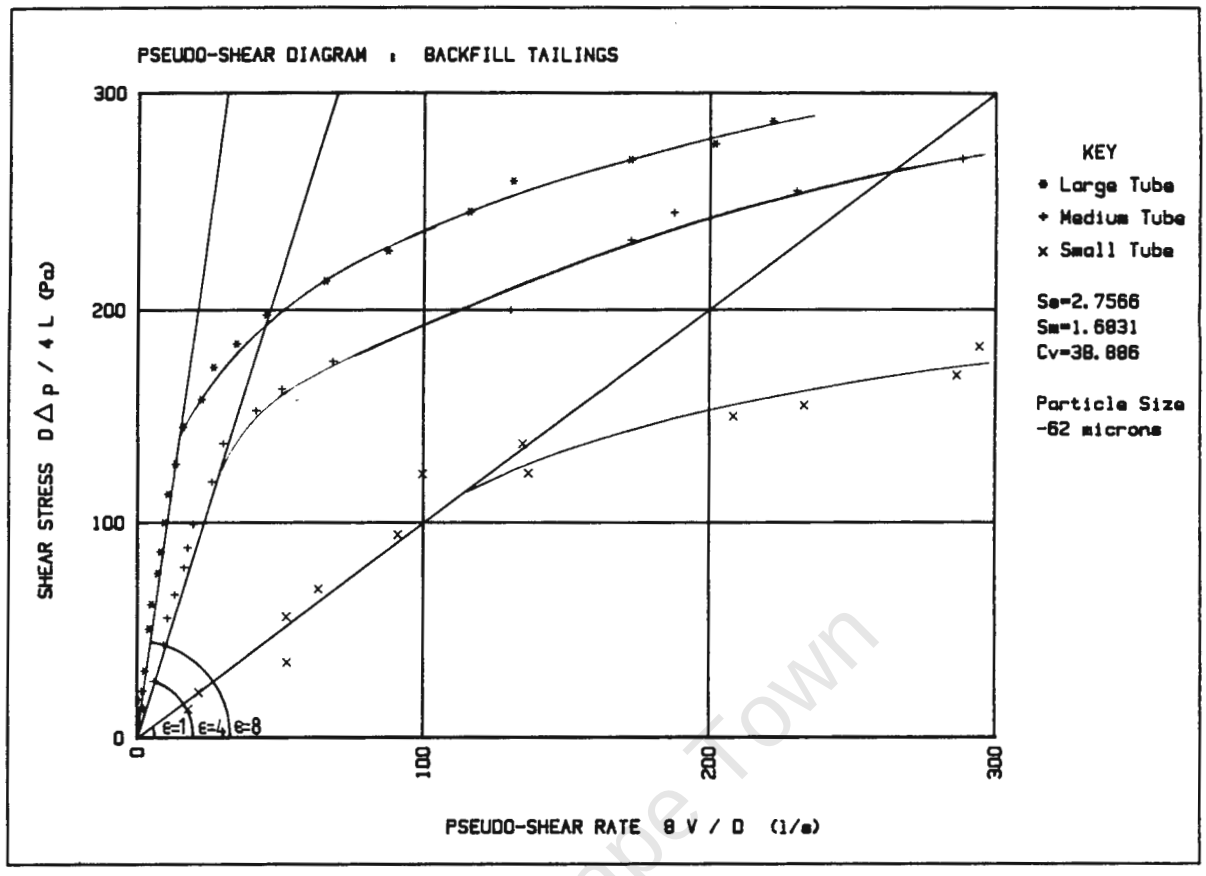

Fig. 7.13 Boundary-layer effect - measured slopes of the initial sections of the pseudo-shear diagrams for each tube diameter.

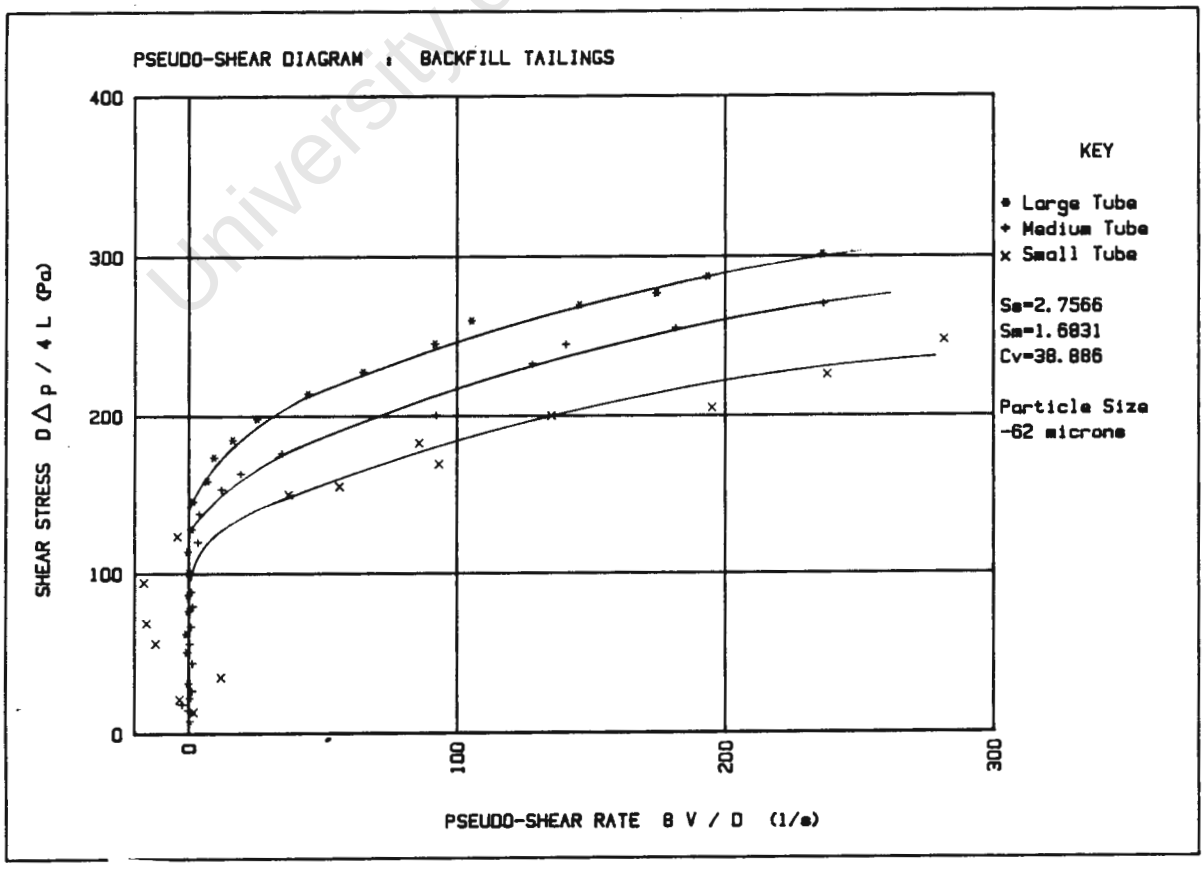

Fig. 7.14 Boundary-layer effect - corrected pseudo-shear diagram.

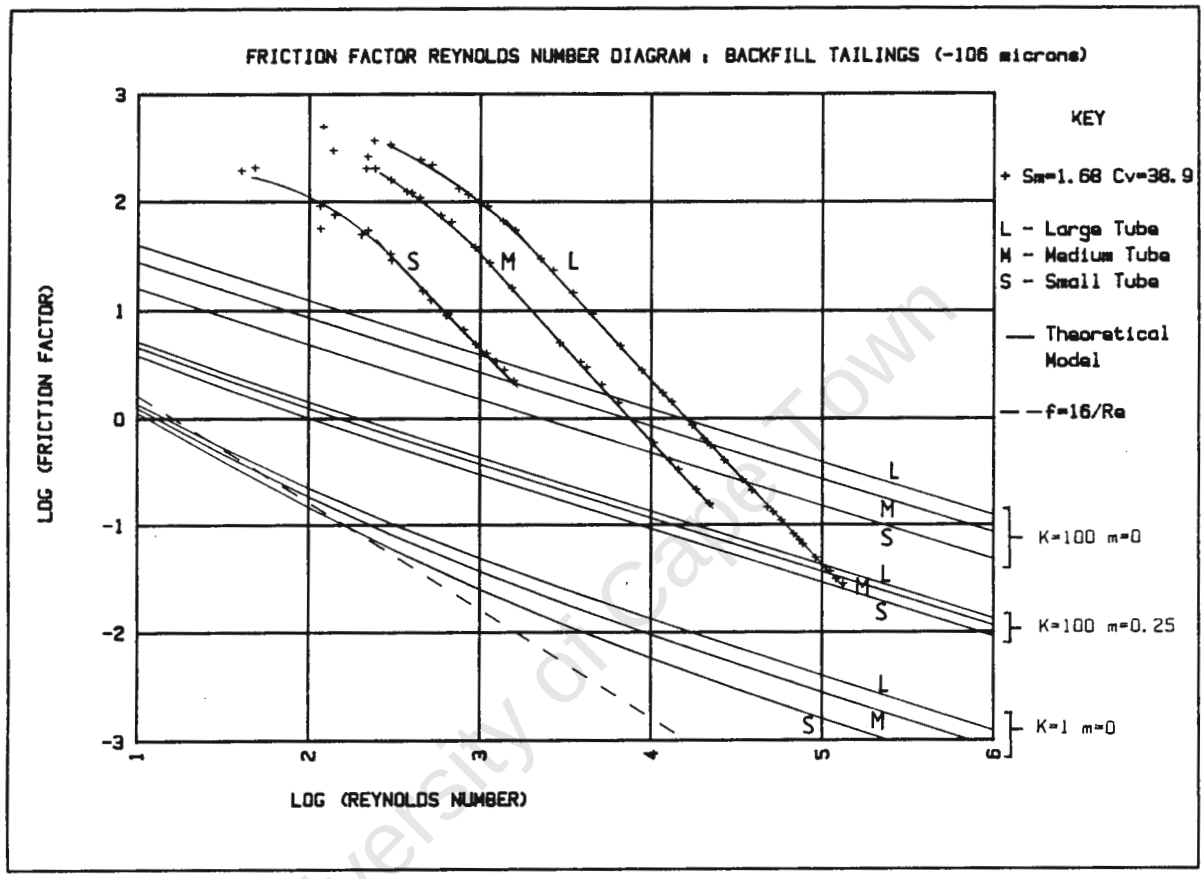

Fig. 7.15 Modified friction factors - friction factor Reynolds number diagram showing experimental and theoretical curves.

CHAPTER 8

CONCLUSIONS AND RECOMMENDATIONS

1. The Balanced Beam Tube Viscometer is an instrument capable of collecting reliable laminar and turbulent flow data as well as the laminar-turbulent transition. The errors in the measurements taken are within acceptable limits.

2. The backfill tailings were tested in the viscometer and exhibited two distinctive types of behaviour depending on concentration.

3. At low concentrations (Cv < 30%, Sm < ± 1.55) the backfill tailings behave as a single phase fluid. At these concentrations the rheology was successfully characterized using the yield-pseudoplastic model and a new curve fitting program.

4. At high concentrations (Cv > 30%, Sm > ± 1.55) the backfill tailings exhibited anomalous behaviour in the form of a marked tube diameter dependence.

5. The anomalous behaviour is not due to incorrect measurements, time dependency, settling of the solid particles or undeveloped flow.

6. Effective slip analysis accounts for diameter dependence but yields negative velocities. If effective slip occurs it can therefore not be corrected for using this technique.

7. The flow is not dense-phase and the overall head loss is not due to sliding fiction caused by the solid particles.

8. The diameter dependence observed is not due to a reduction in *in situ* concentration caused by a wall effect.

9. The existence of a boundary-layer of liquid is credible however it has not yet been proven. Correction for a boundary-layer does not account for the anomalous behaviour.

10. The diameter dependence is theoretically accounted for using a modified friction factor that takes the hydrodynamic lubrication between solid particles and tube wall into account. A comparison between theoretical and predicted hydraulic gradients show that the hydrodynamic lubrication as formulated does not take place.

11. It is recommended that the velocity profile is experimentally determined using wall and traversing velocity probes. The experimental and theoretical (based on the rheology) velocity profiles may be compared thus verifying the rheology. The velocity profile will also enable the existence of a liquid layer near the wall to be investigated.

REFERENCES

BAIN, A.G. and BONNINGTON, S.T. (1970) "The Hydraulic Transport of Solids by Pipeline". Perganon Press Ltd. Oxford.

BAKER, P.J., JACOBS, B.E.A. and BONNINGTON, S.T. (1979) "A Guide to Slurry Pipelines". B.H.R.A.

BARR, G. (1931) "A Monograph of Viscometry". Oxford University Press.

BORNEMANN (1986) "Bornemann Pumpen - Eccentric Helical Rotor Pumps". Joh. Heinr.Bornemann and Co. Obernkirchen, Germany.

BRINKWORTH, B.J. (1968) "An Introduction to Experimentation". English University Press, London.

CHENG, D.C.-H. (1970) "A Design Procedure for the Pipeline Flow of Non-Newtonian Dispersed Systems". Proc. Hydrotransport 1, B.H.R.A., P.J5-77/95.

_____. (1975) "Pipeline Design for Non-Newtonian Fluids". The Chemical Engineer Part 1 September n.300 p.525-528 Part 2 October n.301 p.587-588.

DAVIS, P.K. and SHRIVASTAVA, P. (1982) "Rheological and Pumping Characteristics of Coal-Water Suspensions". Jou. of Pipelines v.3 p.97-107.

DUCKWORTH, R.A., PULLUM L. and LOCKYEAR, C.F. (1983) "The Hydraulic Transport of Coarse Coal at High Concentration". Jou. of Pipelines v.3, p.251-265.

GOULD (1980) "Instruction Manual PDH3000 Series". No. IM136A Gould Inc. California.

GOVIER, G.W. and AZIZ, K. (1972) "The Flow of Complex Mixtures in Pipes". van Nostrand Reinhold Co.

GREEN, H.G. (1949) "Industrial Rheology and Rheological Structures". John Wiley and Sons, Inc. New York.

HANKS, R.W. and HANKS, K.W. (1982) "A New Viscometer for Determining the Effect of Particle Size Distributions and Concentration on Slurry Rheology". Proc. 7th Int. Conf. on Slurry Transportation p.151-161.

HARRIS, J. and QUADER, A.K.M.A. (1971) "Pipes and Pipelines". British Chemical Engineering, v.16, n.4/5.

HORSLEY, R.R. and REIZES, J.A. (1980) "The Effect of Zeta Potential on the Head Loss Gradient for Slurry Pipelines with Varying Slurry Concentrations". Proc. Hydrotransport 7, B.H.R.A. p.D3-163/168.

KENCHINGTON, J.M. (1974) "An Assessment of Methods of Pressure Drop Prediction for Slurry Transport". Proc. Hydrotransport 3, B.H.R.A. p.F1-1/20.

LAZARUS, J.H. (1988) "Mixed Regime Slurries in Pipelines - Part I Mechanistic Model". Accepted for publication by American Society of Civil Engineers, Hydraulics Division.

_____ (1985) "Hydraulic Transport of Solids". Postgraduate Course Notes, University of Cape Town, South Africa.

_____. and SIVE, A.W. (1985) "Final Report on the Hydraulic Transport of Fly Ash Slurries". Hydrotransport Research Report No. COM5/85, University of Cape Town.

_____. and SLATTER, P.T. (1986) "Comparative Rheological Characterization Using a Balanced Beam Tube Viscometer and Rotary Viscometer". Proc. Hydrotransport 10, B.H.R.A. p.J2-291/294.

MAUDE, A.D. and WHITMORE, R.L. (1956) "The Wall Effect and the Viscometry of Suspensions". Brit. Jou. Appl. Phys. v.7, p.98-102.

MOONEY, M. (1931) "Explicit Formulas for Slip and Fluidity". Jou. of Rheology v.2 n.2, p.210-222.

OLDROYD, J.G. (1948) "The Interpretation of Observed Pressure Gradients in Laminar Flow of Non-Newtonian Liquids Through Tubes". Jou. of Colloid Sci. v.4, p.333-342.

REINER, M. (1934) "The Theory of Non-Newtonial Liquids". Physics, v.5, n.11.

SCHOFIELD, R.K. and SCOTT BLAIR (1930) "The Influence of the Proximity of a Solid Wall on the Consistency of Viscous and Plastic Materials". Jou. Phys. Chem. v.34, p.248-262.

SCHRAMM, G. (1981) "Introduction to Practical Viscometry". Gebruder Haake West Germany.

SCOTT BLAIR, G.W. (1969) "Elementary Rheology". Academic Press Inc. London.

SHOOK, C.A. (1985) "Experiments with Concentrated Slurries of Particles with Densities near that of the Carrier Fluid". Can. Jou. of Chem. Eng. v.63, p.861-869.

SIVE, A.W. and LAZARUS, J.H. (1988) "Mixed Regime Slurries in Pipelines - Part II Experimental Evaluation". Submitted to the American Society of Civil Engineers, Hydraulics Division.

SKELLAND, A.H.P. (1967) "Non-Newtonian Flow and Heat Transfer". John Wiley and Sons, Inc. New York.

SLATTER, P.T. (1986) "The Rheological Characterization of Non-Newtonian Slurries Using a Novel Balanced Beam Tube Viscometer". MSc Dissertation, University of Cape Town.

SMOLDYREV, A.Y. and SAFONOV, Y.K. (1979) "Pipeline Transportation of Concentrated Slurries". Terraspace Inc. (Translated from Russian).

STEPANOFF, A.J. (1964) "Pumping Solid-Liquid Mixtures". Mechanical Engineering, September p.29-35.

_____. (1965) "Pumps and Blowers/Two-Phase Flow". John Wiley and Sons, Inc. New York.

STREAT, M. (1986) "Dense-Phase Flow of Solid Water Mixtures in Pipelines: A State-of-the-Art-Review". Proc. Hydrotransport 10, B.H.R.A. p.B1-39/49.

SWECO (1986) "Sweco Vibro-Energy Separators". Lockers Engineers S.A. (Pty) Ltd.

THOMAS, D.G. (1963) "Non-Newtonian Suspensions, Part 1. Physical Properties and Laminar Transport Characteristics". Ind. and Eng. Chem. v.55 n.11, p.18-29.

THOMAS, H.W. (1962) "The Wall Effect in Capillary Instruments". Biorheology 1.

VAN WAZER, J.R., LYONS, J.W., KIM, K.Y. and COLWELL, R.E. (1963) "Viscosity and Flow Measurement - A Laboratory Handbook of Rheology". John Wiley and Sons, Inc. New York.

WASP, E.J., KENNY, J.P. and GHANDI, R.L. (1979) "Solid-Liquid Flow Slurry Pipeline Transportation". Gulf Publishing Co. Houston.

WINDHAB, E. and GLEISSLE, W (1984) " The Flow Behaviour of Highly Concentrated Suspensions Determined with a New Shear- and Slip Flow Separating Method". Proc. 9th Int. Cog. on Rheology.

CONTENTS OF APPENDICES

APPENDIX A

THE RABINOWITSCH-MOONEY RELATION DERIVATION AND ANALYSIS

A.1. INTRODUCTION

The Rabinowitsch-Mooney relation (as applied to tube flow) relates the pseudo-shear rate to the true shear rate at the tube wall. This is useful in tube viscometry in reducing bulk flow parameters to a rheogram.

$$\text{i.e.} \quad \left[-\frac{du}{dr}\right]_o = \frac{8V}{D}\left[\frac{3n' + 1}{4n'}\right] \tag{A1}$$

$$\text{where} \quad n' = \frac{d\,(\ell n\,(\tau_o))}{d\left(\ell n\left(\frac{8V}{D}\right)\right)} \tag{A2}$$

A.2. DERIVATION (Slatter (1986))

We start with the completely general constitutive equation for circular tube flow:-

$$-\frac{du}{dr} = f\,(\tau) \tag{A3}$$

A force balance on a cylindrical element of radius r and length dL yields

$$\pi\, r^2\, dp = 2\pi\, r\, \tau\, dL$$

$$\therefore \quad \frac{dp}{dL} = \frac{2\,\tau}{r}$$

$$\text{and} \quad \frac{dp}{dL} = \frac{2\,\tau_o}{R}$$

$$\therefore \quad r = \frac{R\tau}{\tau_o}, \quad r^2 = \frac{R^2\tau^2}{\tau_o^2} \quad \text{and} \quad dr = \frac{R}{\tau_o}\,d\tau \tag{A4}$$

also $\tau_o = \frac{D\Delta p}{4L}$.

The flow rate can be obtained by integrating the velocity profile:

$$Q = 2\pi \int_o^R u.r.dr \qquad (A5)$$

Integrating by parts:

$$Q = \pi \left[u\, r^2 - \int r^2 \frac{du}{dr}\, dr \right]_o^R \qquad (A6)$$

Assuming that $u_o = 0$ (no slip at the tube wall)

$$Q = -\pi \int_o^R r^2 \frac{du}{dr}\, dr$$

$$= \pi \int_o^{\tau_o} \frac{R^2\tau^2}{\tau_o^2} \cdot \left(-\frac{du}{dr}\right) \cdot \frac{R}{\tau_o} \cdot d\tau \qquad \text{(substituting A4)}$$

$$= \frac{\pi R^3}{\tau_o^3} \int_o^{\tau_o} \tau^2 \cdot f(\tau) \cdot d\tau \qquad (A7)$$

Substituting $R = D/2$

$$\frac{8Q}{\pi D^3} = \frac{2V}{D} = \frac{1}{\tau_o^3} \int_o^{\tau_o} \tau^2 \cdot f(\tau) \cdot d\tau$$

$$\therefore \frac{8V}{D} = \frac{4}{\tau_o^3} \int_o^{\tau_o} \tau^2 \cdot f(\tau) \cdot d\tau \qquad (A8)$$

Now, differentiating with respect to τ_o (product rule)

$$\frac{d\left(\frac{8V}{D}\right)}{d\,\tau_o} = \frac{-12}{\tau_o^4} \int_o^{\tau_o} \tau^2 \cdot f(\tau) \cdot d\tau + \frac{4}{\tau_o^3} \cdot \frac{d}{d\tau_o}\left[\int_o^{\tau_o} \tau^2 \cdot f(\tau) \cdot d\tau \right] \qquad (A9)$$

The first term on the R.H.S

$$\frac{-12}{\tau_o^4}\int_o^{\tau_o}\tau^2\,.\,f(\tau)\,.\,d\tau = \frac{-3}{\tau_o}\left[\frac{4}{\tau_o^3}\int_o^{\tau_o}\tau^2\,.\,f(\tau)\,.\,d\tau\right]$$

$$= \frac{-3}{\tau_o}\,.\,\frac{8V}{D} \qquad \text{(substituting A8)}$$

The second term on the RHS is treated with the Liebniz formula

---

[The Liebniz formula states:-

$$\frac{d}{d\alpha}\int_{u_o(\alpha)}^{u_1(\alpha)} F(x,\alpha)\,dx = f(u_1,\alpha)\frac{d\,u_1}{d\,\alpha} - F(u_o,\alpha)\frac{du_o}{d\,\alpha}$$

$$+\int_{u_o(\alpha)}^{u_1(\alpha)}\frac{\partial F(x,\alpha)}{\partial\alpha}\,.\,dx$$

Now, let $\alpha = \tau_o$; $u_o(\alpha) = 0$; $u_1(\alpha) = \tau_o$; $x = \tau$;
and $F(x,\alpha) = F(\tau,\tau_o) = \tau^2 f(\tau)$ (i.e. $F(\tau)$ only)]

Then $$\frac{d}{d\tau_o}\left[\int_o^{\tau_o}\tau^2\,.\,f(\tau)\,.\,d\tau\right] = \tau_o^2\,.\,f(\tau_o)\,.\,1 - 0 + \int_o^{\tau_o}0\,.\,d\tau$$

$$= \tau_o^2\,.\,f(\tau_o)$$

$$\therefore \quad \frac{d\left(\frac{8V}{D}\right)}{d\,\tau_o} = \frac{-3}{\tau_o}\,.\left(\frac{8V}{D}\right) + \frac{4}{\tau_o^3}\,.\,\tau_o^2\,.\,f(\tau_o)$$

$$\therefore \quad f(\tau_o) = \left(-\frac{du}{dr}\right)_o = \frac{1}{4}\left[3\left(\frac{8V}{D}\right) + \tau_o\frac{d\left(\frac{8V}{D}\right)}{d\tau_o}\right]$$

$$= \frac{\left(\frac{8V}{D}\right)}{4}\left[3 + \frac{\tau_o}{\left(\frac{8V}{D}\right)}\,.\,\frac{d\left(\frac{8V}{D}\right)}{d\tau_o}\right] \qquad \text{(A10)}$$

Examining the last term:-

[Consider

$$\frac{x}{y} \cdot \frac{dy}{dx} = \frac{x}{1} \cdot \frac{1}{y} \cdot \frac{dy}{dx}$$

Now $\frac{d(\ell n\ x)}{dx} = \frac{1}{x}$ and $\frac{d(\ell n\ y)}{dy} = \frac{1}{y}$

$$\therefore \quad \frac{x}{y} \cdot \frac{dy}{dx} = \frac{dx}{d(\ell n\ x)} \cdot \frac{d(\ell n\ y)}{dy} \cdot \frac{dy}{dx}$$

$$= \frac{d(\ell n\ y)}{d(\ell n\ x)} \quad]$$

Similarly

$$\left(-\frac{du}{dr}\right)_o = \frac{\left(\frac{8V}{D}\right)}{4}\left[3 + \frac{d\left(\ell n\ \left(\frac{8V}{D}\right)\right)}{d\ (\ell n\ (\tau_o))}\right] \qquad \text{(A11)}$$

$$\text{Let } n' = \frac{d\ (\ell n\ (\tau_o))}{d\ \left(\ell n\ \left(\frac{8V}{D}\right)\right)} \qquad \text{(A2)}$$

$$\text{Then } \left[-\frac{du}{dr}\right]_o = \frac{8V}{D}\left[\frac{3n' + 1}{4n'}\right] \qquad \text{(A1) q.e.d.}$$

A.3 DISCUSSION

Since no assumptions are made concerning the nature of the fluid, the result is perfectly general, and can be applied to any fluid, provided that there is no slip at the tube wall.

The relation is a unique mapping from a pseudo-shear diagram to a rheogram.

The effect of this relation for yield-pseudoplastic, bingham plastic and yield-dilatant rheologies is shown in Fig. A1, Fig. A2 and Fig. A3 respectively. The relation logarithmically stretches the x axis of the pseudo-shear diagram yielding a rheogram. It is therefore possible using a pseudo-shear diagram to speculate on the shape of the rheogram. This is the basis for the use of the pseudo-shear rate.

Slatter (1986) showed that the errors involved in the use of the relation were too large for it to be of practical use.

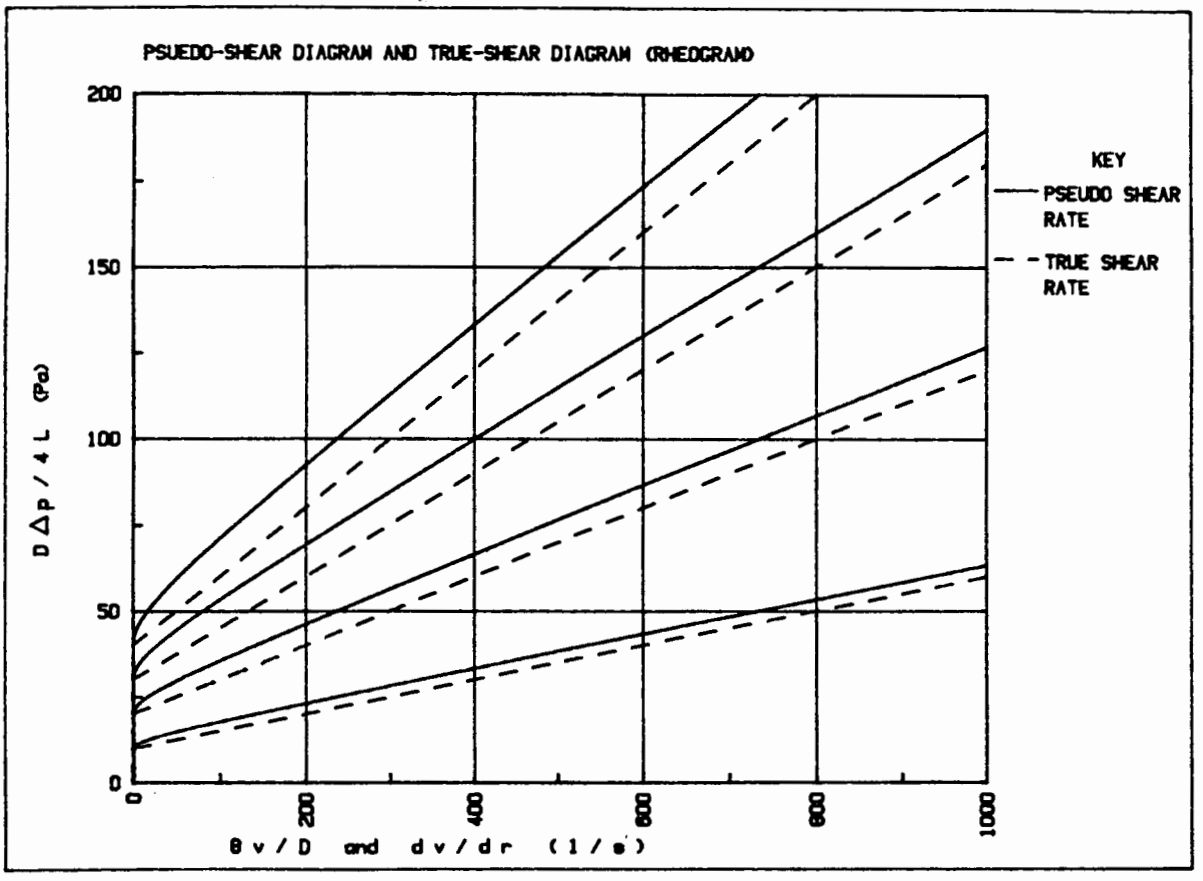

Fig. A1 The effect of the Rabinowitch-Mooney relation on a yield-pseudoplastic rheology.

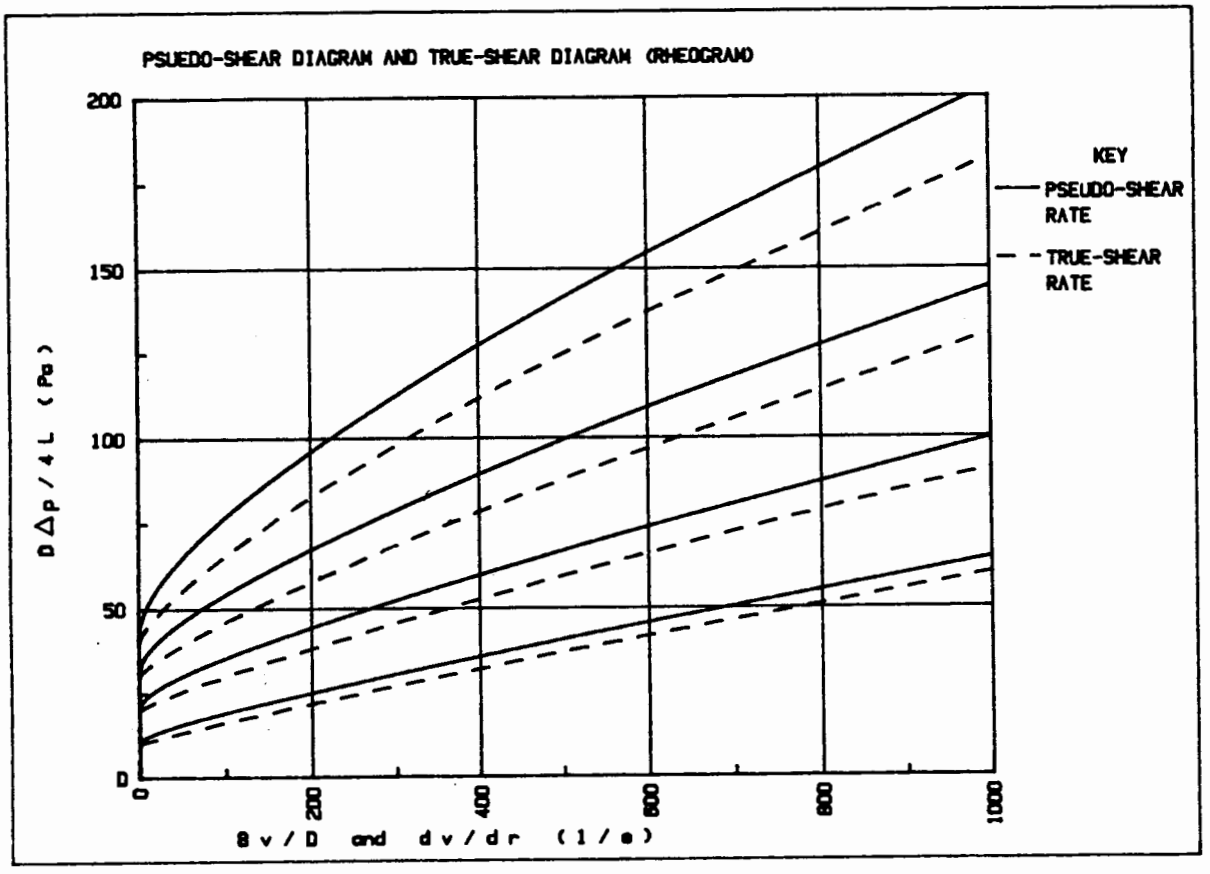

Fig. A2 The effect of the Rabinowitch-Mooney relation on a

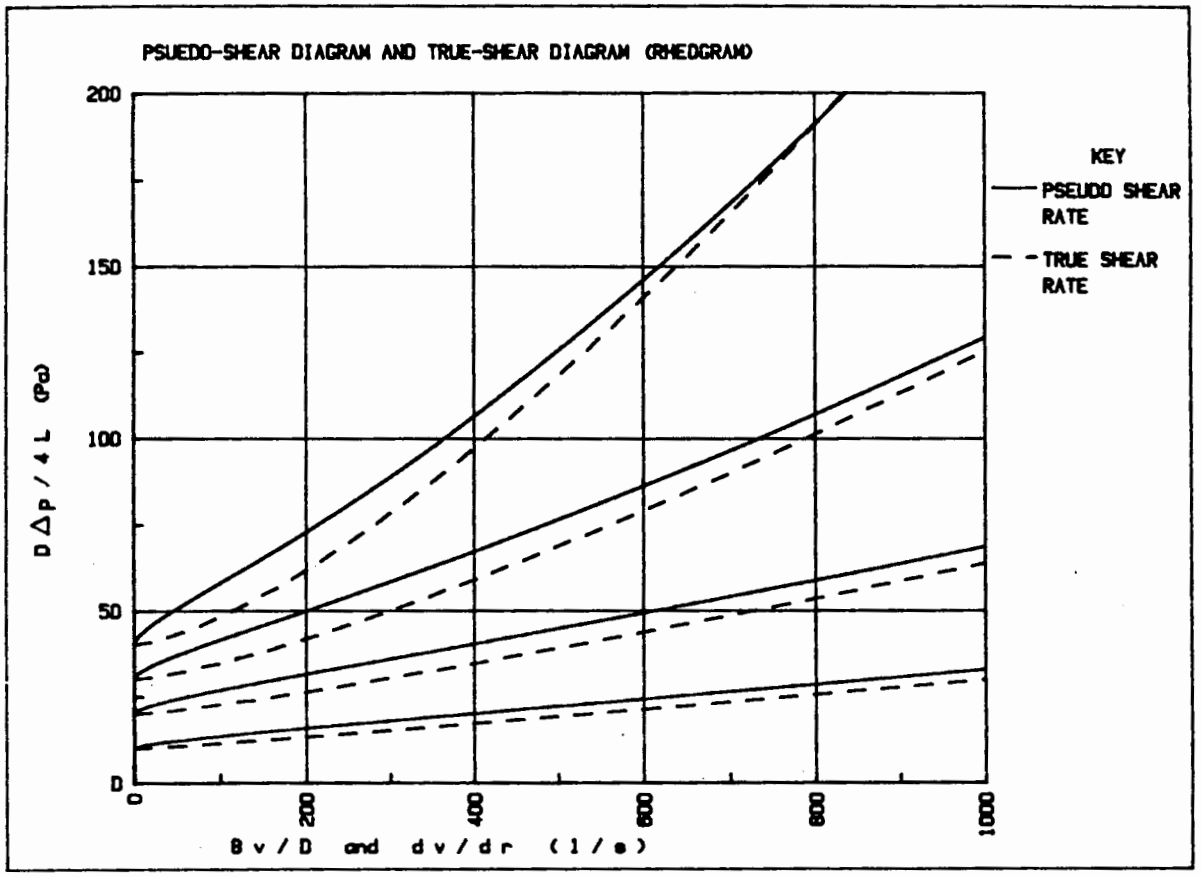

Fig. A3 The effect of the Rabinowitch-Mooney relation on a yield-dilatant rheology.

APPENDIX B

TUBE FLOW DERIVATIONS

B.1 INTRODUCTION

This derivation is based on the yield-pseudoplastic model. By applying various conditions the flow equations for other rheological models are determined.

B.2 YIELD-PSEUDOPLASTIC DERIVATION

The general flow equation A7 from Appendix A given by

$$Q = \frac{\pi R^3}{\tau_o^3} \int_o^{\tau_o} \tau^2 \; f(\tau) \; d\tau \qquad \text{(B1)}$$

Applying the continuity equation $Q = \pi R^2 V$ gives

$$\frac{8V}{D} = \frac{4}{\tau_o^3} \int_o^{\tau_o} \tau^2 \; f(\tau) \; d\tau \qquad \text{(B2)}$$

In the plug region:

$$0 \leq r \leq r_{plug}$$

$$0 \leq \tau \leq \tau_y$$

$$\text{and } f(\tau) = 0 \qquad \text{(B3)}$$

In the sheared region:

$$r_{plug} \leq r \leq R$$

$$\tau_y \leq \tau \leq \tau_o$$

$$\text{and } f(\tau) = \left(\frac{1}{K}\right)^{1/n} (\tau - \tau_y)^{1/n} \qquad \text{(B4)}$$

For fluids with a yield stress equation B2 becomes

$$\frac{8V}{D} = \frac{4}{\tau_o^3} \left[\int_0^{\tau_y} \tau^2 f(\tau)\, d\tau + \int_{\tau_y}^{\tau_o} \tau^2 f(\tau)\, d\tau \right] \qquad \text{(B5)}$$

Applying the conditions B3 and B4 gives

$$\frac{8V}{D} = \frac{4}{\tau_o^3} \left(\frac{1}{K}\right)^{1/n} \int_{\tau_y}^{\tau_o} \tau^2 (\tau - \tau_y)^{1/n}\, d\tau \qquad \text{(B6)}$$

$$\text{set } x = \tau - \tau_y$$

$$\text{then } dx = d\tau$$

$$\text{and } \tau = x + \tau_y$$

Equation B6 becomes

$$\frac{8V}{D} = \frac{4}{\tau_o^3}\left(\frac{1}{K}\right)^{1/n}\int_{\tau_y}^{\tau_o}\tau^2\,(x-\tau_y)^2\,x^{1/n}\,dx$$

$$= \frac{4}{\tau_o^3}\left(\frac{1}{K}\right)^{1/n}\int_{\tau_y}^{\tau_o}\left(x^{\frac{2n+1}{n}} + 2\tau_y\,x^{\frac{n+1}{n}} + \tau_y^2\,x^{\frac{1}{n}}\right)dx$$

$$= \frac{4n}{\tau_o^3}\left(\frac{1}{K}\right)^{1/n}\left[\frac{x^{\frac{3n+1}{n}}}{\frac{3n+1}{n}} + 2\tau_y\frac{x^{\frac{2n+1}{n}}}{\frac{2n+1}{n}} + \tau_y^2\frac{x^{\frac{n+1}{n}}}{\frac{n+1}{n}}\right]_{\tau_y}^{\tau_o}$$

$$= \frac{4n}{\tau_o^3}\left(\frac{1}{K}\right)^{1/n}\left[\frac{(\tau-\tau_y)^{\frac{3n+1}{n}}}{3n+1} + 2\tau_y\frac{(\tau-\tau_y)^{\frac{2n+1}{n}}}{2n+1} + \tau_y^2\frac{(\tau-\tau_y)^{\frac{n+1}{n}}}{n+1}\right]_{\tau_y}^{\tau_o}$$

$$= \frac{4n}{\tau_o^3}\left(\frac{1}{K}\right)^{1/n}\left[\frac{(\tau_o-\tau_y)^{\frac{3n+1}{n}}}{3n+1} + 2\tau_y\frac{(\tau_o-\tau_y)^{\frac{2n+1}{n}}}{2n+1} + \tau_y^2\frac{(\tau_o-\tau_y)^{\frac{n+1}{n}}}{n+1}\right]$$

$$= \frac{4n}{\tau_o^3}\left(\frac{1}{K}\right)^{1/n}(\tau_o-\tau_y)^{\frac{n+1}{n}}\left[\frac{(\tau_o-\tau_y)^2}{3n+1} + 2\tau_y\frac{(\tau_o-\tau_y)}{2n+1} + \frac{\tau_y^2}{n+1}\right] \qquad (B7)$$

B.3 BINGHAM PLASTIC (n = 1)

Applying the condition n = 1 to equation B7 gives

$$\frac{8V}{D} = \frac{4}{K\tau_y^3}(\tau_o - \tau_y)^2\left[\frac{(\tau_o-\tau_y)^2}{4} + 2\tau_y\frac{(\tau_o-\tau_y)}{3} + \frac{\tau_y^2}{2}\right]$$

$$= \frac{4}{K\tau_y^3}(\tau_o - \tau_y)^2\left[\frac{\tau_o^2}{4} + \frac{(\tau_o\,\tau_y)}{6} + \frac{\tau_y^2}{12}\right]$$

$$= \frac{4}{K}\left[1 - \frac{4}{3}\left(\frac{\tau_y}{\tau_o}\right) + \frac{1}{3}\left(\frac{\tau_y}{\tau_o}\right)^4\right]$$

Setting $\alpha = \frac{\tau_y}{\tau_o}$, $\eta_p = K$ and making τ_o the subject of the equation yields the Buckingham equation given by

$$\tau_o = \frac{8V}{D}\eta_p \frac{1}{(1 - 4/3\alpha + \alpha^4/3)} \qquad (B8)$$

B.4 POWER LAW ($\tau_y = 0$)

Applying the condition of $\tau_o = 0$ to equation (B7) gives

$$\frac{8V}{D} = \frac{4n}{\tau_o^3}\left(\frac{1}{K}\right)^{1/n}\tau_o^{\frac{n+1}{n}}\frac{\tau_o^3}{1+3n}$$

$$= \frac{4n\,\tau_o^{1/n}}{K^{1/n}(1+3n)} \qquad (B9)$$

B.5 NEWTONIAN ($\tau_y = 0$, $n = 1$)

Applying the conditions of $\tau_y = 0$ and $n = 1$ to equation (B7) gives

$$\frac{8V}{D} = \frac{\tau_o}{K}$$

Setting $\mu = K$ and making τ_o the subject of the equation gives

$$\tau_o = \mu \frac{8V}{D} \qquad \text{(B10)}$$

Substituting in the continuity equation yields the Hagen-Poiseuille equation given by

$$Q = \frac{\pi R^3}{4 \mu} \tau_o \qquad \text{(B11)}$$

B.6 CONCLUSIONS

These equations are all identical to the equations presented in Skelland (1967), Govier and Aziz (1972) and Wasp (1979).

APPENDIX C

YIELD-PSEUDOPLASTIC CURVE FITTING PROGRAM DESCRIPTION

C.1 INTRODUCTION

This program fits the yield-pseudoplastic equation given by

$$\frac{8V}{D} = \frac{4n}{K^{1/n}\tau^3}(\tau - \tau_y)^{\frac{n+1}{n}}\left[\frac{(\tau-\tau_y)^2}{3n+1} + \frac{2\tau_y(\tau-\tau_y)}{2n+1} + \frac{\tau_y^2}{n+1}\right] \qquad (C1)$$

to a set of data on pseudo-shear diagram.

C.2 DESCRIPTION

The value of the yield stress (τ_y) is read off the pseudo-shear diagram directly. Using this value the program selects the values of K and n that give the minimum error in 8V/D on a graph of 8V/D versus τ_o. The error for fixed value of τ_y, K and n is given by

$$\text{Error} = \sqrt{\sum_{i=1}^{n}\left(\left(\frac{8V_i}{D}\right)_{obs} - \left(\frac{8V_i}{D}\right)_{calc}\right)^2 / n-1}$$

$$= \sqrt{\sum_{i=1}^{n}\left(\left(\frac{8V_i}{D}\right)_{obs} - \left(\frac{4n}{K^{1/n}\tau_i^3}(\tau_i - \tau_y)^{\frac{n+1}{n}}\left[\frac{(\tau_i-\tau_y)^2}{3\,n+1} + \frac{2\tau_y(\tau_i-\tau_y)}{2n+1} + \frac{\tau_y^2}{n+1}\right]\right)\right)^2 / n-1} \qquad (C2)$$

At a fixed value of n the minimum value for K is obtained by setting dError/dK = 0. This gives

$$K_{min} = 1/\left[\frac{2\sum_{i=1}^{n}\left(V_i/D\right)}{n\sum_{i=1}^{n}\left(\left(\frac{(\tau_i-\tau_y)^2}{3n+1} + \frac{2\tau_y(\tau_i-\tau_y)}{2n+1} + \frac{\tau_y^2}{n+1}\right)/\tau_y^3\right)}\right]^n \qquad (C3)$$

The program calculates the error over a range of n values at the minimum K value. By zooming in on the value of n with the lowest error the best fit values of K and n are obtained. The error in the fit is calculated as error in 8V/D per point using equation C2.

C.3 CONCLUSION

The program is capable of efficiently selecting the values of K and n associated with the minimum error.

APPENDIX D

ANCILLARY TESTS

D.1 SOLIDS RELATIVE DENSITY DETERMINATIONS

Aim : To determine the solids relative density.

Method : Find the mass of a clean dry density bottle of known volume. Fill the bottle with the mixture to the etched level remove any air bubbles with a vacuum pump and weigh. Empty the bottle into a weighed evaporation dish using water to rinse off all the solid particles. Dry the dish at 102°C and weigh. The relative density is determined twice using the calculation procedure. The average of the two relative densities is calculated if their difference is less than 0.01.

Readings :

Volume of bottle	= v	ml
Mass of dry bottle	= m1	g
Mass of bottle + mixture	= m2	g
Mass of dry evaporation dish	= m3	g
Mass of evaporation dish + dried mixture	= m4	g

Calculations :

Mass of mixture	= m2 - m1	g
Mass of solids	= m4 - m3	g
Mass of liquid	= m2 - m1 - m4 + m3	g
Volume of liquid	= (m2 - m1 - m4 + m3)/0.9982	ml
Volume of solids	= v - ((m2 - m1 - m4 + m3)/0.9982)	ml

$$\text{Density of solids } (\rho_s) = \frac{m4 - m3}{(v - ((m2 - m1 - m4 + m3)/0.9982))} \text{ g/ml}$$

$$\text{Relative density of solids } (S_s) = \frac{\rho_s}{0.9982}$$

Masses were determined using a Mettler scale accurate to ± 0.01 mg. The accuracy of this determination is approximately 0.3%.

D.2 MIXTURE RELATIVE DENSITY DETERMINATIONS

Aim : To determine the mixture relative density.

Method : Find the mass of a clean dry density bottle of known volume. Fill the bottle with the mixture until it is almost full and weigh. Fill the bottle with water to the etched level and remove any air bubbles with a vacuum pump and weigh again. Empty the the bottle and rinse with water. Refill the bottle with water to the etched mark and weigh again.

Readings :

Mass of dry bottle	= m1	g
Mass of bottle + mixture	= m2	g
Mass of bottle + mixture + water	= m3	g
Mass of bottle + water	= m4	g

Calculations :

Mass of mixture	= m2 - m1	g
Mass of added water	= m3 - m2	g
Volume of added water	= (m3 - m2)/0.9982	ml
Mass of water	= m4 - m1	g
Volume of water	= (m4 - m1)/0.9982	ml
Volume of mixture	= (m4 - m1 - m3 + m2)/0.9982	ml
Density of mixture (ρ_m)	$= \frac{m2 - m1}{(m4 - m1 - m3 + m2)/0.9982}$	g/ml

Relative density of mixture (S_m) $= \frac{\rho_m}{0.9982}$

Masses were determined using a Mettler scale accurate to ± 0.01 mg. The accuracy of this determination is 0.3%.

D.3 pH DETERMINATION

pH determinations are made using a Radiometer model pHM 80 pH meter and a GK 2401C glass electrode calibrated using Radiometer buffer (Disodium hydrogen phosphate / potassium dihydrogen phosphate) of pH = 7.02 (±0.001) at 20°C, calibrated at the measuring temperature shown in Fig. D1.

D.4 PARTICLE SIZE DISTRIBUTION DETERMINATIONS

The particle size distributions were determined using a Malvern 2600/3600 Particle Sizer VF.6. The instrument is calibrated using particles of a known diameter. Three lenses (63 mm, 100 mm and 300 mm) may be used. The particle ranges of each lense are shown in Table D1. The 300mm lens is used because it has the most appropriate particle sizes range.

Table D1 Malvern lenses

Lens (mm)	Size Range (μm)
63	1.2 - 118.4
100	1.9 - 188.0
300	5.8 - 564.0

D.5 MICROGRAPHS

The micrographs were taken using an optical microscope. The microscope is equipped with 10 mm, 16 mm and 40 mm dry lenses and side and bottom lighting.

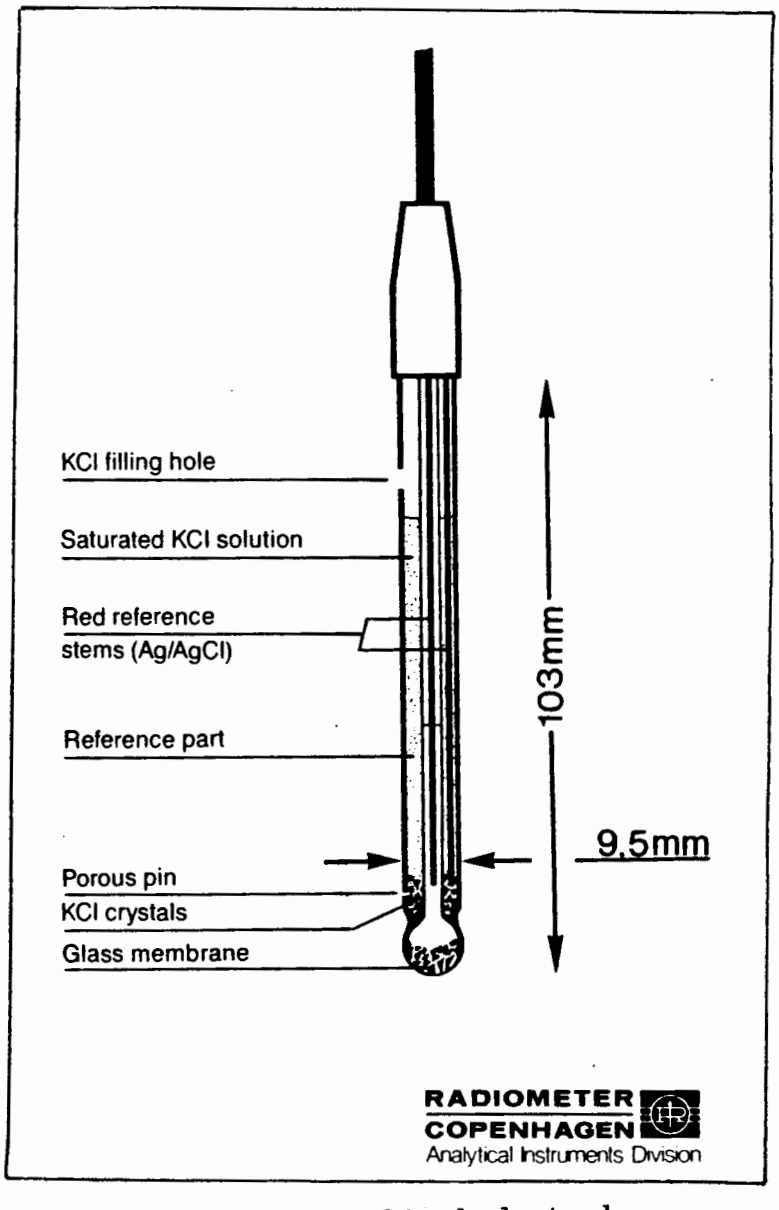

Fig. D1 GK2401C Combined electrode.

APPENDIX E

COMPARATIVE TESTS BETWEEN FULL PLANT TAILINGS (FPT) AND BELT FILTERED TAILINGS (BFT)

E.1 INTRODUCTION

The similarity between two types of backfill tailings is investigated in this appendix. The two tailings are the result of the same process but may differ in geographic origin.

E.2 COMPARATIVE TESTS

The two tailings were scalped using a 18" Sweco Vibro-Energy Separator at 106 μm and 62 μm. The -106 μm and the -62 μm fractions of each of the tailings are compared.

E.2.1 Particle Size Distribution

The particle size distributions of the two slurries were determined using the Malvern Particle Sizer described in Appendix D. The results are shown together in Fig. E1 and Fig. E2.

E.2.2 Solids Relative Density

The solids relative density of each of the two tailings was determined using the procedure outlined in Appendix D. The results of the tests are presented in Table E1.

Table E1 Summary of the comparative solids relative densities

Tailings	Particle Size (μm)	Solids Relative Density (S_s)
FPT	-106	2.747
BFT	-106	2.745
FPT	- 62	2.754
BFT	- 62	2.749

E.2.3 Rheology

The two tailings were tested in the Balanced Beam Tube Viscometer. A summary of the tests done is presented in Table E2.

Table E2 Summary of the comparative tests.

Tailings	Particle Size (μm)	Mixture Relative Densities (S_m)	Volumetric Concentration (C_v)
FPT	-106	1.704	40.30 %
BFT	-106	1.701	40.17 %
FPT	- 62	1.605	34.50 %
BFT	- 62	1.607	33.47 %

The pseudo-shear diagrams at each concentration and particle size for each of the tailings are plotted together for comparison and shown in Fig. E3 to Fig. E4.

E.3 CONCLUSIONS

The differences in the above tests are considered to be insignificant with reference to the rheology. The differences in the rheograms are ascribed to small variations in the mixture relative densities shown in Table E2 and experimental error. Assuming that no variables have been overlooked the tests show that all the variables that affect rheology for each of the tailings are for all intents and purposes the same. This conclusion enables a more cohesive analysis to be made.

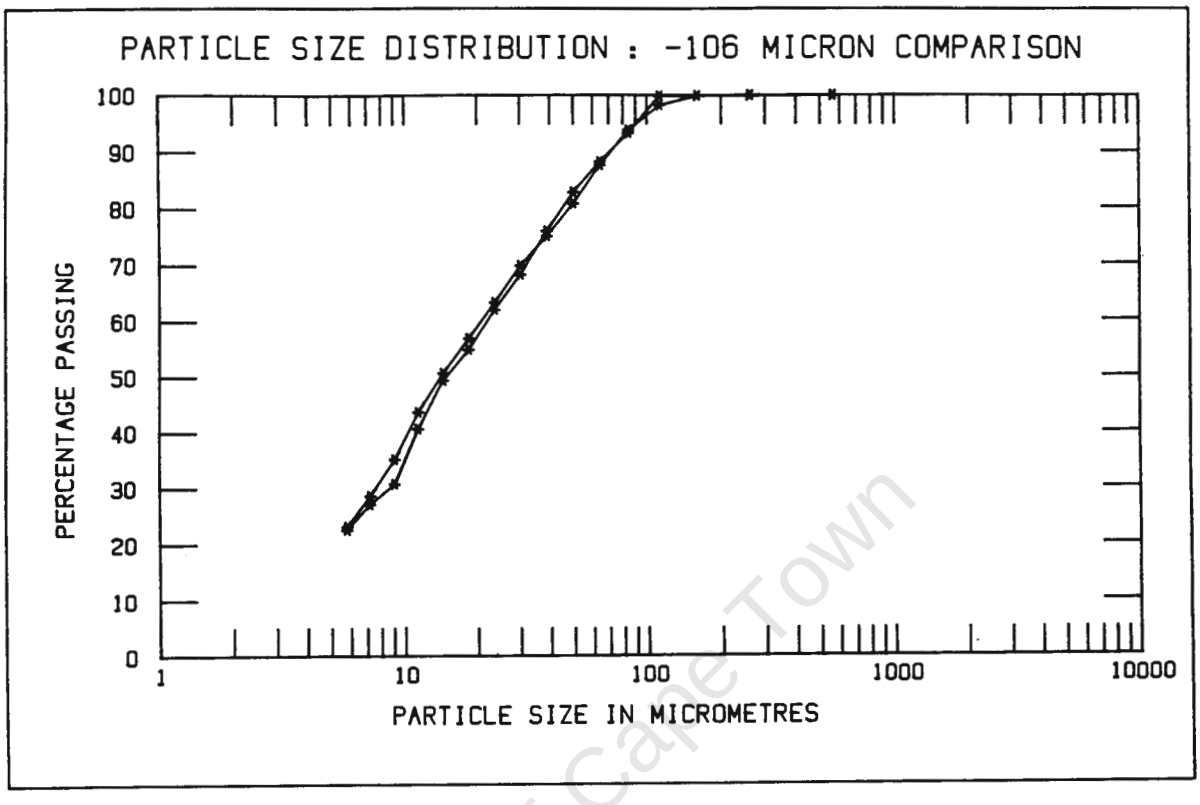

Fig. E1 Particle size distribution comparison between the -106 μm fraction of FPT and BFT.

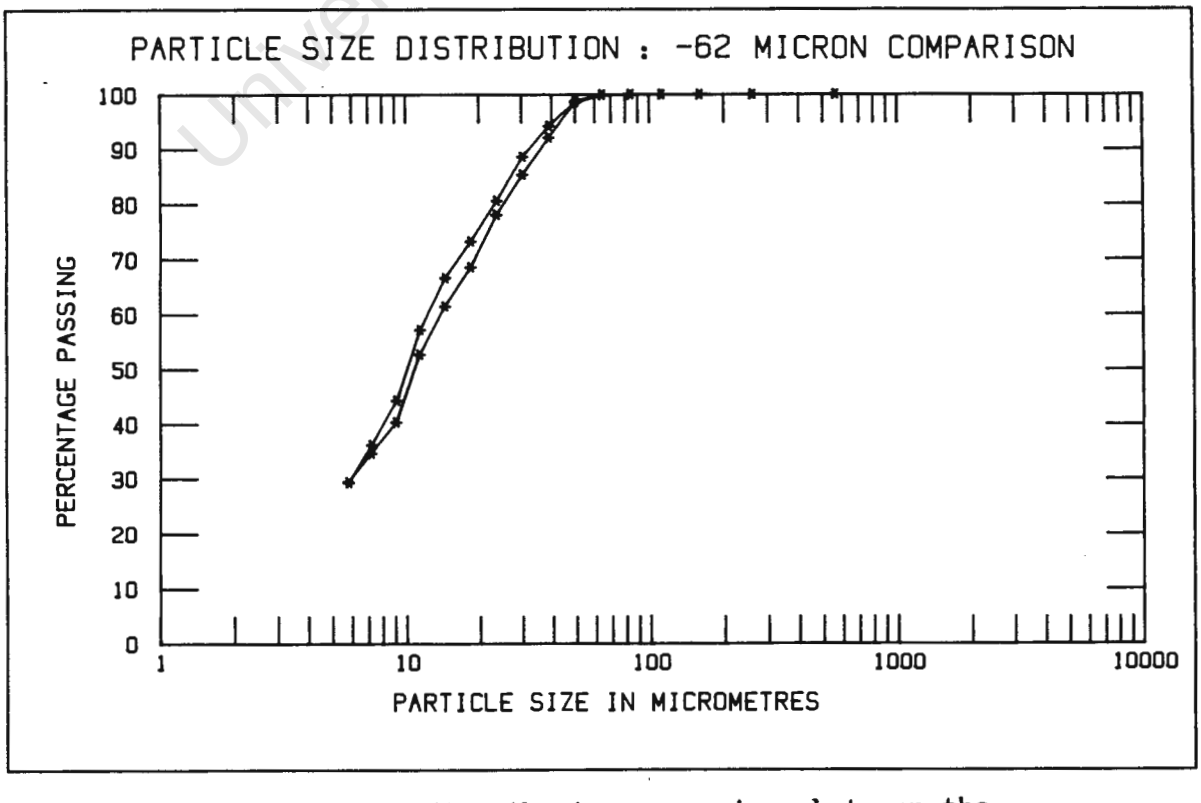

Fig. E2 Particle size distribution comparison between the -62 μm fraction of FPT and BFT.

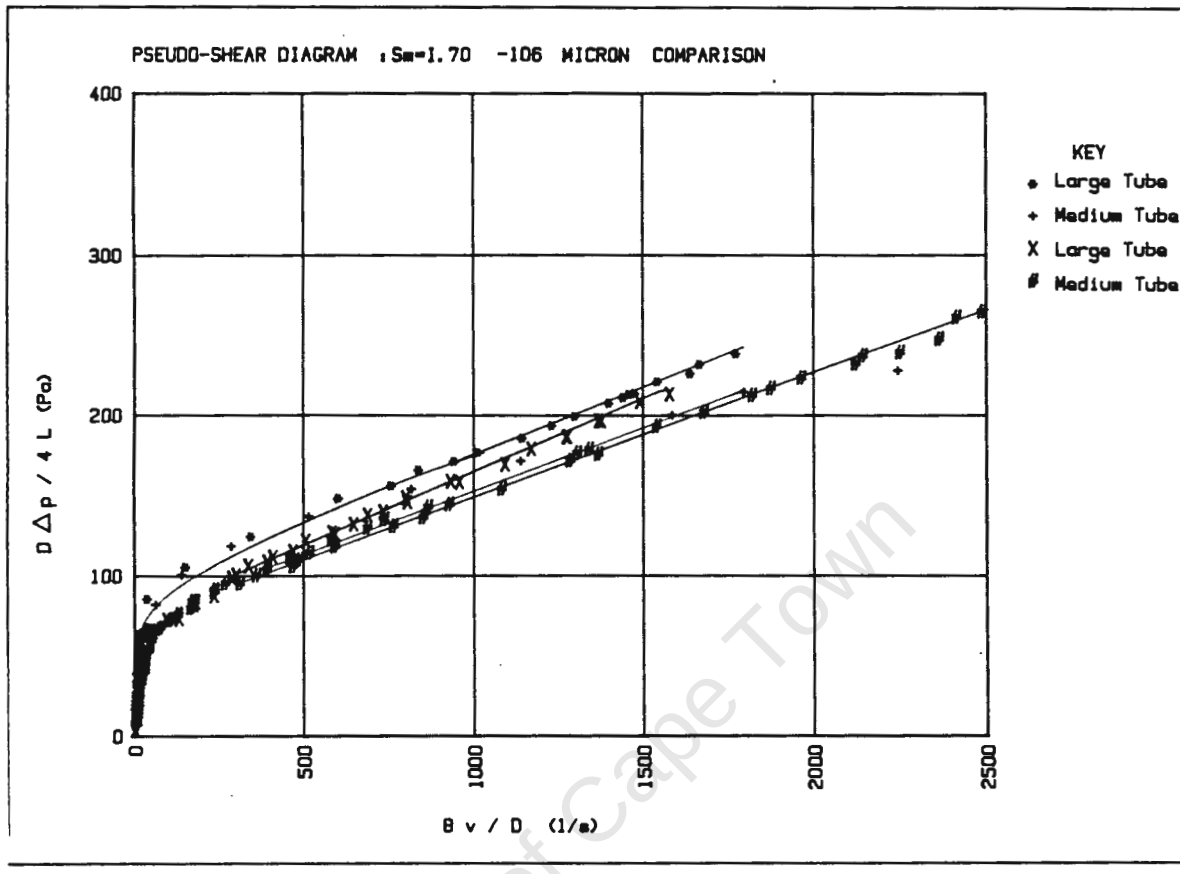

Fig. E3 Rheological comparison between the -106 μm fraction of FPT and BFT.

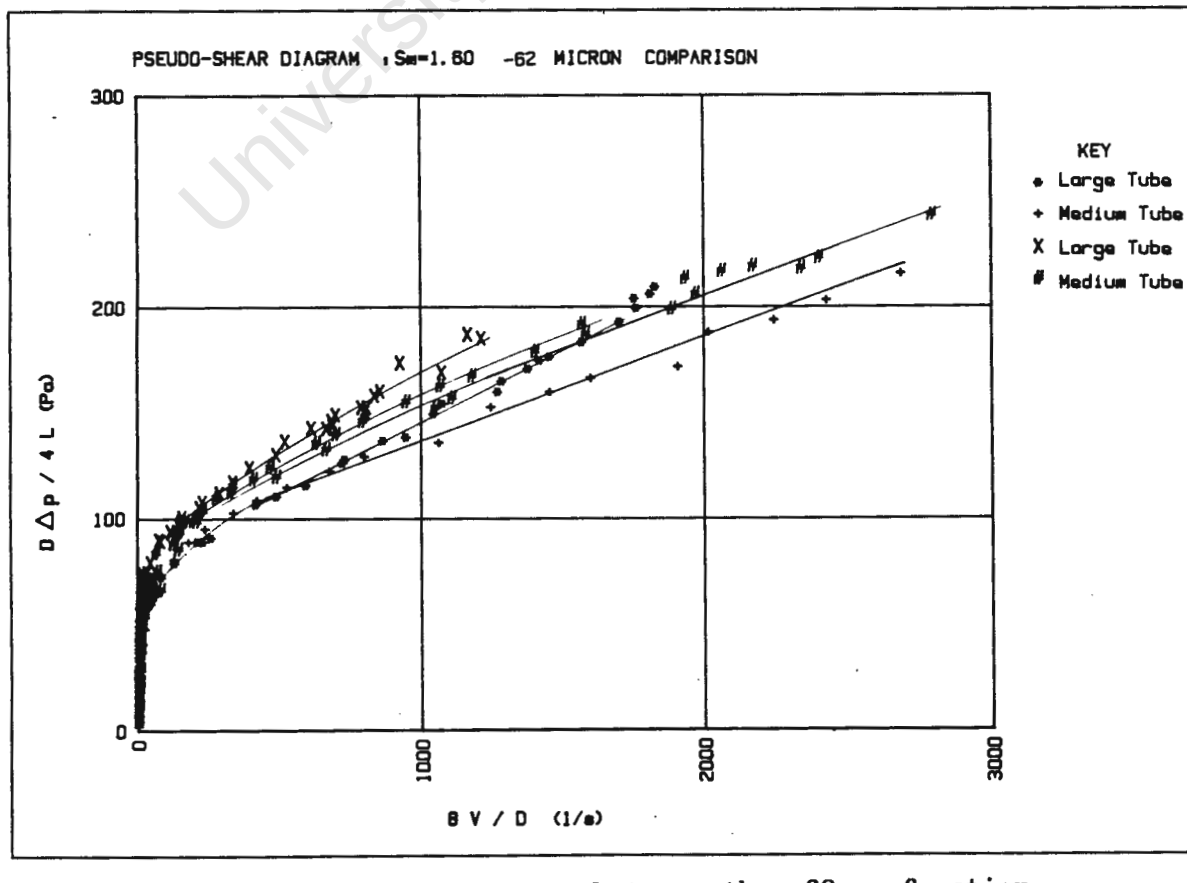

Fig. E4 Rheological comparison between the -62 μm fraction of FPT and BFT.

APPENDIX F

EXAMINATIONS WRITTEN BY AUTHOR IN COMPLETION OF THE MSc DEGREE REQUIREMENTS

Examination		Credit Rating
CIV 516F	Coastal Hydraulics	5
CIV 525S	Contract Law	3
CIV 526F	Properties of Concrete	4
CIV 524Z	Irrigation Systems	3
END 507Z	Management for Engineers	5
Thesis	"The Rheology and Flow Behaviour of High Concentration Mineral Slurries"	20
	TOTAL	40

Credit requirements for degree = 40